1967

The ignition transient in small solid propellant rocket motors of practical configuration

Lukenas, Leo Allen

Princeton, New Jersey; Princeton University

THE IGNITION TRANSIENT IN SMALL SOLID PROPELLANT ROCKET MOTORS OF PRACTICAL CONFIGURATIONS

by

Leo A. Lukenas
LCDR USN

PRINCETON UNIVERSITY
DEPARTMENT OF
AEROSPACE AND MECHANICAL SCIENCES

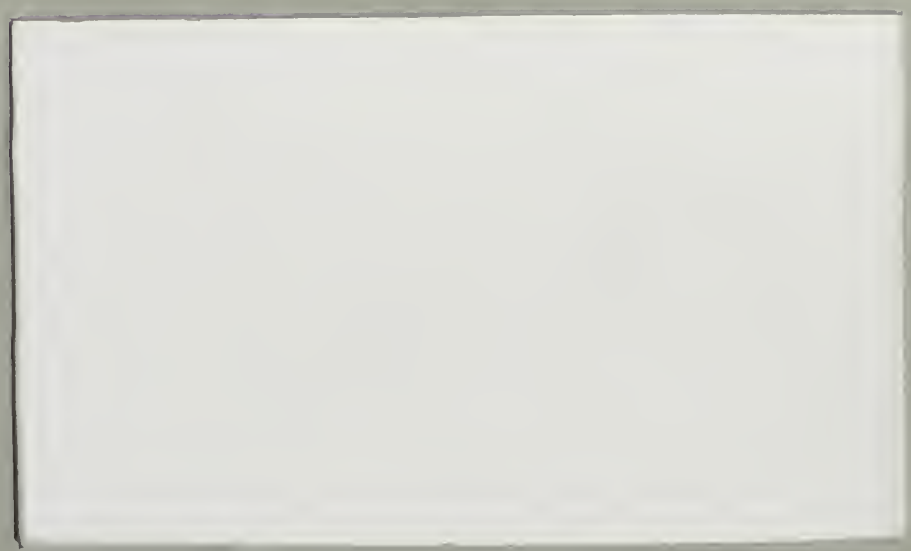

THE IGNITION TRANSIENT IN SMALL SOLID PROPELLANT ROCKET MOTORS OF PRACTICAL CONFIGURATIONS

by

Leo A. Lukenas
LCDR USN

Submitted in partial fulfillment
of the requirements for
the degree of Master of Science in Engineering
from Princeton University, 1967

ACKNOWLEDGEMENTS

I am grateful to the United States Navy for the opportunity to attend Princeton University under the provisions of the U.S. Naval Postgraduate Education Program. While at Princeton, it was my privilege to work under Professor Martin Summerfield. Professor Summerfield proposed the project for this report and supervised the overall effort. I thank him for his confidence and invaluable guidance.

The background experience and many suggestions of Mr. Peter L. Stang, a member of the Professional Technical Staff of the Guggenheim Laboratories, enabled me to avoid many pitfalls during the course of this research. Mr. Stang's encouragement and interest were constant and are greatly appreciated.

My introduction to experimental research was under the able assistance of graduate student, Mr. William J. Most. He was never too busy to discuss problems as they arose, and he was always eager to help. His contributions are deeply appreciated and gratefully acknowledged.

I wish to acknowledge the time and efforts devoted to the computer work by undergraduate, Mr. Lawrence H. Linden, Princeton 1968.

I am grateful to Mr. Chris R. Felsheim for his able and enthusiastic support in the areas of propellant processing and equipment manufacture and modification.

My righthand man and project technician was Mr. Samuel O. Morris, a patient listener whose optimism was ever-present. I am grateful for his able assistance which was often above and beyond the call of duty.

I wish also to acknowledge Mr. James H. Semler for the expert machining of the many required parts and Mr. Roy E. Crosby for the photographic work.

Financial support for this research was provided by NASA Research Grant NsG 200-60. The computer facilities used in this report are supported in part by the National Science Foundation Grant NSF-GP 579.

Moral support was provided by my wife and children. They were patient, understanding and uncomplaining while sacrificing a normal family life for the duration of my postgraduate education. For their sacrifice, I am proud. By their love, I was buoyed.

TABLE OF CONTENTS

TABLE OF CONTENTS - Cont'd.

LIST OF TABLES

LIST OF FIGURES

LIST OF FIGURES - Cont'd.

ABSTRACT

An understanding of the ignition transient of a solid propellant rocket motor becomes increasingly more important as larger and more sophisticated solid propellant rocket motors are developed. Cost considerations alone require the minimal use of empirical methods in rocket development. Consideration of structural strength limitations, possible critical trajectory guidance and vehicle attitude control requirements, and the problem of ignition shock to sensitive instrumentation require that the ignition transient response be known and used as a basis for design. The ignition transient includes the entire time from initiation of the ignition signal to the attainment of design operating conditions within the rocket motor. The ignition transient can be separated into three intervals: the ignition lag interval - the delay between the initial ignition signal and the igniting of the first propellant element; the flame spreading interval - the time required for the propellant surface to become wholly ignited following first ignition; and the chamber filling interval - the time from completion of flame spreading to the attainment of design operating conditions.

This research is the logical extension of the modified ignition transient prediction theory of Summerfield, Parker, and Most[1] to small solid propellant rocket motors with practical configurations. The object was to design, develop, and test-fire small rocket motors with practical configurations using a realistic igniter and to compare the experimental results with computer predicted ignition transients. Two case bonded motors were developed, one with a circular port and the other with a star shape port. A combined

total of 57 circular and star shape motors were tested using various exit nozzle areas and propellant grain lengths of 3.5, 7.625, and 9.5 inches.

A large discrepancy was found between the predicted and experimental results in the flame spreading interval, with a smaller difference occurring in the chamber filling interval. Three possible reasons are considered for the slow pressure rise; back flame spreading, back chamber filling, and cooling-off of the igniter gas as it flows along the motor length. Based on diagnostic firing runs, it was determined that back flame spreading did not occur and that back chamber filling was only a minor contributor to the slow pressure rise. Cooling-off of the igniter gas is considered the major probable cause for the slow pressure increase.

Completion of flame spreading was determined to take place after 50% of the equilibrium chamber pressure was reached. This indicates a need to assign equal importance to the flame spreading and chamber filling intervals when considering ways to control the ignition transient.

The ignition prediction theory of Summerfield, Parker, and Most appears to be fundamentally correct. The results of this research indicate a need for refinement in the theory, particularly in the flame spreading interval in order to better predict the performance of rocket motors of practical configuration.

CHAPTER I

INTRODUCTION

As larger and more sophisticated solid propellant rocket motors are developed, it becomes increasingly more important and necessary to understand the ignition transient. Trial-and-error techniques are costly and must be avoided when possible. With a knowledge of the dynamics of the ignition transient, the design engineer can better cope with the associated problems. A detailed knowledge of the thrust response during the ignition transient is required for motors used for critical trajectory guidance and vehicle attitude control. Unexpected pressure overshoots during the ignition transient could cause a rupture of the motor casing. High rates of pressurization could cause cracking of the propellant grain especially at low ambient temperatures. With guidance systems or other payloads highly sensitive to acceleration forces, the problem of ignition shock must be avoided.

An ignition transient prediction theory was developed by Summerfield, Parker, and Most[1] for an experimental solid propellant slab motor. Di Lauro[2] modified the theory to include the effects of a gas torch igniter and used the modified theory to obtain computer predictions of the ignition transient of a slab motor using a gas torch igniter. Series of predictions were obtained by varying igniter flow rate, port area, throat area, or igniter duration. Work is underway to obtain experimental firing runs of a laboratory rocket motor employing flat slab grains to verify the predictions.

The purpose of the work reported herein is the logical extension of the modified ignition transient prediction theory to small solid propellant

rocket motors with practical configurations. The object was to design, develop, and test-fire small rocket motors with practical configurations using a realistic igniter and to compare the experimental results with computer-predicted ignition transients. Two internal-burning, case-bonded motors were developed, one with a circular port cross-section and the other with a star-shape port cross-section. The motor with the circular port cross-section will be referred to as the circular motor throughout this report.

CHAPTER II

THEORETICAL DISCUSSION

The ignition transient is the time from initiation of the ignition signal to the attainment of design operating conditions within the rocket motor. The ignition transient can be separated into three intervals: the ignition lag interval - the delay between the ignition signal and igniting of the first propellant element; the flame spreading interval - the time required for the propellant surface to become wholly ignited following first ignition; and the chamber filling interval - the time from completion of flame spreading to the attainment of design operating conditions. Detailed discussions of the three intervals are presented in References 1 through 4.

The ignition lag interval is dependent on delays inherent in igniter initiation and on the process by which an element of the propellant grain ignites. The latter is a complex process that is not fully understood. However, for the purpose of this report, the ignition criterion is assumed to be simply the attainment of a critical temperature by the propellant element.[1,2,3,4]

The equations governing the flame spreading and chamber filling intervals can be derived from the conservation equations for the combustion chamber. The derivation of the equations is given in detail in Reference 1 and 2 and will not be repeated here. The assumptions used in the derivation include the uniform-pressure and uniform-temperature combustor, negligible reaction in the control volume, longitudinal streamline flow, ideal nozzle exhaust flow, low Mach number flow within the combustion chamber, identical product gas composition for the igniter and motor propellants, and a simple power law for the burning rate.

Using these assumptions, the conservation equations may be written for the combustion chamber.

1. Momentum

$$\nabla P_c \approx 0 \qquad \text{III-1}$$

2. Continuity

$$\frac{dm_c}{dt} = \dot{m}_b + \dot{m}_{ign} - \dot{m}_n \qquad \text{III-2}$$

3. Energy

$$\frac{1}{\gamma}\frac{d}{dt}(m_c T_c) + \dot{m}_n T_c - \dot{m}_b T_f - \dot{m}_{ign} T_{c_{ign}} = 0 \qquad \text{III-3}$$

(For the definition of symbols, refer to the list of symbols, page xi

After some algebraic manipulation, the conservation equations take the dimensionless form:

$$\frac{dP}{d\tau} = \gamma\left[SP^n - PT^{1/2} + P_{ign}\, T_{ign}^{1/2}\, \frac{A_{t_{ign}}}{A_t}\, f(\tau)\right] \qquad \text{III-4}$$

$$\frac{dT}{d\tau} = \frac{T}{P}\left[(\gamma - T)\, SP^n - (\gamma - 1)PT^{1/2} + \frac{P_{ign}}{T_{ign}^{1/2}}\, \frac{A_{t_{ign}}}{A_t}(T - \gamma T_{ign}) f(\tau)\right] \qquad \text{III-5}$$

Equations III-4 and III-5 apply to both the chamber filling and flame spreading intervals. Because of the appearance of the instantaneous burning area, $S = S(\tau)$, there is no general solution for the equations during the flame-spreading interval.

For the chamber filling interval, S = 1, by definition. It can be shown that the dimensionless chamber temperature, T, does not vary much from unity.[1,2]

Using S = 1 and the assumption $T \approx 1$, equations III-4 and III-5 may be reduced to a single differential equation of the Bernoulli type:

$$\frac{dP}{d\tau} = \gamma(P^n - P) \qquad \text{III-6}$$

The analytical solution of which is

$$P = \left[1 - (1 - P_I^{1-n})e^{-\gamma(1-n)\tau}\right]^{\frac{1}{1-n}} \qquad \text{III-7}$$

It should be noted that the maximum value of the time rate of change of chamber pressure, $dP/d\tau$, occurs at the beginning of the chamber filling interval. It should also be noted that $ln\left[1 - P^{1-n}\right]^{-1}$ is proportional to time, τ. This relationship will be used later to determine the end of flame spreading, i.e., the start of chamber filling, for the experimental firing-runs.

In order to apply equations III-4 and III-5 to the flame spreading interval, the instantaneous burning area, S, must be considered. The process of flame spreading can best be explained by the hypothesis of successive independent ignitions.[1,2] Based on this hypothesis and an ignition criterion, flame spreading can be determined if the energy flux to the propellant from the flowing hot gas is known. As already indicated, the ignition criterion assumed for this report is the attainment of a critical temperature by a propellant element. The energy flux to the propellant is provided by the empirical heat transfer correlation determined by Summerfield, Parker, and Most[1] and reproduced in Figure 1. In order to allow for the probable location of the leading edge of the boundary layer ahead of the leading edge of the propellant, the x = 0 point, the empirical heat transfer correlation is transformed as follows:[2]

$$N_{u(a+x)} = 0.09\ R_{e(a+x)}^{0.8}$$

where "a" is the distance between the boundary layer leading edge and the propellant leading edge. The empirical heat transfer correlation is of the conventional form for a turbulent boundary layer flow over a rough flat plate (i.e., a flat slab of propellant). The heat transfer correlation for the circular and star shape motor grains is expected to be about the same as that determined for the slab motor. Any difference would probably involve only a small coefficient change.

CHAPTER III

EXPERIMENTAL APPARATUS

The small experimental rocket motors designed and developed for this project consisted of a solid propellant pyrogen igniter and an internal-burning case-bonded solid propellant motor grain. An exploded view of the motor is given in Figure 2. A photograph of the assembled motor on the test stand is shown in Figure 3.

A primary design objective was the duplication of selected parameters of the two-dimensional rocket motor of Summerfield, Parker, and Most.[1] The selected parameters were chamber volume, propellant grain length, and propellant composition. The solid pyrogen igniter was designed to duplicate the typical performance of the gas torch igniter of Most,[5] i.e., the same durations and mass flow rates of hot gases. The purpose of the duplication of selected parameters was to allow an independent assessment of the three-dimensional effects of the practical configuration and no other variables would be introduced.

Design of the star shape grain was undertaken after the design and development of the circular grain were completed, and its dimensions were chosen to be compatible with the available equipment developed for the circular grain. The amount of propellant needed for each test was minimized by choosing a small web thickness, just sufficient to permit trouble-free casting. A simple calculation showed that a web thickness of as little as 1 mm would have been sufficient to last through the entire transient; therefore, the minimum practical requirements for smooth casting determined the thickness.

A table of experimental parameters including igniter and motor data is contained in Appendix A.

A. Solid Pyrogen Igniter

One of the objectives in the development of a realistic practical igniter was a square wave pressure response having the same duration and mass flow rate obtained by Most with the gas torch igniter.[5] A typical gas torch run produced a flow rate of 0.02 lbs. per second for 0.2 seconds. The resulting solid pyrogen igniter was a miniature internal-burning case-bonded solid propellant rocket motor with a circular port cross-section. One end of the grain was tapered in order to provide neutral burning. Overall length of the igniter grain was 0.524 in. with a port diameter of 0.5 in. and a web thickness of 0.09375 in. The firing time with this web thickness proved excessive, i.e., the igniter operated throughout the ignition transient resulting in pressure overshoots above the equilibrium operating level. Igniter duration was reduced by decreasing the charge web thickness. The goal was to have termination of the igniter coincident with motor ignition. From tests in which the web thickness was changed, a minimum value of 0.0465 in. was determined. Further reduction resulted in a delay fire or misfire. Proper web thickness was obtained by machining the cast igniter port to a diameter of 0.594 in. With this final design, the average igniter duration was 150 msec, with igniter termination usually occurring during the ignition transient. A typical igniter trace is given in Figure 4.

A modified composite double base propellant was selected for the igniter, i.e., a plastisol propellant. The composition of the plastisol

propellant is given in Table I. The burning rate curve is provided by Figure 5. The plastisol propellant was made in the Solid Propellant Processing Laboratory at Princeton using techniques reported in Reference 6.

In order to provide the igniter with a neutral burning pressure response, an inert tapered section of epoxy cement was cast into one end of the disposable phenolic shell prior to the processing and casting of the propellant. The tapered insert was designed to maintain the propellant burning area constant during igniter operation, provided the ends of the grain were properly inhibited. The inert tapered insert served to inhibit one end, while a layer of epoxy cement was used to inhibit the other end. Figure 6 shows the several stages of igniter grain preparation.

Initiation of the igniter grain was accomplished with an Atlas Electric Match Assembly, Type 14104. Firing current was provided by two 90-volt dry cell batteries connected in series. The assembled igniter is shown in Figure 7.

Results of initial igniter tests were less than satisfactory. Delays in ignition of the igniter propellant of as much as 1.1 second were obtained. This difficulty was eliminated by providing a closure for the igniter nozzle designed to rupture at some mid-pressure, a technique often used to improve the ignition of practical rocket motors.[7] By sealing the chamber, the products of the electric match actuation were retained momentarily within the chamber while the pressure rose to the rupture level for the seal. The pressure build-up was probably a significant contributor to successful ignition. Double base propellants often require ignition pressures of as much as 400 psia to avoid the problem of chuffing or hangfires.[7] On the basis of tests using sealed igniters, a triple thickness of heavy duty aluminum foil was selected.

Using a nozzle closure and a 0.0937 inch diameter exit throat, average total igniter duration was approximately 150 msec., including the time from electric match initiation to completion of igniter pressure decay. Average igniter chamber equilibrium pressure was 400 psia. Average flow rate for the steady state portion of the igniter response was 0.022 lb. per second.

B. Solid Propellant Motor

Two grain configurations were developed for this study, the circular grain and the star shape grain. Both grain configurations were produced and fired with propellant grain lengths of 3.5, 7.625, and 9.5 inches. The composite propellant used was a 20% polybutadiene-acrylic acid binder with 80% bimodal ammonium perchlorate. This is designated as PBAA-80BM. This is the same propellant used in the two dimensional motor work.[1,3,4] The composition of PBAA-80BM is given in Table II. The burning rate curve is shown in Figure 8. The propellant grains were cast in disposable phenolic shells. The propellant was made in the Princeton Solid Propellant Processing Laboratory using techniques reported in Reference 8.

1. Circular Grain

The original objective of the circular grain design was the duplication of selected parameters of the two dimensional motor with the flat slab grain: chamber volume, propellant length, and propellant composition. The basic circular grain therefore had a propellant grain length of 9.5 in. and a port area of 0.624 $in.^2$, with a port diameter of 0.891 in. and a web-thickness of 0.179 in. Circular grains were also made in 3.5 in. and 7.625 in. lengths. The weight of the propellant for the 3.5, 7.625, and 9.5 inch motors was

55, 120, and 150 grams respectively. The propellant port surface was smooth in appearance. Average motor firing duration was approximately one second. Figure 9 is a photograph of a phenolic shell, a teflon mandrel, and the teflon mold pieces. Figure 10 shows a circular motor prior to removal of the mandrel and mold pieces along with two cured circular motors.

The ends of the motor were inhibited with washers cast with RTV (Room Temperature Vulcanizing) silicone rubber. Figure 11 shows an RTV washer and the required mold parts. The washers were cemented to the ends of the propellant grain using silicone rubber cement.

Although the circular motor has a progressive burning response, for the short duration of the ignition transient the exposed propellant surface was assumed constant.

2. Star Shape Grain

The objective of the star-shape development was to make the design compatible with the existing materials and equipment used with the circular grain motors. A procedure developed by Stone[9] was used to design a neutral burning six-pointed star having a port area of 0.331 $in.^2$ The star mandrel was machined from aluminum bar stock and teflon coated. Figure 12 shows a mandrel and a cured star shape motor. The propellant used for the 3.5, 7.625, and 9.5 inch star shape motors weighed approximately 82, 180, and 220 grams respectively. Both ends of the star shape grain were inhibited with a layer of epoxy cement. Rubber O-ring seals were used to provide a gas-tight seal with adjacent hardware.

C. Hardware Description

The hardware discussed below is shown in Figures 2 and 3. Copper was used for the igniter adapter section, the aft section assembly, and all nozzles. Stainless steel was used for the igniter assembly and motor housings. The assembled rocket was hydrostatically tested to 1650 psia and certified for working pressures up to 1000 psia.

1. Igniter Assembly

The purpose of the igniter assembly was to house the solid pyrogen igniter grain and provide for the mounting of a pressure transducer and a Conax sealing gland used with the electric match. Protection against overpressurization was provided by a stainless steel rupture disc incorporated into the igniter assembly.

2. Igniter and Motor Nozzles

The igniter and motor nozzles consisted of copper plates with a hole of the desired diameter and a rounded entrance region. Nozzle port dimensions were checked periodically throughout the program. Erosion of the motor nozzles was negligible. One igniter nozzle was used for all runs. During the course of the testing program, an increase in nozzle area of approximately 6% occurred. The original diameter was 0.09375 in. and the final diameter was 0.0969 in. No apparent effect on motor response was observed due to the small reduction of mass flow resulting from the igniter nozzle area increase.

3. Igniter Adapter

The igniter adapter section was to provide for the smooth expansion of the igniter gases from the igniter nozzle exit to the motor entrance. The slope of the sides of the expansion section was approximately 15^{o}. The purpose of this expansion section was to provide a full flowing diffuser and

avoid impingement of the igniter gas jet downstream of the propellant leading edge. It was recognized that separation would probably occur within the expansion section, but photographic observations of the igniter gas jet from the igniter adapter exit plane showed an apparent full flow condition. This suggests that, although the gas stream may have separated from the diffuser, it reattached itself before reaching the adapter exit plane. The stream entering the port of the rocket motor grain was therefore subsonic, but probably non-uniform as a result of the internal decelerating shocks. The pattern was probably fairly reproducible, although no direct tests were made of this point.

4. Motor Housing Assembly

The propellant grains were loaded into the motor housing assembly for the firing runs. The basic motor housing had an overall length of 10 in., and an internal diameter of 1.38 in. For the 3.5 in. and 7.625 in. propellant grains, the 4 in. motor housings used in earlier ignition studies[10,11,12] were used. The availability of the 4 in. motor housings determined the variations of the propellant grain length to be tested.

5. Aft Section Assembly

The purpose of the aft section assembly was to provide for the mounting of a pressure transducer to measure the combustion chamber pressure. A burst disc assembly was incorporated into the design to protect against dangerous overpressurization. The design of this section was essentially the same one used in References 10, 11, and 12, except that the transducer mounting was modified to accept a different pressure transducer from that used in the previous research.

D. Instrumentation

Igniter chamber pressure and motor chamber pressure were measured with the use of two Dynisco strain gauge type pressure transducers, Model PT76. These transducers have no provision for coolant flow, but can withstand short periods of heating when properly protected. The transducers were mounted on the igniter assembly and on the aft section assembly of the main chamber. See Figures 2 and 3 . Protection from the hot chamber gases was provided by RTV silicone rubber discs approximately 0.25 in. thick glued to the transducer head, a technique of transducer protection that was developed by Most[5]. The natural frequency of each transducer with the RTV plug in place was determined by shock tube tests, and it was found to be 20,450 cps. Reference to previous pressure transducer evaluation programs indicated that this would result in a flat $\pm 5\%$ amplitude versus frequency response out to approximately 8,000 cps. The manufacturer's specification for this model pressure transducer is 25,000 cps. It was concluded, therefore, that the accuracy of pressure measurement would be excellent for the frequencies associated with the ignition transient, and in fact, that the transducer frequency response capability would exceed that of the other instrumentation components.

Periodically throughout the motor firing program the transducers were calibrated using a hydraulic dead weight tester. They were also gas calibrated before and after a series of runs or when long delays occurred between runs. The gas calibration was obtained by pressurizing the assembled rocket motor with nitrogen gas, and by regulating the nitrogen pressure, readings of the transducer output signal were taken at 50 psi intervals from 0 psig to 1000 psig.

The 10-volt d.c. excitation signal was supplied to the pressure transducers by B & F Transducer Conditioning Modules. These units have a ripple level of less than 0.5 millivolts peak to peak.

The pressure signals were amplified by Dana D.C. Amplifiers. These are essentially zero impedance amplifiers. They were selected for their low noise-to-signal ratio of 4 microvolts RMS referenced to the wide band filter and a gain of 1000. They also feature a wide gain selection and internal filters with band pass widths ranging from wide band and 10 kc down to 0.01 kc.

After amplification the pressure signals were recorded simultaneously on a Honeywell Visicorder oscillograph, Model 1508, and a Honeywell Tape Recorder, Model 8100. The visicorder used galvanometers with a natural frequency of 1650 cps. The time required for the galvanometer to initially reach the desired value is approximately 0.4 msec. The damping resistors for each galvanometer were adjusted to give an optimum 7% overshoot response to a step change.

In order to obtain the desired millisecond resolution, the visicorder was operated at a speed of 60 inches of paper per second. A few runs were made at a speed of 120 inches of paper per second. At both speeds, 0.01 second timing marks were used.

The tape recorder was operated at a speed of 30 ips with a 10 kc band pass filter. This results in a low signal-to-noise ratio of 45 db. while retaining sufficiently high frequency response capabilities.

Primary data reduction was done from the original visicorder traces since these exhibited the lowest signal-to-noise ratio. The magnetic tapes are a permanent record of all runs and were used to playback each trace on a reduced time scale to permit rapid visualization of the entire run. For these reduced time scale playbacks it was necessary to use a 1 kc filter to keep the signal-to-noise ratio low.

Arrangement of the equipment on the instrumentation console is shown in Figure 13. A list of test apparatus and materials is included as Appendix B.

CHAPTER IV

EXPERIMENTAL RESULTS AND DISCUSSION

A total of 57 small solid propellant rocket motors were fired. Of the total number, 46 were circular and 11 were star shape grains. Firing runs were made with both designs using varying exit nozzle areas and propellant grain lengths of 3.5, 7.625, and 9.5 inches. A list of the several motor variations is included in Table III. The pressure traces in real time, t, for runs 54 and 84 are given respectively in Figures 14 and 15 . The results of runs 54 and 84 are representative of the data obtained for circular and star shape motors and are used throughout the discussion unless otherwise noted.

A. Comparison of Predicted and Experimental Results

The primary objective of this study was to determine the applicability of the ignition transient prediction theory to motors of practical configuration. In order to obtain predictions for the circular and star shape motors the computer program of di Lauro was used.[2] From the beginning, it was recognized that the computer program based on the slab motor model would probably not yield accurate predictions of circular and star shape motor response. The main difference was that the computer program was based on flat plate heat transfer and the rocket motors used in this project did not have flat plate propellant grains. The predictions were expected to serve as rough approximations which, when compared with the experimental data, would reveal areas in need of refinement or suggest effects not previously considered.

The computer input data were based, in part, on the experimental results in order to insert the proper values for the igniter characteristics and the combustion performance of the main propellant. The criterion used for the initiation of igniter cut-off was the measured combustion chamber pressure at which the igniter chamber pressure began to decay. When the predicted combustion chamber pressure reached the experimental value, a linear decay of igniter chamber pressure was introduced. Based on measured igniter performance, a decay period of 35 msec. was incorporated into the computer program. Characteristic velocity for the motor, C^*, was calculated using measured motor chamber pressure. The average value of C^* based on pressure measurements was 4170 ft/sec for circular motors and 4310 ft/sec for star shape motors. Theoretical C^* was 4397 ft/sec. Equations used for the calculation of experimental motor parameters are included in Appendix A. By using experimental data as computer input allowance was made for actual motor inefficiencies. If the computer prediction program could accurately characterize the ignition transient of circular and star shape motors, then the predictions based on measured performance parameters should approximate the experimental results. Large deviations would suggest possible errors in program formulation and/or in the assumed theoretical model for which the chamber filling equations were developed.

Comparison of computer predictions with experimental runs is included in Figures 16 and 17 . A large discrepancy in the flame spreading region and a lesser difference in the chamber filling interval are apparent. The discrepancy in the chamber filling region was greater with the 3.5 in. motors than with the 9.5 in. motors. With respect to the chamber filling

interval, if the actual C^* was less than the steady-state value as a result of the cooling off of the combustion product gases at motor parts that had not yet reached equilibrium, the rate of rise in that interval would be slower. In all cases, the predicted rate of pressure increase was more rapid throughout the ignition transient. Predicted overshoots were from 3% to 10% greater than measured. By comparing a circular motor run, Figure 16 , with a star shape motor run, Figure 17 , it can be observed that the rate of pressure rise is greater for the star shape motor. This is as expected since the port area of the star motor is about one half that of the circular motor while the igniter mass flow is approximately the same for both. Although the star shape motors consistently have more rapid ignition transients, the slow pressure buildup in the flame spreading interval persists and will be considered in detail later.

B. Delayed Ignition

During the testing program, a few cases of delayed ignition of the main motor grain were experienced. Delays of from 0.24 sec to 1.93 sec were obtained. Such "delay fires" were characterized by normal igniter actuation followed by a period of no observable pressure within the motor chamber and then motor ignition with a rapid ignition transient. This delayed ignition is unexplained by the theoretical model considered. Once the igniter terminates, there is no further hot gas flow and therefore no further heat transfer to the propellant. According to the ignition theory, the motor propellant should not ignite. Since the motor does eventually ignite, other reactions must have been initiated by the hot igniter gas flow. These reactions must

continue to function after igniter termination to raise the temperature of elements of the propellant to the critical temperature, causing ignition. The possible mechanisms involved in a "delay fire" were beyond the scope of the simple analysis underlying the computer program, and, although we note this phenomenon here, it will not be treated in this work. This additional heat generation may not be a strong factor in normal ignition when there is adequate heat transfer from the igniter gas, but obviously it serves to convert a non-ignition to an ignition with a delay.

C. Analysis of Experimental Flame Spreading

When compared to computer predictions, the experimental pressure traces display a much more gradual pressure rise during the initial part or flame spreading interval of the pressure transient. Three possible hypothetical reasons are offered in explanation of the slow pressure rise in the chamber. The three possibilities will be referred to as back flame spreading, back chamber filling, and cooling-off of the igniter gas.

1. Back Flame Spreading

If the igniter gas flow from the upstream igniter enters the port of the rocket motor in such a way that the hot gas jet strikes the propellant downstream of the leading edge, the area of most intense heat transfer would not be the leading edge. Ignition or first flame would occur downstream. If downstream ignition occurs, flame spreading would proceed simultaneously toward both the leading and trailing edges of the propellant grain. Flame spreading toward the leading edge is referred to as back flame spreading.

It is apparent that the back flame spreading, without benefit of a large hot gas flow upstream for heat transfer, would proceed at a slower rate than the downstream flame spreading. In a recent report issued by United Technology Center, dealing with ignition and flame propagation in solid propellant motors, downstream impingement of igniter gases and downstream ignition were observed.[13] The back flame spreading was reported to have a relatively constant rate while the downstream flame spreading rate accelerated. The overall flame spreading would therefore take longer than for the case of leading edge ignition. The slower overall flame spreading rate could contribute to the slow pressure rise measured during the flame spreading interval.

In order to determine if downstream ignition was occurring with the circular and star shape motors, a series of modified firing tests was performed. If first flame occurs near the leading edge, proper ignition would be disrupted by replacing the first section of the propellant with inert material. If ignition occurs downstream, no appreciable effect on normal ignition would be observed. By varying the amount of inert material or spacer placed upstream of the propellant leading edge, it was determined that first flame does occur near the leading edge and not downstream. "Delay fires" were caused using inert sections as short as one-half inch. Photographic observation of igniter gas flow showed that the igniter gases fill the exit port of the igniter adapter section with no apparent downstream impingement.

On the basis of the tests performed, it is concluded that back flame spreading is not a factor in the slow pressure rise measured during the flame spreading interval of the circular and star shape motors.

2. Back Chamber Filling

Use of the igniter adapter section for smooth expansion of the igniter gases introduces an additional amount of volume upstream of the motor combustion chamber. As flame spreading takes place, pressurization of the stagnant gases within this upstream volume may retard the pressure build up. Pressurization of the upstream stagnant volume is referred to as back chamber filling.

In order to test this hypothesis, firing runs were made in which the size of the volume upstream of the propellant grain was varied. The volume change was accomplished by using inert spacer sections with lengths of 1/2 in., 1 in., and 1 1/2 in. Figure 18 compares the results of tests performed with 3.5 in. motors using a 1/2 in. spacer, run 109, and a 1 1/2 in. spacer, run 110. From the test results, it is concluded that back chamber filling makes only a minor contribution to the slow rate of chamber pressure increase in the flame spreading interval and does not account for the large discrepancy between predicted and measured response.

3. Cooling-off of Igniter Gas

Although the leading edge of the propellant may be heated with the intensity predicted by the computer program and ignited properly, the remaining portion of the grain may be heated more slowly because of a cooling-off of the igniter gas axially down the grain. The downstream sections of the propellant may be exposed to lower temperature gas and would

therefore be heated to a lesser degree than the leading section. Combustion gases produced by the ignition of the upstream propellant must provide a greater amount of the total heat required to raise the temperature of the downstream propellant elements to the ignition point. The result would be a reduced rate of pressure increase. Support for this hypothesis is provided by the consideration of the combustion chamber exit temperatures calculated from chamber pressure measurements for inert motor grain firing runs. The calculated temperatures indicate a large temperature difference between the igniter and motor exits. The average temperature difference was approximately 720^{o} K. Similar temperature differences were measured by Most[5] for the slab motor.

Of the three possible causes of the slow experimental pressure rise in the flame spreading interval, the most probable explanation appears to be the cooling-off of the igniter gas.

D. Determination of the Completion of Flame Spreading

With the solution to the Bernoulli type differential equation developed in Chapter II, it was noted that $\ln\left[1 - P^{1-n}\right]^{-1}$ was proportional to time, τ. This relation can be shown to be linear only in the chamber filling interval with no igniter flow and with burning area, S, equal to unity. From a plot of the quantity $\ln\left[1 - P^{1-n}\right]^{-1}$ versus τ, the beginning of the chamber filling interval can be determined as the time at which the curve becomes linear. With this time, the pressure at completion of flame spreading can be determined from the plot of pressure, P, versus time, τ.

On plots of $\ln\left[1 - p^{1-n}\right]^{-1}$ versus τ for run 54, Figure 19 , and run 84, Figure 20 , it is shown that flame spreading is completed after 50% of equilibrium pressure is reached in the combustion chamber. In all instances of regular pressure transient response flame spreading was determined to be completed after the 50% pressure value. There were a few runs with irregular pressure transients. Some of the irregularities could be associated with "delay fires" while others had no apparent explanation.

The predictions developed by di Lauro[2] showed flame spreading to be complete well before the 50% pressure level. In many cases, the value was closer to 35%. UTC[13] determined that flame spreading was completed by the time 10% of equilibrium pressure was reached. The computer predictions obtained for the circular and star shape motors show the value to be approximately 25%. While these results suggest that attention should be focused on the chamber filling process in order to control the pressure rise curve, the results obtained for the motors of practical configuration presented in this report indicate that the flame spreading and the chamber filling intervals are of equal importance when considering control of the pressure rise of the ignition transient.

CHAPTER V

CONCLUSIONS AND RECOMMENDATIONS

The solid pyrogen igniter designed and developed for this report has proven to be a reliable research tool but it is somewhat less versatile than the gas torch igniter.[5] As a more basic transition from the slab motor to practical motor configurations, the testing of the circular and star shape motors using the gas torch igniter is recommended. By doing this, the additional problems introduced by the new type igniter, the solid pyrogen igniter, would be avoided and the effect of changes in motor configuration would be more readily observable.

While investigating the possible causes of the slow pressure rise during the flame spreading interval of the circular motors, it was determined that the forward section of the propellant was extremely important for successful ignition and reduced induction periods. It is concluded that no downstream impingement of the igniter gases on the motor grain occurs in the igniter-motor configurations used for the experimental runs and that initial ignition occurs within the first one-half inch of the propellant length. Back chamber filling could contribute to the slow pressure rise, but the effect would be small.

The greatest probable cause of the slow pressure rise in the flame spreading interval is the cooling-off of the igniter gas along the length of the combustion chamber. The heating of the aft portion of the propellant grain by the igniter gas is less intense than allowed for by the computer prediction program.

Flame spreading in the experimental circular and star shape motors is completed after 50% of combustion chamber equilibrium pressure is reached. The flame spreading and chamber filling processes should be treated as approximately equal in importance when considering ways of controlling the pressure rise during the ignition transient.

The prediction theory is believed fundamentally correct. Additional refinements and especially a better understanding of heat transfer effects are required to predict adequately the ignition transients of circular and star shape rocket motors. Heat transfer measurements for the circular and star shape motors are recommended in order that a better heat transfer correlation may be determined. As a first step in the refinement of the computer prediction program, modification of the program to incorporate a temperature gradient for the igniter gas flow in the combustion chamber is recommended.

REFERENCES

1. Summerfield, M., Parker, K. H., and Most, W. J., "The Ignition Transient in Solid Propellant Rocket Motors," Aerospace and Mechanical Science Report No. 769, Princeton University, Princeton, New Jersey, 10 February, 1966.

2. Di Lauro, G. F., "Theoretically Predicted Ignition Transients of Solid Propellant Rocket Engines," M.S.E. Thesis, Department of Aerospace and Mechanical Sciences, Princeton University, March 1967.

3. Parker, K. H., Most, W. J., and Summerfield, M., "The Ignition Transient in Solid Propellant Rocket Motors," AIAA Preprint No. 66-666, June 1966.

4. Parker, K. H., Wenograd, J., and Summerfield, M., "The Ignition Transient in Solid Propellant Rocket Motors," AIAA Preprint No. 64-126, January 1964.

5. Unpublished data, Guggenheim Laboratories, Princeton University, Princeton, New Jersey.

6. Waesche, R. H. W., and Summerfield, M., "Solid Propellant Combustion Instability: Oscillatory Burning of Solid Rocket Propellants," Aerospace and Mechanical Science Report No. 751, Princeton University, Princeton, New Jersey, August 1965.

7. Barrere, M., Jaumotte, A., Fraeijs de Veubeke, B., and Vandenkerckhove, J., Rocket Propulsion, Elsevier, Amsterdam, 1960.

8. Kurylko, L., "An Experimental Study of the Ignition of Solid Propellants," M.S.E. Thesis, Department of Aerospace and Mechanical Sciences, Princeton University, March 1967.

9. Stone, M. W., "A Practical Mathematical Approach to Grain Design," Jet Propulsion 26, No. 9, September 1956.

10. Grant, E. H., Jr., Lancaster, R. W., Wenograd, J., and Summerfield, M., "A Study of the Ignition of Solid Propellants in a Small Rocket Motor," AIAA Preprint No. 64-153, January 1964.

11. Grant, E. H., Jr., Wenograd, J., and Summerfield, M., "Research on Solid Propellant Ignitability and Igniter Characteristics," Aeronautical Engineering Report No. 662, Princeton University, Princeton, New Jersey, 31 October 1963.

12. Lancaster, R. W., and Summerfield, M., "Experimental Investigation of the Ignition Process of Solid Propellants in a Practical Motor Configuration," Aeronautical Engineering Report No. 548, Princeton University, Princeton, New Jersey, 3 May 1961.

REFERENCES

(Continued)

13. Jensen, G. E., Cose, D. A., Brown, R. S., MacLaren, R. O., Anderson, R., and Corcoran, W. J., "Studies in Ignition and Flame Propagation of Solid Propellants," Report No. UTC 2117-FR, United Technology Center, Sunnyvale, California, June 1966.

LIST OF SYMBOLS

Latin

a	distance between boundary layer leading edge and propellant grain leading edge
A_b	total exposed grain surface
A_p	main rocket port area
A_{ign}	igniter port area
A_t	main rocket nozzle throat area
$A_{t_{ign}}$	igniter nozzle throat area
C_p	specific heat of propellant gas products
C^*	characteristic velocity $\equiv \frac{\sqrt{RT_t}}{\Gamma}$
d_t	diameter of main rocket nozzle throat
$d_{t_{ign}}$	diameter of igniter nozzle throat
h	heat transfer coefficient
k	constant in burning rate law, $r_{ss} = k P_c^{\,n}$
l	length of propellant grain
L^*	characteristic length $\equiv \frac{V_c}{A_t}$
$\dot{m}_b$	mass burning rate
m_c	mass of gas in combustion chamber
m_{eq}	mass of gas in combustion chamber at equilibrium
$\dot{m}_{ign}$	mass flow rate from igniter
$\dot{m}_n$	mass flow rate through main rocket nozzle
$\mathfrak{M}$	molecular weight
n	exponent in burning rate law, $r_{ss} = k P_c^{\,n}$

LIST OF SYMBOLS (continued)

Latin

$N_{u_{(a+x)}}$	Nusselt number $\equiv \left[\frac{h(a+x)}{\lambda_g}\right]$
P	dimensionless chamber pressure $\equiv \frac{P_c}{P_{eq}}$
P_c	chamber pressure
$P_{c_{ign}}$	igniter chamber pressure
P_{eq}	chamber pressure at equilibrium
P_I	initial chamber pressure
P_{ign}	dimensionless igniter chamber pressure $\equiv \frac{P_{c_{ign}}}{P_{eq}}$
Q_s	heat flux to propellant surface
r_{ss}	quasi-steady burning rate
R	specific gas constant
$R_{e_{(a+x)}}$	Reynolds number based on a + x; $\equiv \left(\frac{\rho_g u x}{\mu_g}\right)$
S	dimensionless burning area $\equiv \frac{S_b}{A_b}$
S_b	instantaneous burning area
t	time
t^*	characteristic time $\equiv \frac{L^*}{\Gamma^2 C^*}$
T	dimensionless chamber temperature $\equiv \frac{T_c}{T_f}$
T_c	chamber temperature
$T_{c_{ign}}$	temperature of igniter gas
T_f	flame temperature
T_{IG}	ignition temperature of propellant
T_{ign}	dimensionless igniter gas temperature $\equiv \frac{T_{c_{ign}}}{T_f}$
T_o	initial temperature of propellant

LIST OF SYMBOLS (continued)

Latin

T_s	surface temperature of propellant
u	gas velocity
V_c	chamber volume
w	web thickness
x	axial distance

Greek

α_p	thermal diffusivity of propellant
γ	ratio of specific heats
Γ	a function of γ ; $\equiv \sqrt{\gamma \left(\frac{2}{\gamma-1}\right)^{\frac{\gamma+1}{\gamma-1}}}$
λ_g	thermal conductivity of chamber gases
λ_p	thermal conductivity of propellant
μ_g	viscosity of chamber gases
ρ_g	density of chamber gases
ρ_p	density of propellant
τ	dimensionless time $\equiv {}^{t}/_{t^*}$
τ_{IND}	induction time of rocket motor

TABLE I

COMPOSITION OF PLASTISOL

Component	% by Weight
TEGDN	43.3
Ball Powder "A"	21.5
AP (5μ)	11.6
AP (45μ)	23.6
	100.0

TABLE II

COMPOSITION OF PBAA - 80BM

Component	% by Weight
PBAA	17
EPON 828	3
AP (15μ)	24
AP (180μ)	56
	100

TABLE III

INDEX OF EXPERIMENTAL ROCKET MOTOR VARIATIONS

Note: Runs 98 through 114 are not listed below. These were diagnostic runs for which grain lengths and/or chamber volumes were varied from the basic motor combinations listed.

a. Circular Grain

l(in.)	$A_p(in^2)$	$A_t(in^2)$	Run
9.5	0.624	0.1415	37,38,39,42,43 86,88,90,91
		0.1060	36,54,55,79,80 81
7.625	0.624	0.1415	48,52,68,74
		0.1060	49,75
3.5	0.624	0.0730	51,76,82,83,96,97
		0.0491	53,77
		0.0431	50,78

b. Star Shape Grain

9.5	0.331	0.1415	69,70
		0.1060	84
7.625	0.331	0.1415	71,72,85
		0.1060	73
3.5	0.331	0.1415	92
		0.0730	95
		0.0491	93
		0.0431	94

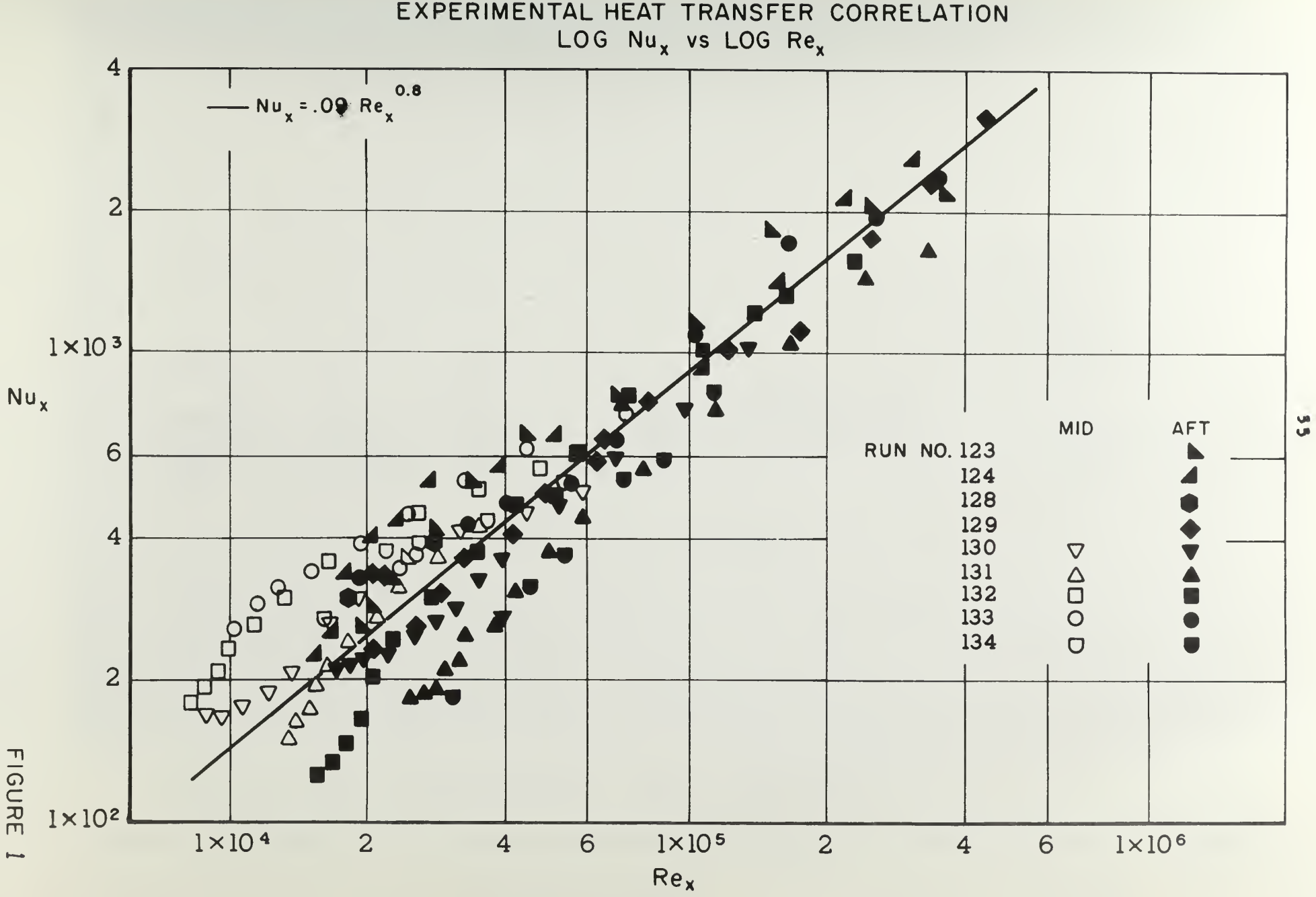
EXPERIMENTAL HEAT TRANSFER CORRELATION
LOG Nu_x vs LOG Re_x
$Nu_x = .029\ Re_x^{0.8}$
Nu_x
Re_x
4
2
1×10^3
6
4
2
1×10^2
1×10^4
2
4
6
1×10^5
2
4
6
1×10^6
MID
AFT
RUN NO. 123
124
128
129
130
131
132
133
134

FIGURE 1

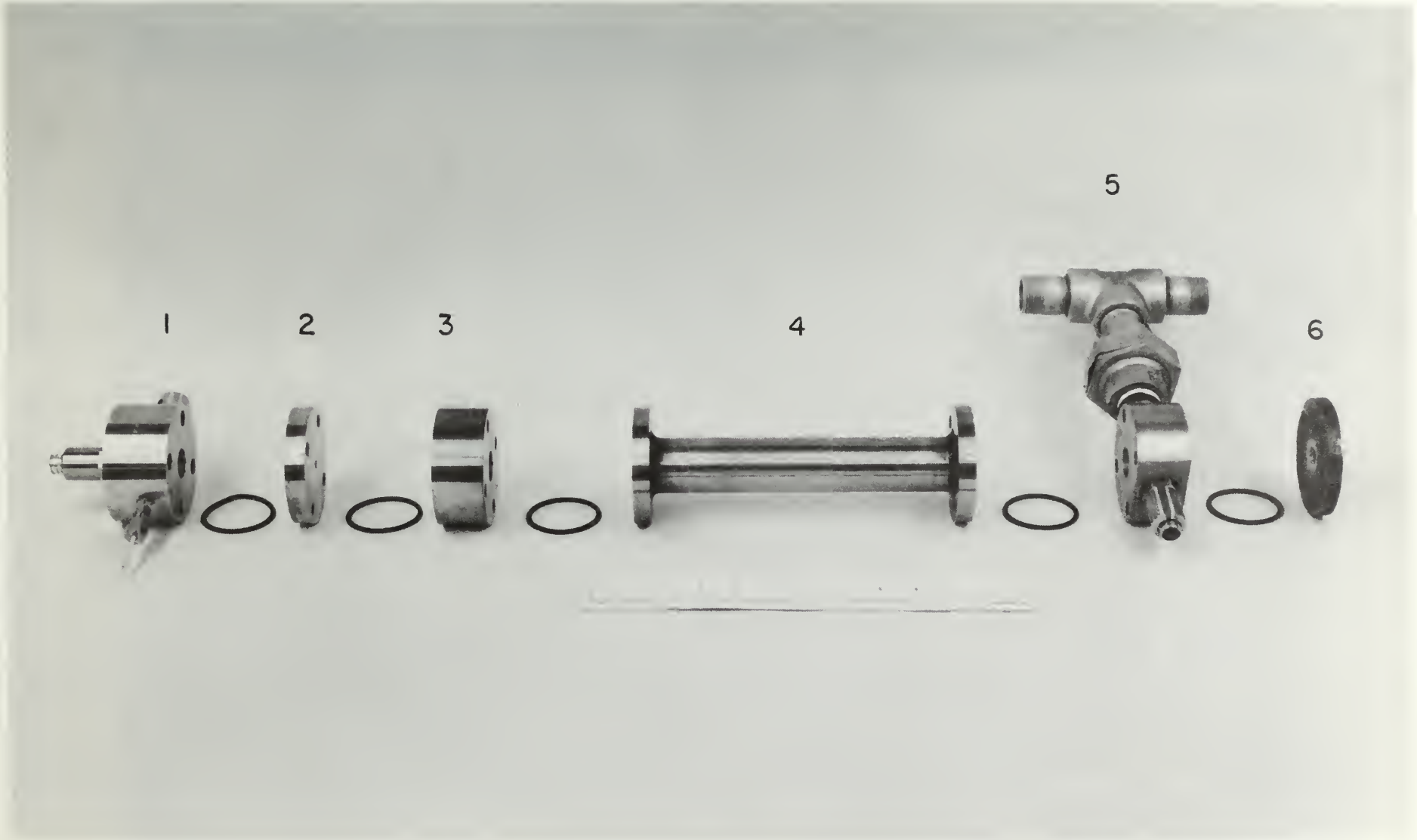

FIGURE 2

EXPLODED VIEW OF EXPERIMENTAL ROCKET MOTOR

1. IGNITER ASSEMBLY
2. IGNITER NOZZLE
3. IGNITER ADAPTER SECTION
4. MOTOR HOUSING
5. AFT SECTION ASSEMBLY
6. MOTOR NOZZLE

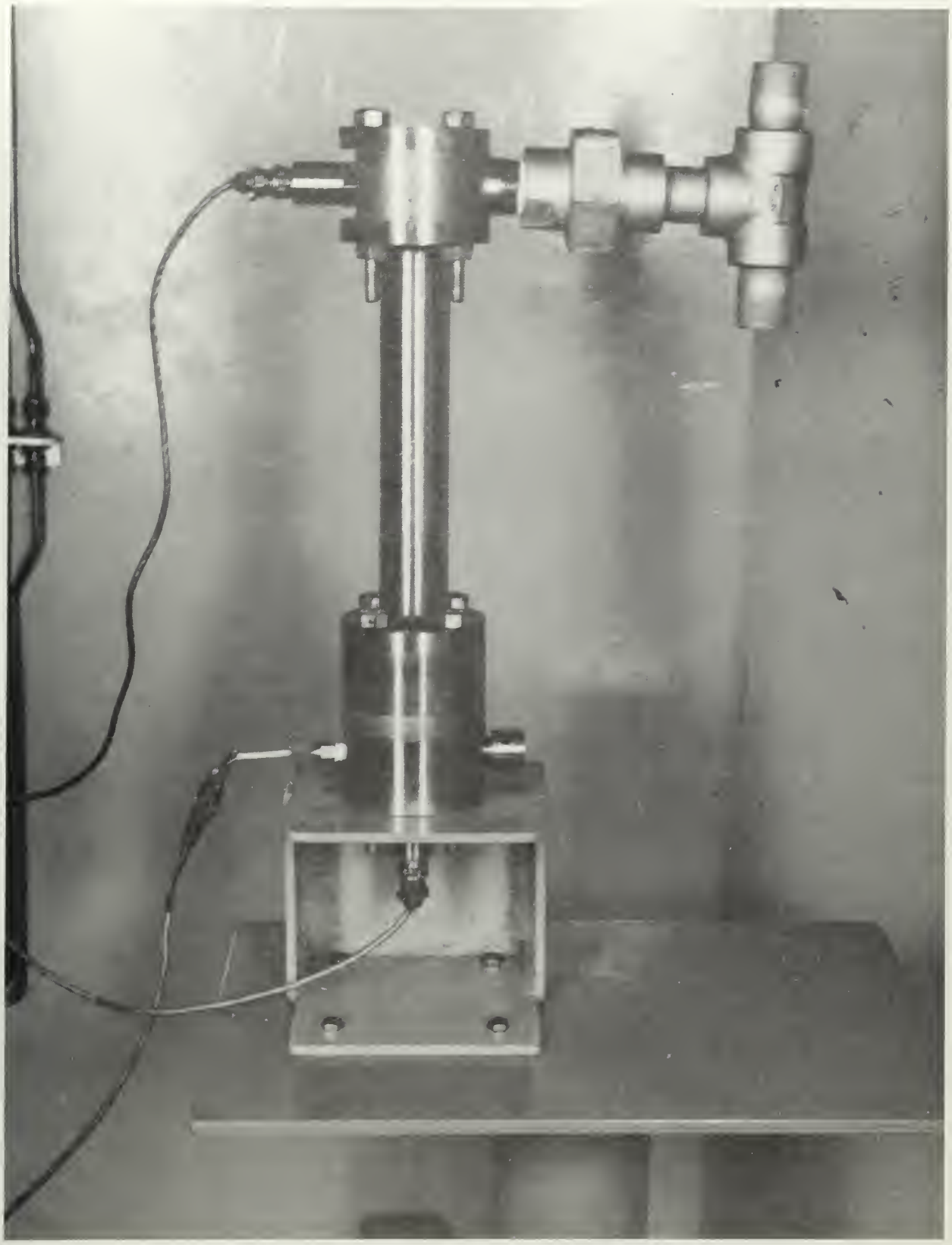

EXPERIMENTAL ROCKET MOTOR ASSEMBLED
ON TEST STAND

FIGURE 3

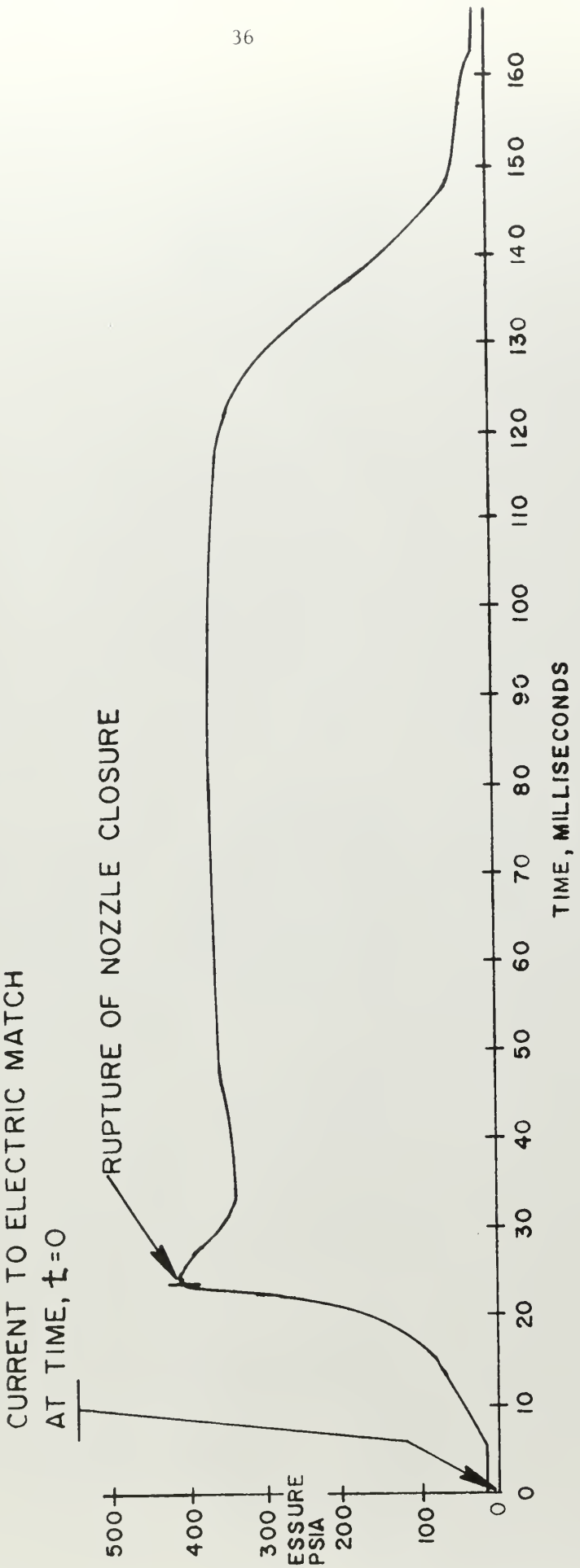

TYPICAL IGNITER CHAMBER PRESSURE RESPONSE OF EXPERIMENTAL SOLID PYROGEN IGNITER

FIGURE 4

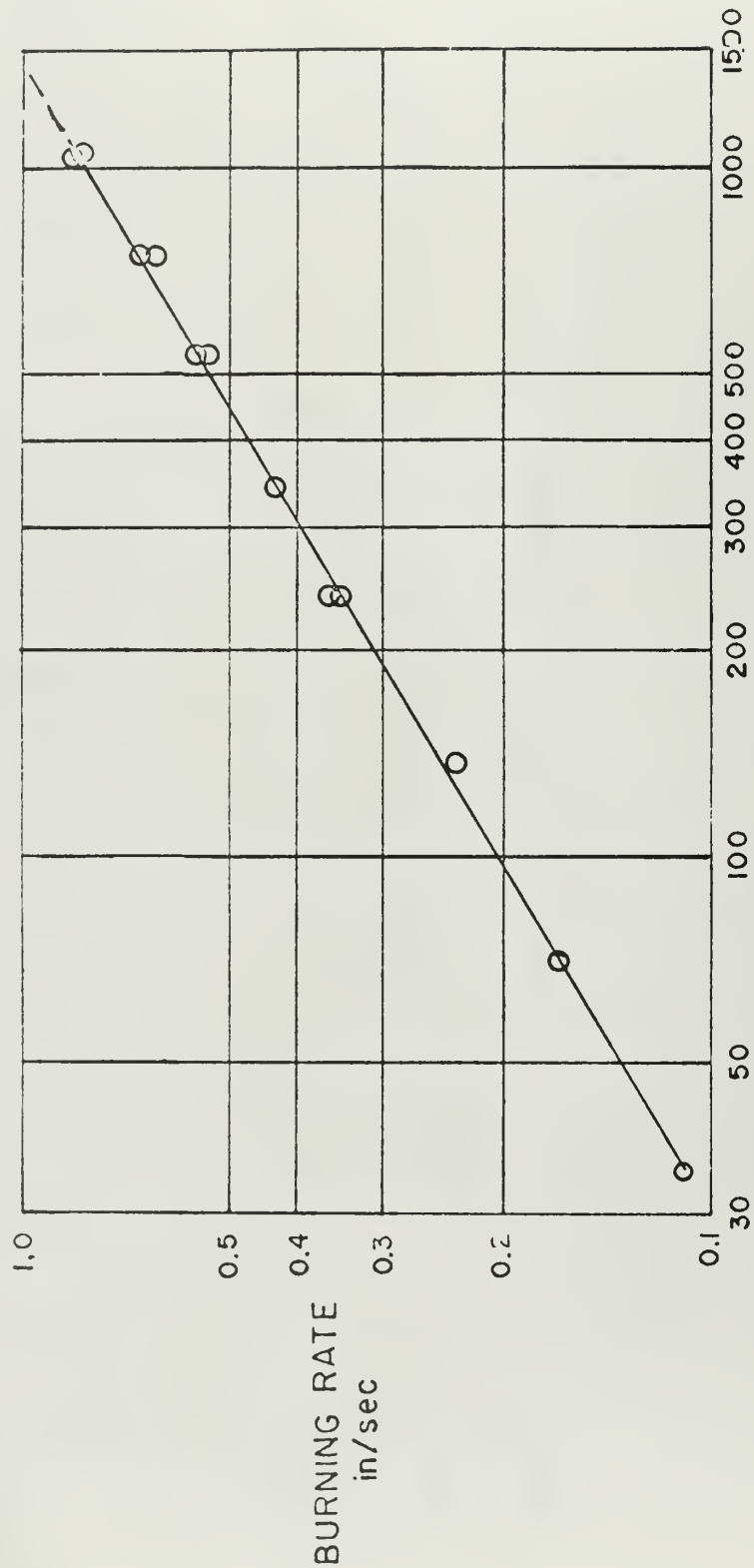

BURNING RATE CURVE FOR PLASTISOL PROPELLANT

FIGURE 5

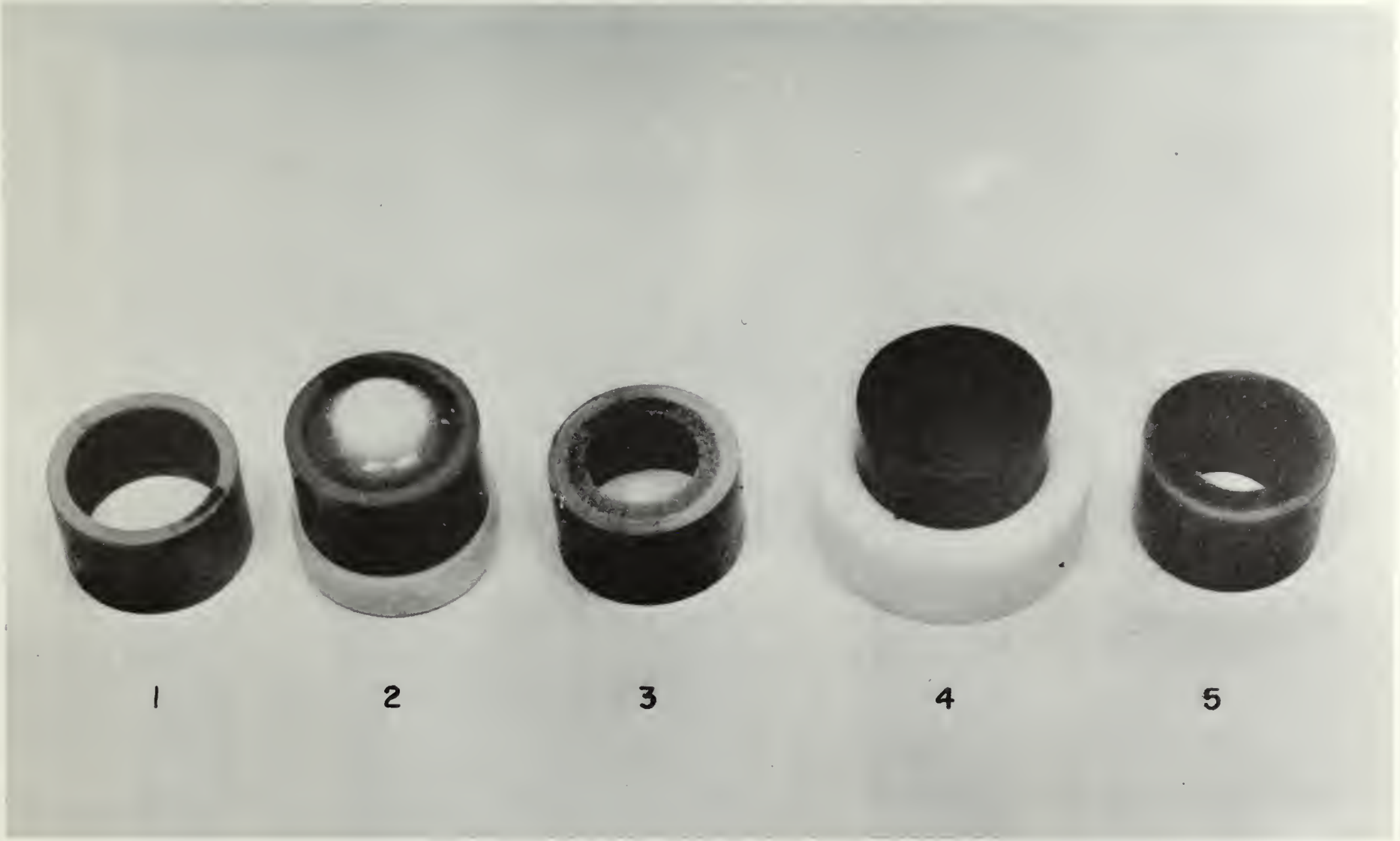

FIGURE 6

STAGES IN PREPARATION OF SOLID PYROGEN IGNITER GRAIN

1. IGNITER PHENOLIC SHELL
2. CASTING OF INERT TAPERED INSERT
3. TAPERED SECTION AFTER MACHING
4. CASTING OF PLASTISOL PROPELLANT
5. COMPLETED IGNITER GRAIN

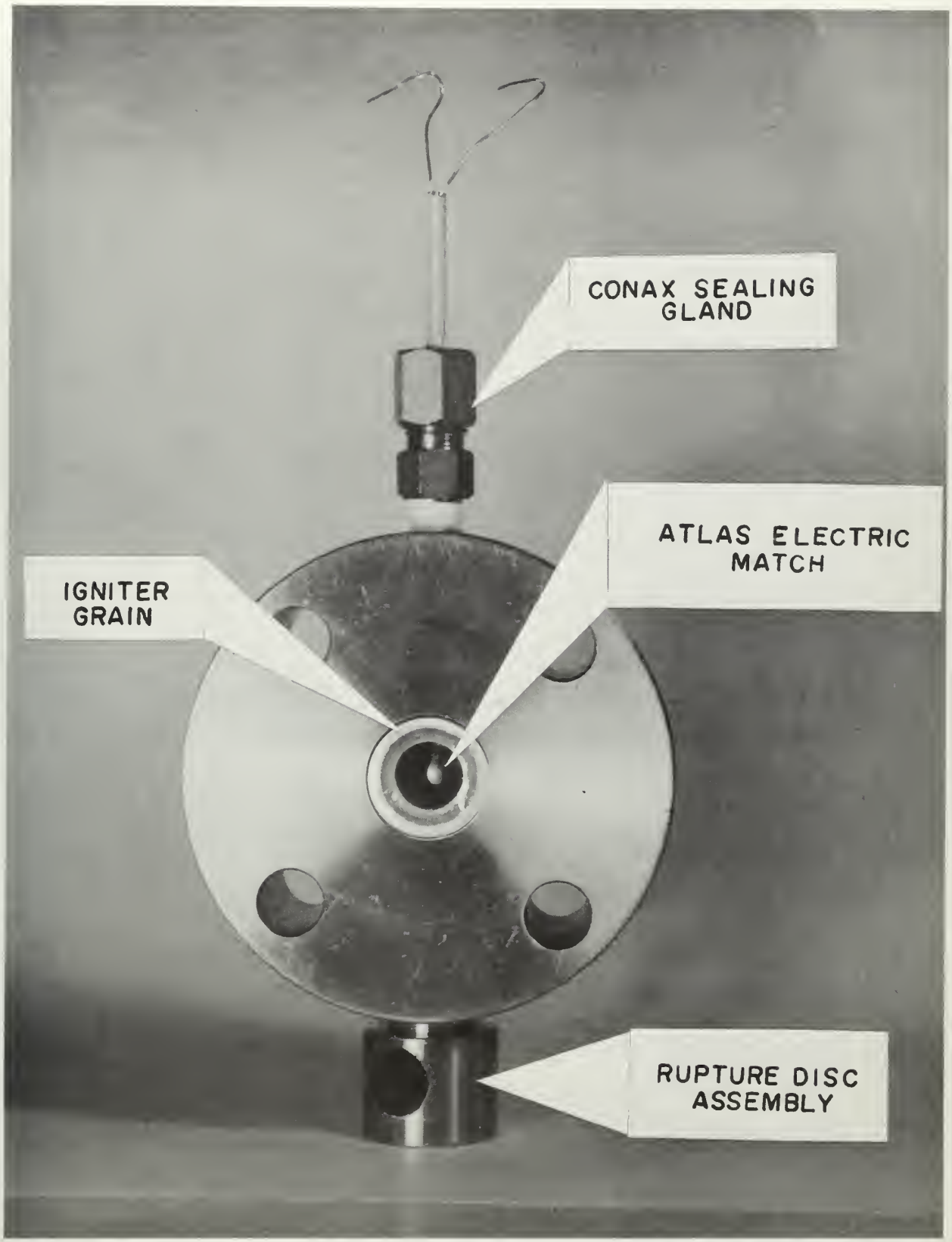

ASSEMBLED EXPERIMENTAL SOLID PYROGEN IGNITER

FIGURE 7

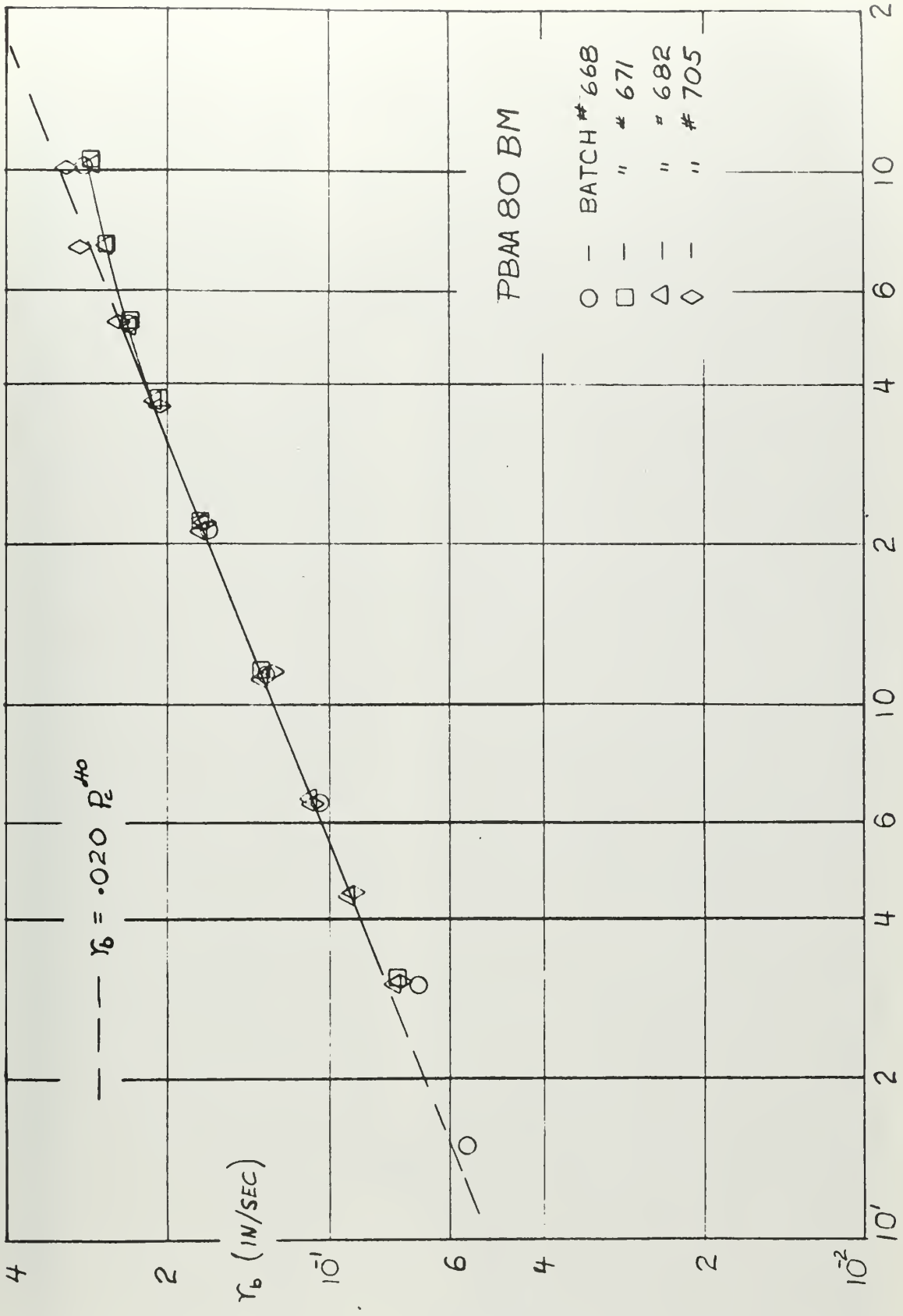

BURNING RATE CURVE OF PBAA 80 BM

FIGURE 8

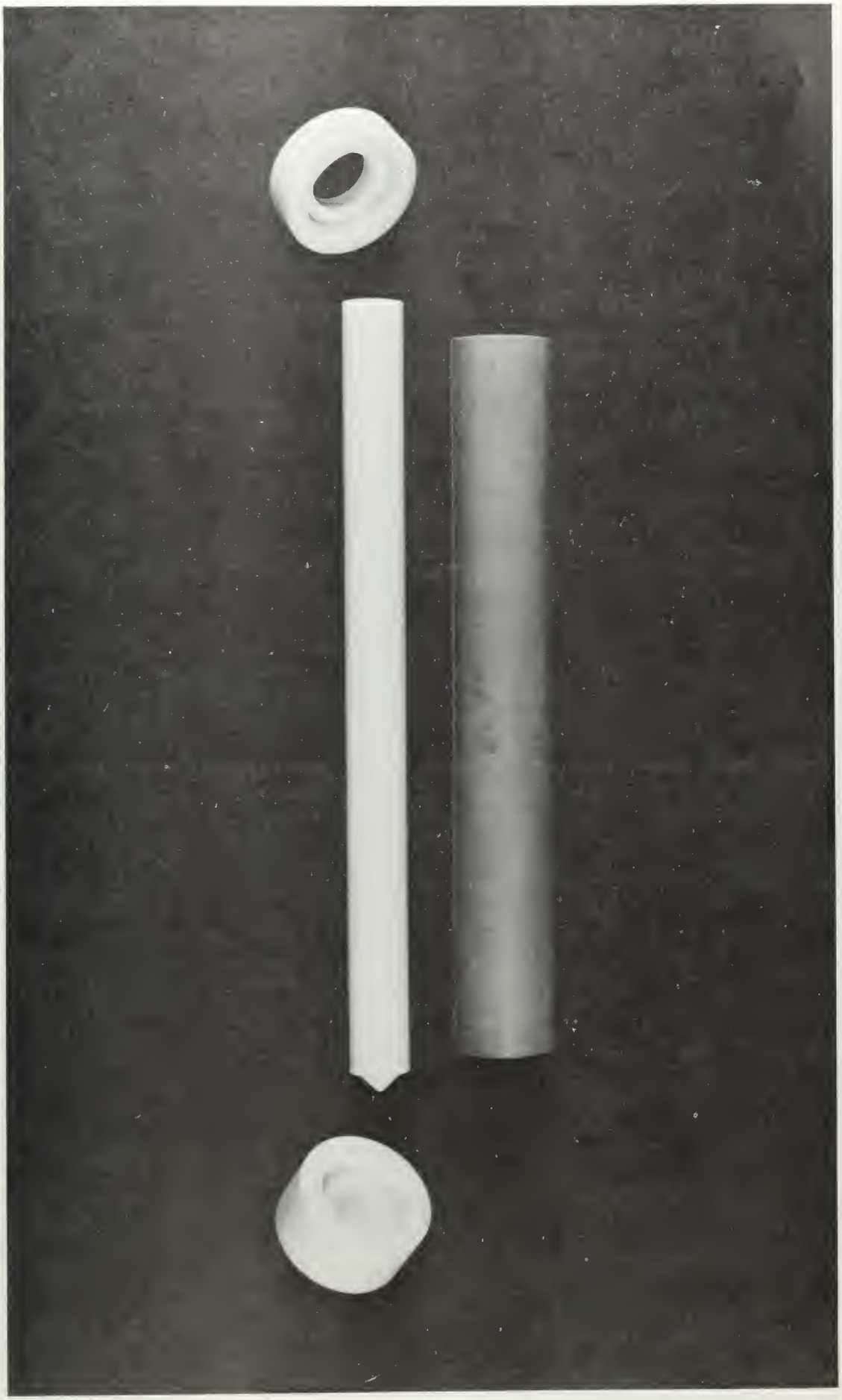

EXPLODED VIEW OF A SOLID PROPELLANT ROCKET MOTOR MOLD WITH PHENOLIC SHELL

FIGURE 9

CIRCULAR GRAINS AND MOLD FOR EXPERIMENTAL ROCKET MOTOR

FIGURE 10

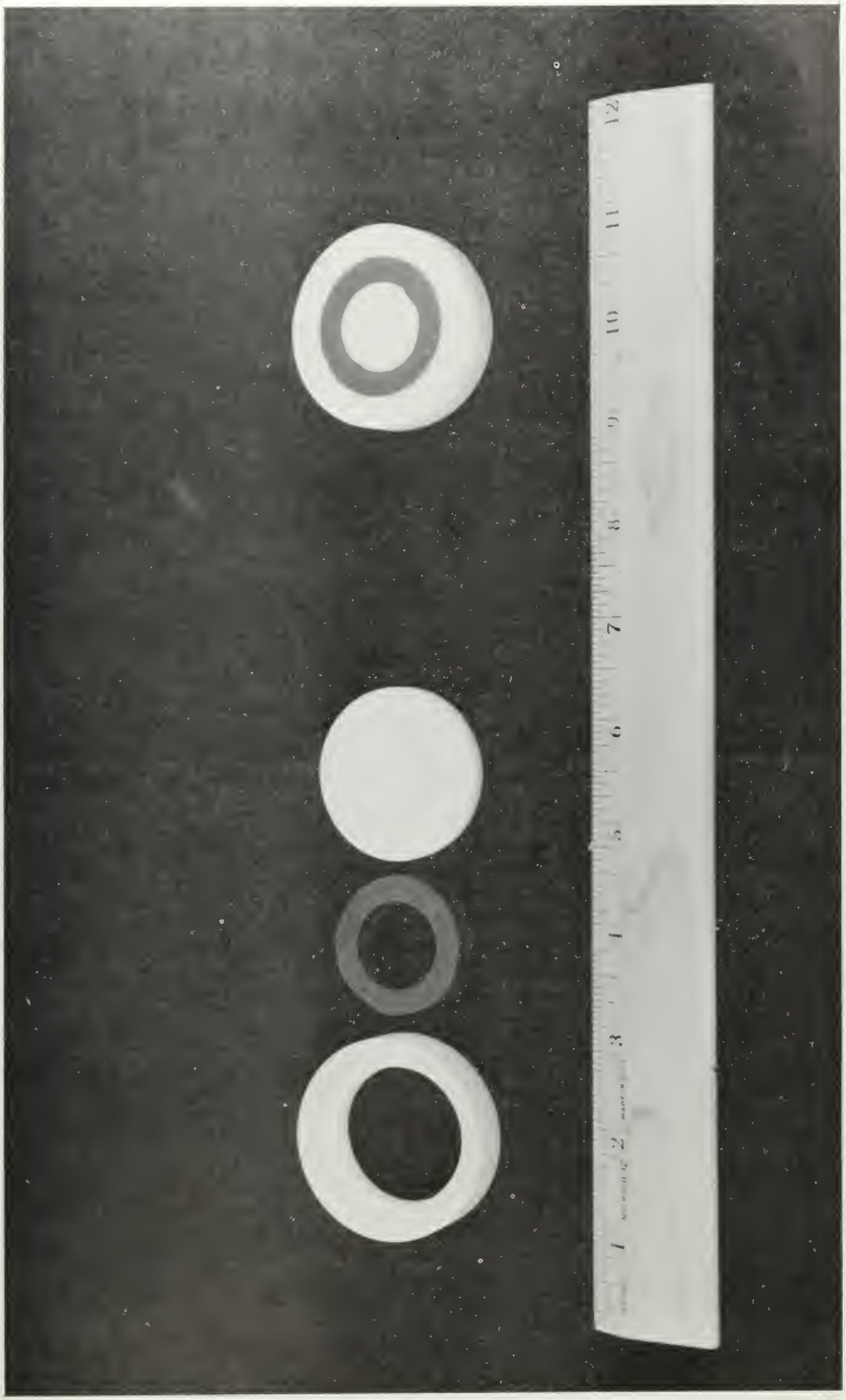

EXPERIMENTAL ROCKET MOTOR INHIBITOR WASHERS AND MOLDS

FIGURE 11

STAR SHAPE GRAIN AND MANDREL FOR EXPERIMENTAL ROCKET MOTOR

FIGURE 12

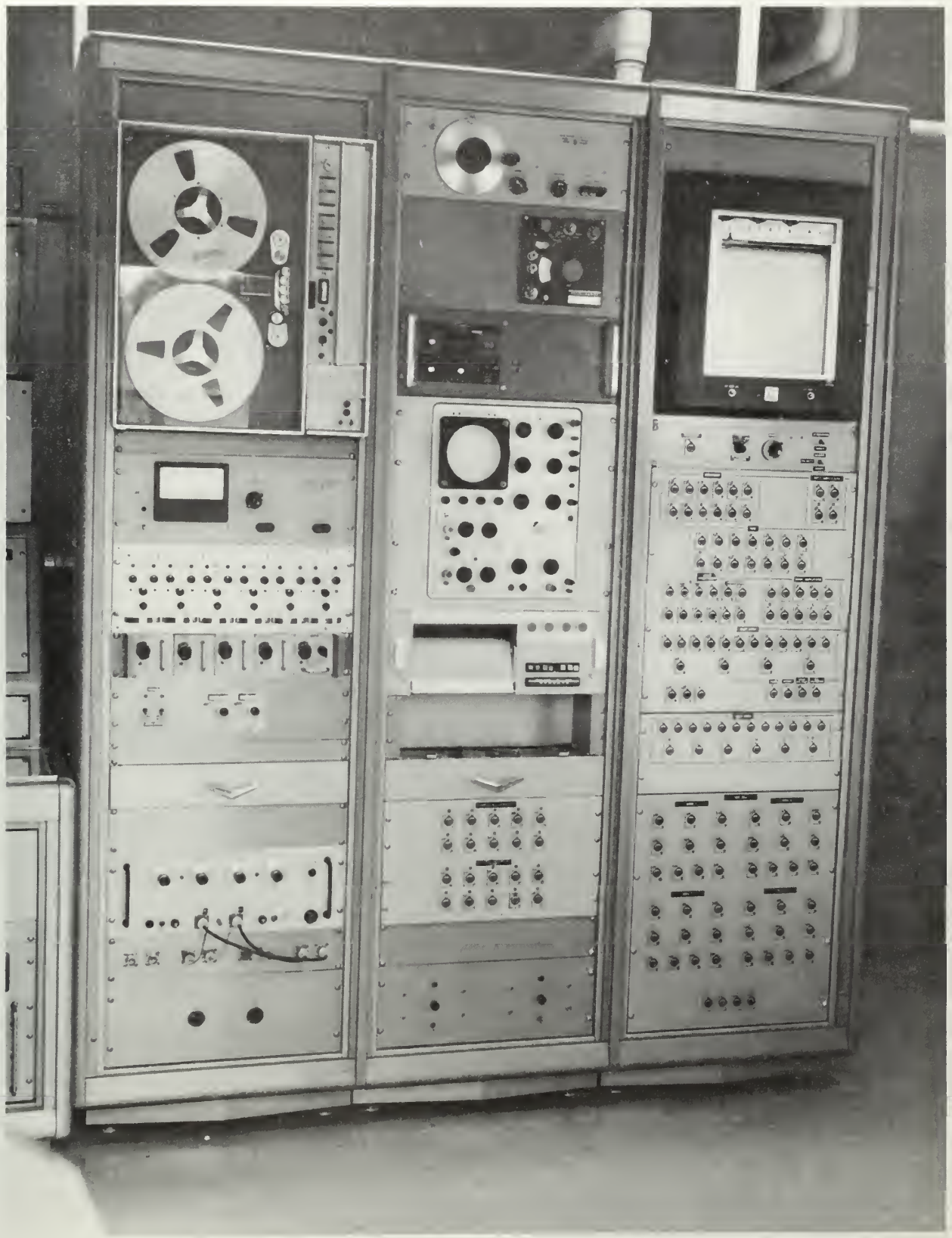

INSTRUMENTATION CONSOLE

FIGURE 13

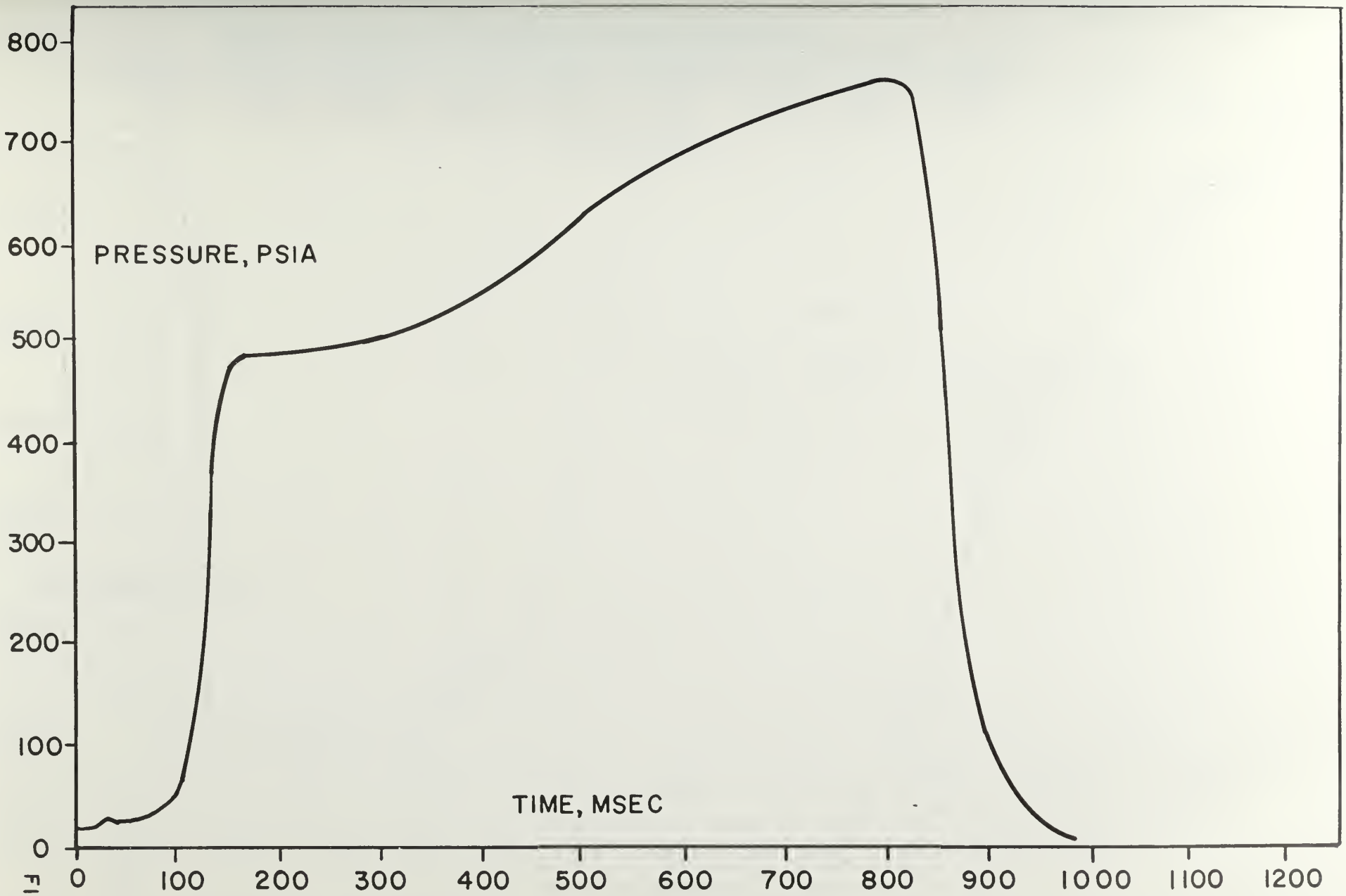

FIGURE 14

TYPICAL CHAMBER PRESSURE TRACE FOR EXPERIMENTAL CIRCULAR GRAIN SOLID PROPELLANT ROCKET MOTOR; RUN NO. 54

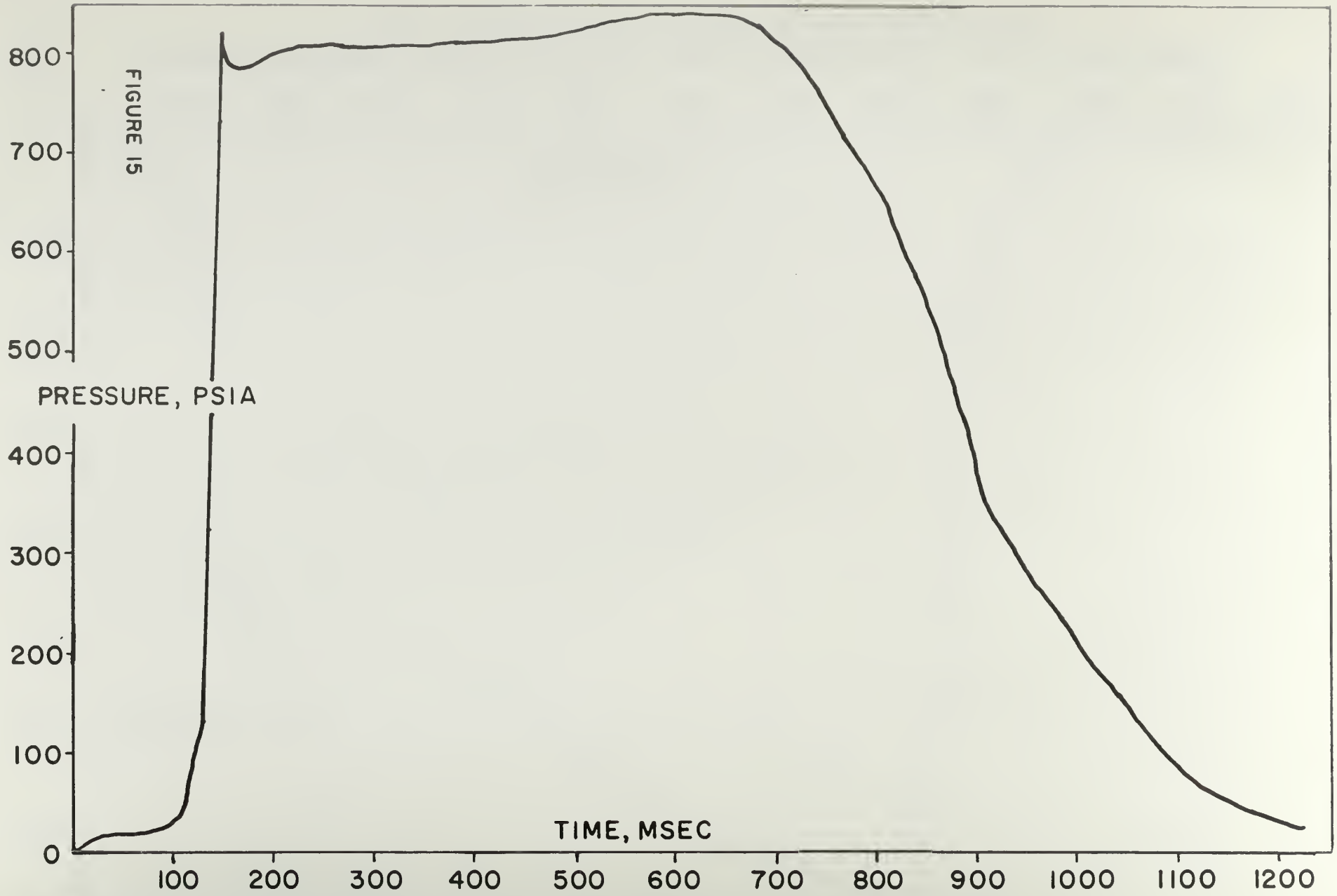

TYPICAL CHAMBER PRESSURE TRACE FOR EXPERIMENTAL STAR SHAPE GRAIN SOLID PROPELLANT ROCKET MOTOR; RUN NO. 84

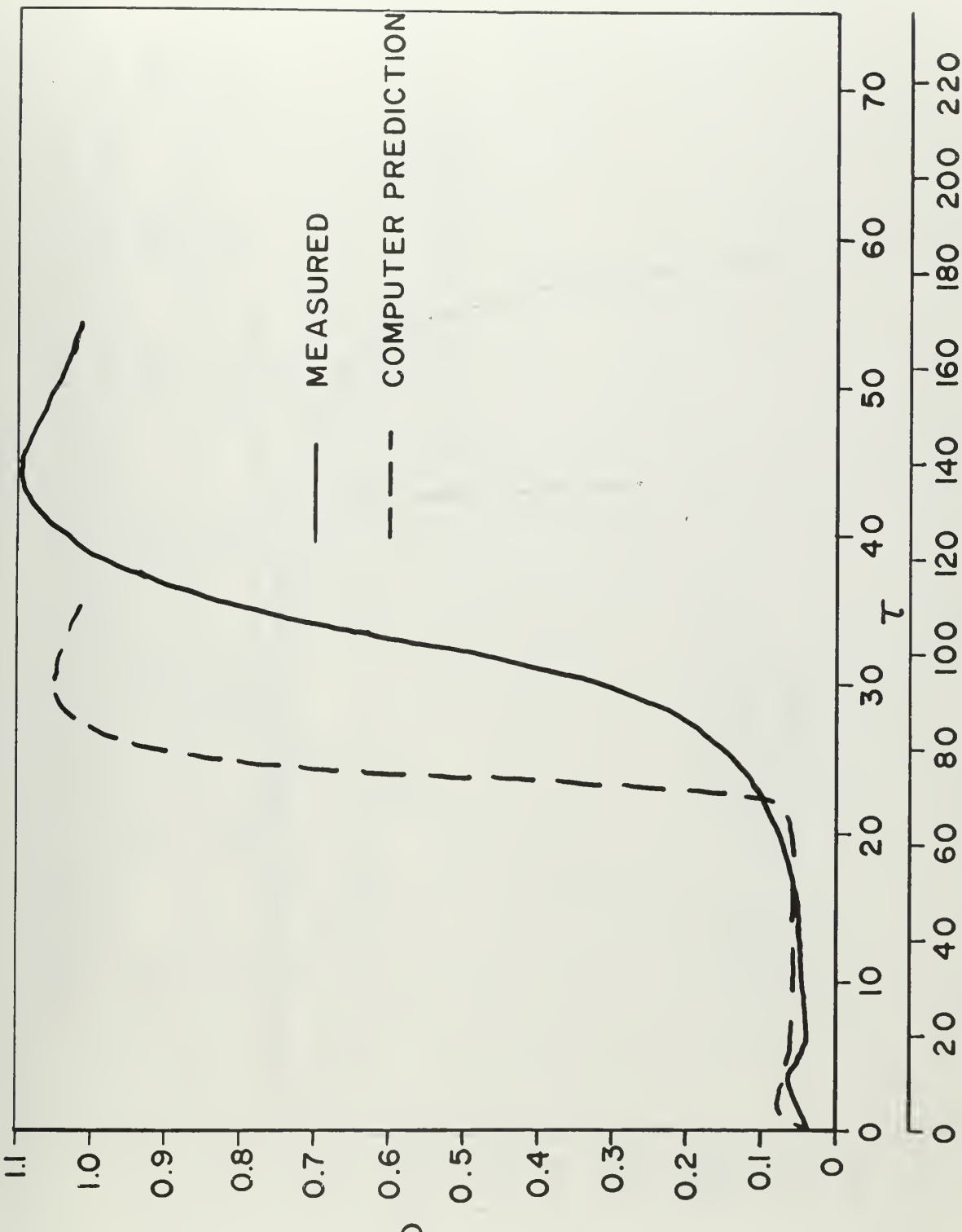

COMPARISON OF COMPUTER PREDICTION AND MEASURED PRESSURE TRACE FOR A TYPICAL CIRCULAR GRAIN ROCKET MOTOR; RUN NO. 54

FIGURE 16

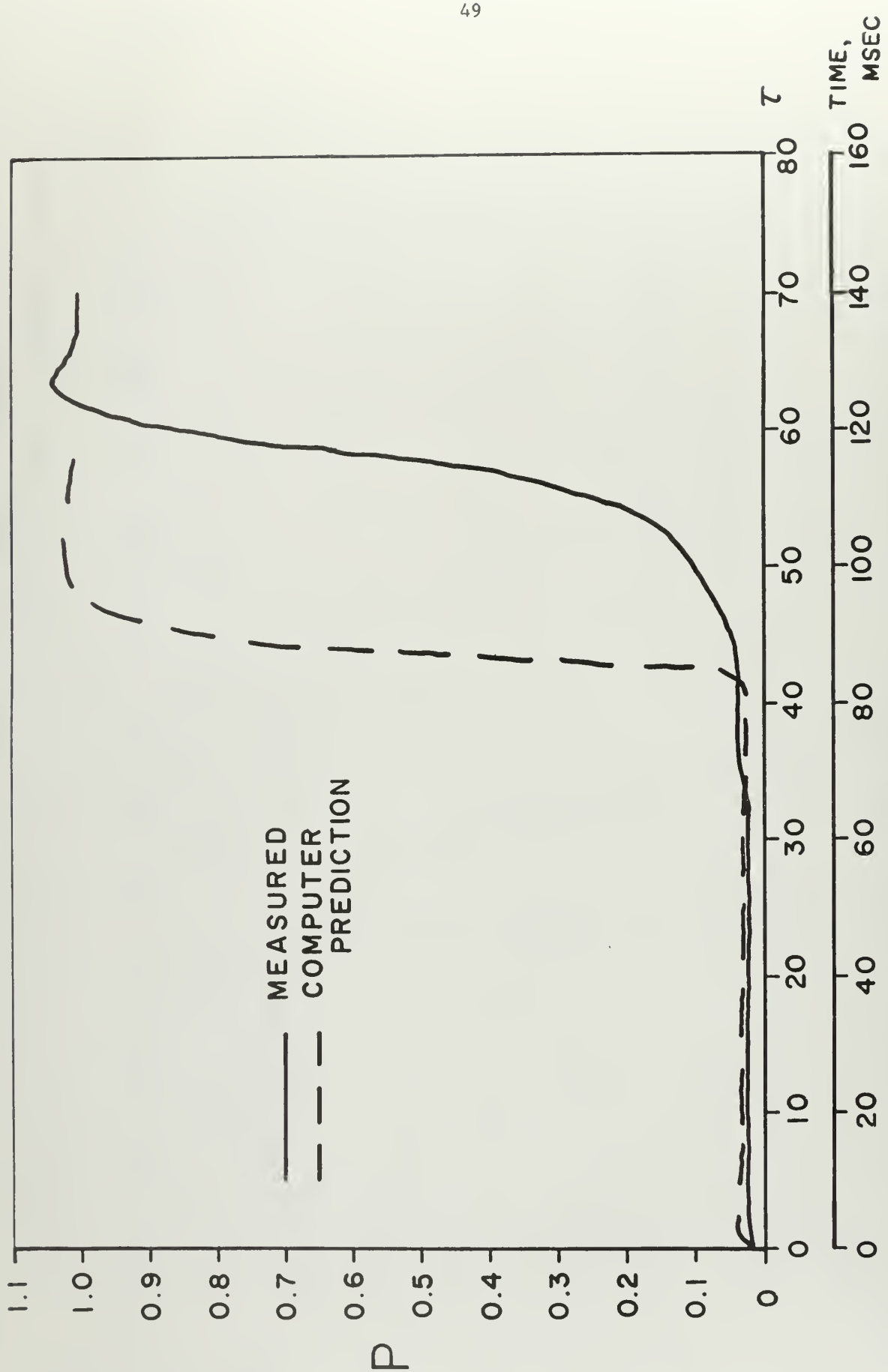

COMPARISON OF COMPUTER PREDICTION AND MEASURED PRESSURE TRACE FOR A TYPICAL STAR SHAPE GRAIN ROCKET MOTOR; RUN NO. 84

FIGURE 17

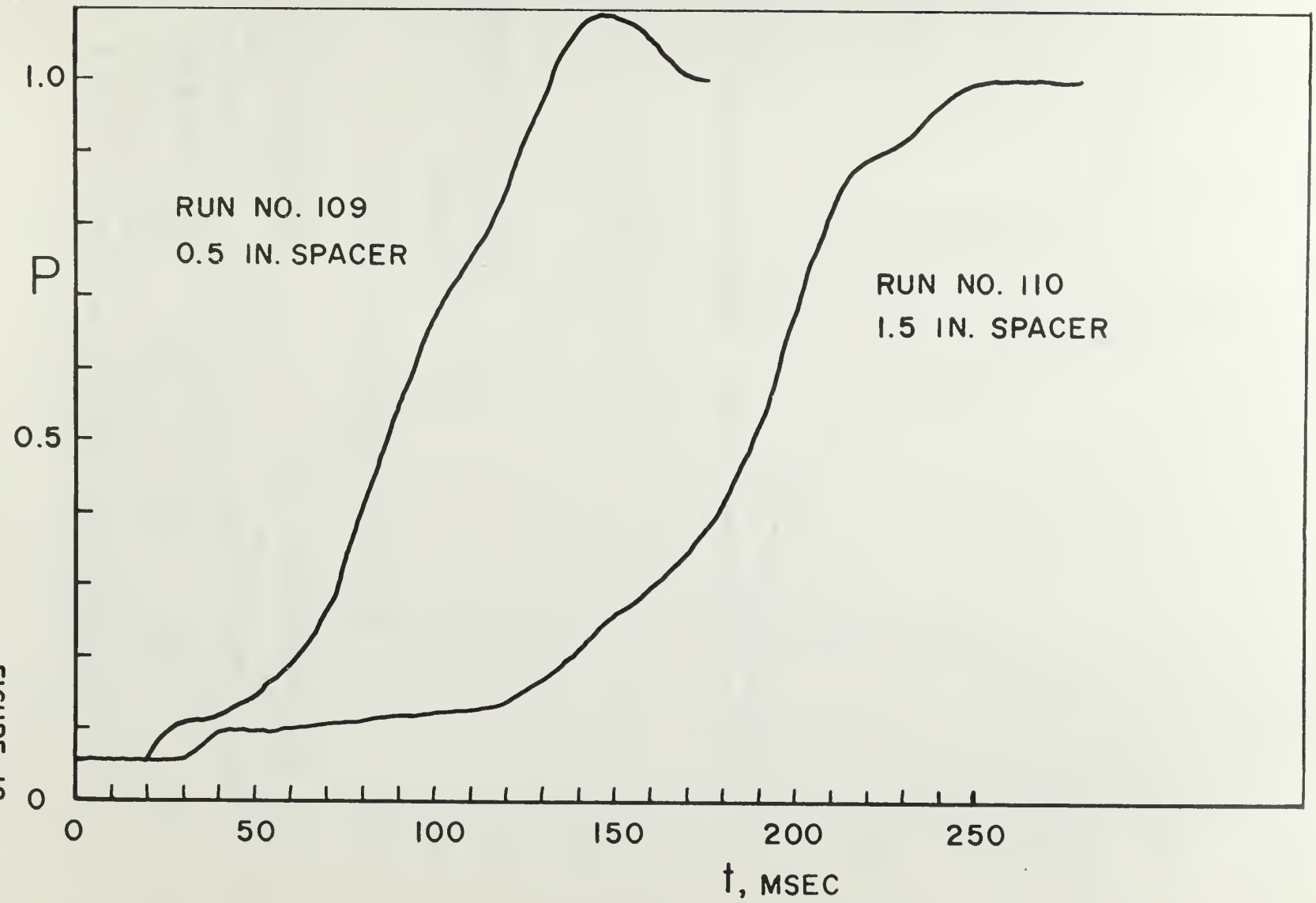

FIGURE 18

PLOT OF RESULTS OF BACK CHAMBER FILLING TESTS;
RUNS 109 AND 110

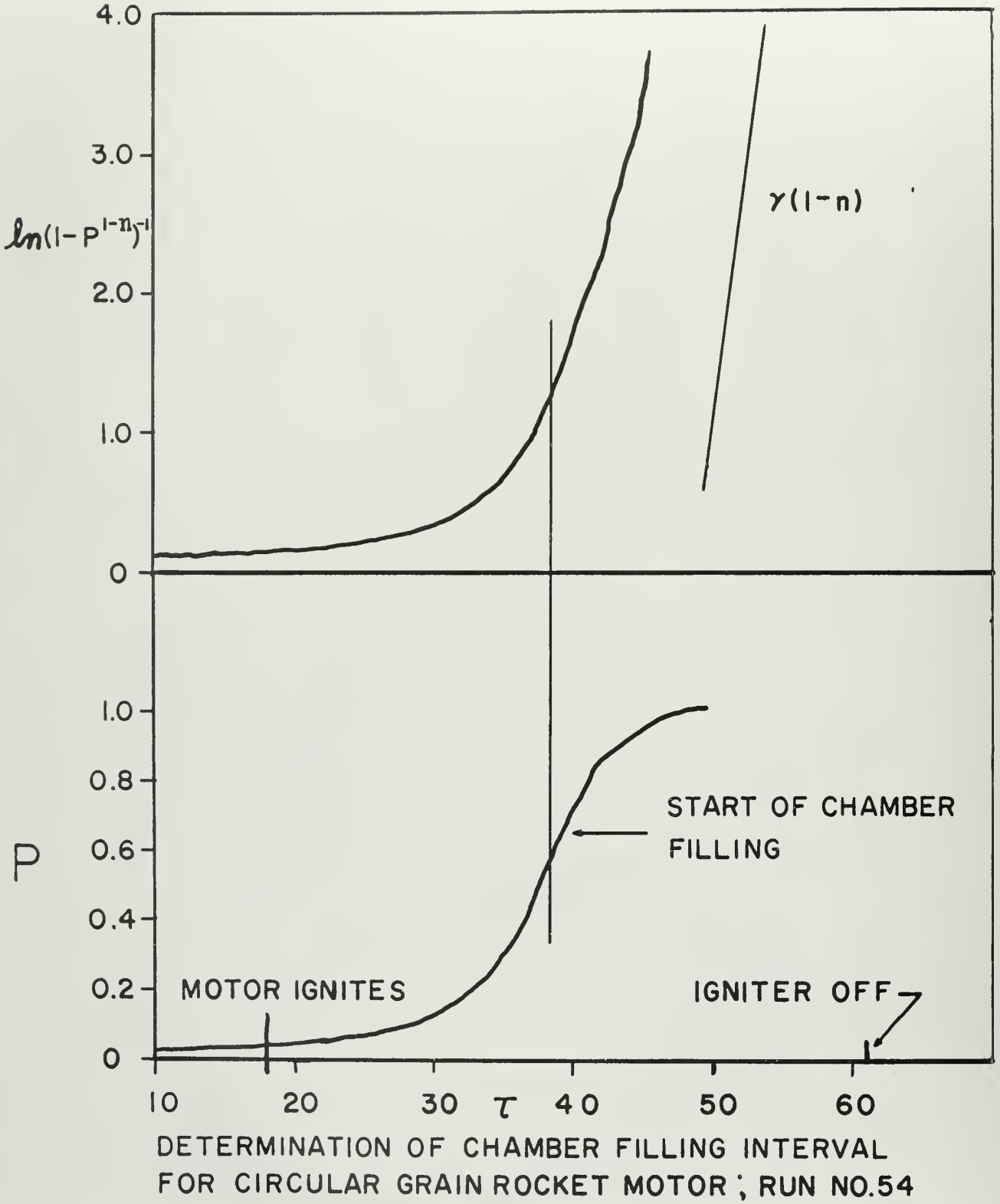

DETERMINATION OF CHAMBER FILLING INTERVAL FOR CIRCULAR GRAIN ROCKET MOTOR; RUN NO.54

FIGURE 19

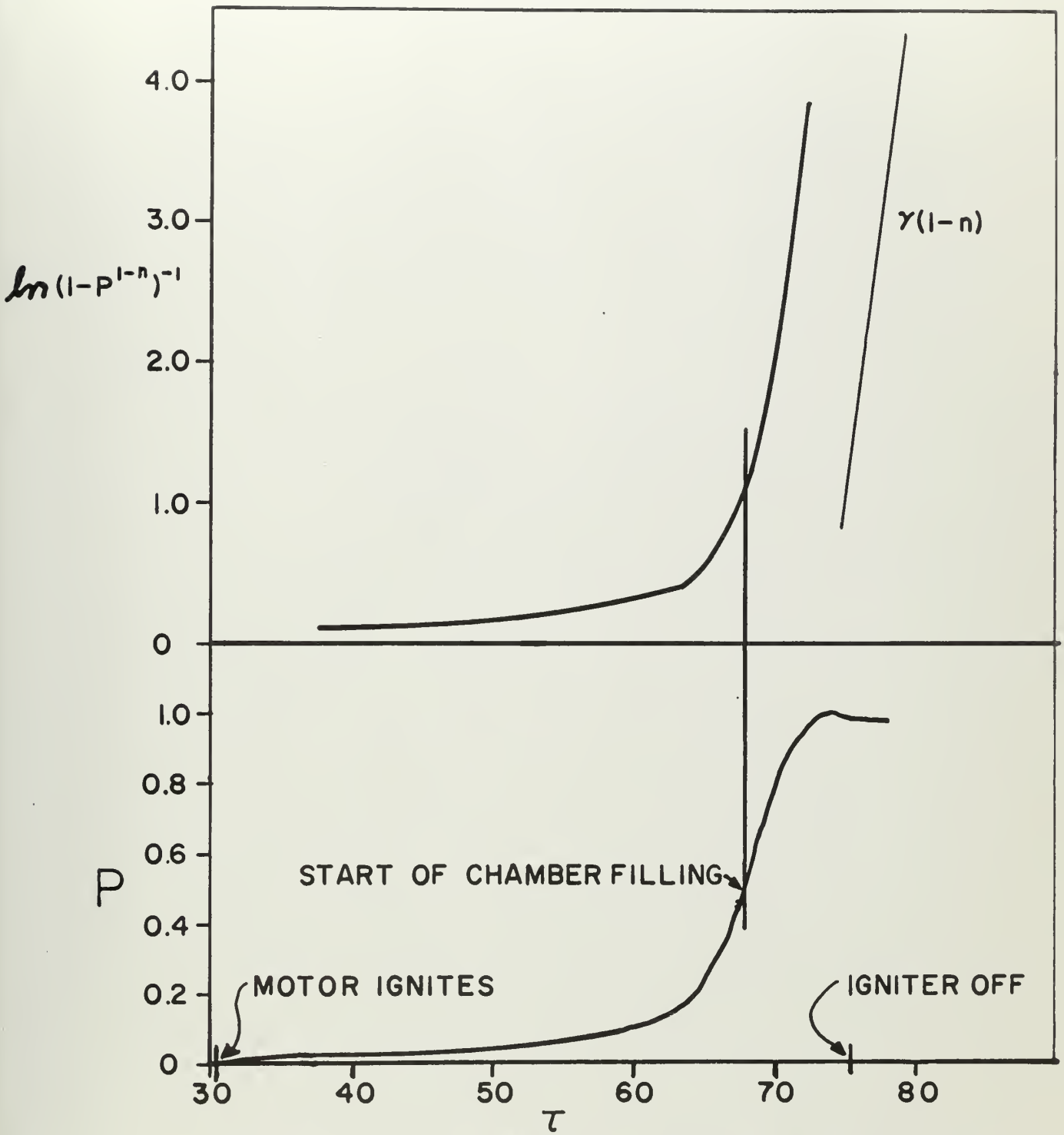

DETERMINATION OF CHAMBER FILLING INTERVAL FOR STAR SHAPE GRAIN ROCKET MOTOR; RUN NO. 84

FIGURE 20

APPENDIX A

COLLECTION OF EXPERIMENTAL RESULTS

The experimental data collected during the course of the research discussed in this report are presented in this appendix in the form of three tables. Table A-I contains the experimental parameters measured and calculated for the rocket motor tests. Table A-II is a list of equations used for the calculation of experimental parameters. Table A-III is a list of all of the experimental motor runs with pertinent parameters and general results.

TABLE A-I

TABLE OF EXPERIMENTAL PARAMETERS

Note: Source of listed values is indicated where appropriate.

a. Solid Pyrogen Igniter

Igniter Rocket Motor

$A_{t_{ign}}$ = 0.0071 in.^{2} (average value)

$V_{c_{ign}}$ = 0.25 in.^{3} (Free Volume. Igniter adapter section not included)

l = 0.442 in.

$A_{p_{ign}}$ = 0.277 in.^{2}

L^* = 2.93 ft. (average value)

t^* = 1.46 msec. (average value)

Propellant: Plastisol

n = 0.41 (see Figure 5)

k = 0.037 $\frac{\text{in.}}{\text{sec.}} \left(\frac{1}{\text{psia}}\right)^{0.41}$ (see Figure 5)

ρ_p = 1.6 g/cm^3 (Ref. 6)

T_f = 2700°K (Ref. 6)

C^*(frozen) = 4790 ft/sec (Ref. 6)

γ = 1.20 (Ref. 6)

$\eta_g \approx$ 25

b. Solid Propellant Motor

Rocket Motor

1. Circular Grain

ℓ = 3.5, 7.625, 9.5 in.

A_p = 0.624 in.^{2}

A_b = 9.8, 2.14, 26.6 in.^{2} (initial value)

TABLE A-I

(Continued)

V_c = 4.03, 6.60, 7.77 $in.^3$ (Free Volume. Includes igniter adapter and aft section assembly)

A_t = (See Table III, page 29 , for variations)

2. Star Shape Grain

l = 3.5, 7.625, 9.5 in.

A_p = 0.331 $in.^2$

A_b = 13.8, 30.0, 37.35 $in.^2$

V_c = 2.85, 4.05, 4.84 $in.^3$ (Free Volume. Includes igniter adapter and aft section assembly)

A_t = (See Table III, page 29, for variations)

Propellant: PBAA-80BM (1)

n = 0.4 (see Figure 8)

k = 0.02 $\frac{in.}{sec.}$ $(psia)^{-0.4}$ (see Figure 8)

ρ_p = 1.6 g/cm^3

C_p = 0.3 cal/g^oC

λ_p = 9×10^{-4} $cal/cm\ sec^oC$

T_{IG} = 420^oC

Combustion Gases (1)

Theoretical @ 90 psia

T_f = 2076^oK

C^*(frozen) = 4384 ft/sec

TABLE A-I

(Continued)

C^*(equilibrium) = 4397 ft/sec

C_g = 0.441 cal/g^oC

m_g = 22.22

Theoretical @ 300 psia

T_f = 2078^oK

C^*(frozen) = 4386 ft/sec

C^*(equilibrium) = 4397 ft/sec

C_g = 0.441 cal/g^oC

m_g = 22.23

γ = 1.26

μ_g(2000^oK) = 6.6×10^{-4} g/cm sec

μ_g(1200^oK) = 4.9×10^{-4} g/cm sec

λ_g(2000^oK) = 3.6×10^{-4} cal/cm sec^oC

λ_g(1200^oK) = 2.4×10^{-4} cal/cm sec^oC

Composition

Species	Mole Fraction
CO	0.256
H_2O	0.242
H_2	0.215
HCl	0.152
N_2	0.176
CO_2	0.060

TABLE A-II

EQUATIONS USED FOR CALCULATION OF EXPERIMENTAL PARAMETERS

$$C^* = \frac{P_c^{(1-n)} \; g \; A_t}{\rho \; k \; A_b}$$

$$L^* = \frac{V_c}{A_t}$$

$$t^* = \frac{L^*}{\Gamma^2 C^*}$$

$$R_{e_{(a+x)}} = \left(\frac{P_{eq} \; A_t \; 1}{C^* \; A_p \; \mu_g} \right) \frac{a + x}{e} \quad \frac{P}{T}^{1/2} + \; 1 - \frac{x}{e} \; \frac{d}{d}^{(P/T)}$$

$$N_{u_{(a+x)}} = 0.09 \; R_{e_{(a+x)}}^{0.8} = \frac{h(a+x)}{\lambda_g}$$

$$h = 0.09 \; \frac{\lambda_g}{(a+x)} \; R_{e_{(a+x)}}^{0.8}$$

$$q(t) = h(T_c - T_s)$$

TABLE A-III

LIST OF EXPERIMENTAL MOTOR RUNS

Definitions

1. Length (ℓ): Length of the propellant grain.

2. Induction Time: The total time from application of the igniter firing current to the electric match to the time of first departure of motor chamber pressure from the pre-ignition pressure level.

3. 50% Time: The time from the completion of the induction period to the time at which 50% of the chamber equilibrium pressure is reached.

4. Total Igniter Duration: The total time from application of the igniter firing current to completion of igniter pressure decay.

5. $t^* = \frac{L^*}{c^* \Gamma}$ where c^* is taken to be the theoretical value.

Constants

A_p(circular) = 0.624 in^2
A_p(star) = 0.331 in^2
$A_{t\,ign}$ = 0.071 in^2 (Average value - see discussion on page 12)

A. Motor Data

Run	Type	Length	A_t	Spacer	L^*	t^*	P_{eq}	Pre-Ignition Pressure	Induction Time	50% Time	Overshoot % P_{eq}
		(in)	(in^2)	Type, length, position	(ft)	(msec)	(psia)	(psia)	(msec)	(msec)	
36	Circular	9.5	.106	None	6.11	3.20					
37	"	"	.1415	"	4.58	2.40	280	20	100	62	111.0
38	"	"	"	"	"	"	285	17	115	59	117.5
39	"	"	"	"	"	"	260	20	70	85	110.0
42	"	"	"	"	"	"	295	19	110	63	0
43	"	"	"	"	"	"	265	18	70	90	107.6
48	"	7.625	"	"	3.88	2.03	215	17	70	60	111.6
49	"	"	.106	"	5.19	2.72	315	18	50	56	111.0
50	"	3.5	.0431	"	7.78	4.06	405	44	46	29	131.0
51	"	"	.073	"	4.60	2.41	185	30	52	24	124.2
52	"	7.625	.1415	"	3.88	2.03	230	19	1280	60	108.8
53	"	3.5	.0491	"	6.82	3.57	355	34	58	33	125.5
54	"	9.5	.106	"	6.11	3.20	440	20	60	63	108.0
55	"	"	"	"	"	"	395	18	80	60	0
68	"	7.625	.1415	"	3.88	2.03	205	17	60	102	0

A. Motor Data

Run	Type	Length (in)	A_t (in^2)	Spacer Type, length, position	L^* (ft)	t^* (msec)	P_{eq} (psia)	Pre-Ignition Pressure (psia)	Induction Time (msec)	50 % Time (msec)	Overshoot % P_{eq}
69	Star	9.5	.1415	None	2.85	1.49	575	19	95	31	116.5
70	"	"	"	"	"	"	585	20	85	27	117.0
71	"	7.625	"	"	2.39	1.25	—	—	—	—	—
72	"	"	"	"	"	"	325	20	80	32	118.5
73	"	"	.106	"	3.19	1.67	505	20	75	50	127.0
74	Circular	"	.1415	"	3.88	2.03	200	20	90	60	0
75	"	"	.106	"	5.19	2.72	315	"	80	"	105.0
76	"	3.5	.073	"	4.60	2.41	175	30	50	22	143.0
77	"	"	.0491	"	6.82	3.57	340	40	45	29	131.0
78	"	"	.0431	"	7.78	4.06	400	45	40	40	121.0
79	"	9.5	.106	"	6.11	3.20	355	19	100	79	103.0
80	"	"	"	"	"	"	370	"	70	99	107.0
81	"	"	"	"	"	"	390	18	80	66	101.0
82	"	3.5	.073	"	4.60	241	145	25	50	41	138.0
83	"	"	"	"	"	"	"	"	45	30	131.0

A. Motor Data

Run	Type	Length (in)	A_t (in^2)	Spacer Type, length, position	L^* (ft)	t^* (msec)	P_{EQ} (psia)	Pre-Ignition Pressure (psia)	Induction Time (msec)	50 % Time (msec)	Overshoot % P_{EQ}
84	Star	9.5	.106	None	3.80	1.99	7.90		75	65	103.5
85	"	7.625	.1415	"	2.39	1.25	315	19	100	40	122.1
86	Circular	9.5	"	"	4.58	2.40	295	18	1700	43	101.2
87	"	"	"	"	"	"	—	—	—	—	—
88	"	"	"	"	"	"	—	—	—	—	106.0
89	"	"	"	No igniter adaptor	4.29	2.24	—	—	—	—	—
90	"	"	"	"	"	"	260	18	95	28	104.0
91	"	"	"	None	4.58	2.40	285	17	65	62	105.2
92	Star	3.5	"	"	1.68	0.88	85	17	75	25	0
93	"	"	.0491	"	4.84	2.53	460	45	45	38	127.0
94	"	"	.0431	"	5.51	2.88	545	46	"	37	112.0
95	"	"	.0730	"	3.25	1.70	185	28	55	45	113.5
96	Circular	"	"	"	4.60	2.41	155	29	40	25	129.0
97	"	"	"	"	"	"	160	33	35	20	115.8
98	"	9.0	.1415	1/2" inert section aft	4.58	2.40	245	17	120	55	0
99	"	"	"	1/2" inert section fwd.	"	"	"	18	—	—	0

A. Motor Data

Run	Type	Length (in)	A_t (in^2)	Spacer Type, length, position	L^* (ft)	t^* (msec)	P_{eq} (psia)	Pre-Ignition Pressure (psia)	Induction Time (msec)	50% Time (msec)	Overshoot % P_{eq}
101	Circular	9.0	.1415	1/2" inert section aft	4.58	2.40	205	18	130	62	0
102	"	"	"	1/2" inert section fwd	"	"	260	16	110	45	106.0
103	"	8.5	"	1" inert section aft; 1/2" spacer forward	4.75	2.48	240	18	80	62	114.0
104	"	"	"	1" inert section aft; 1 1/2" spacer forward	5.14	2.69	265	19	595	63	103.8
105	"	"	"	1" inert section aft; 1" spacer forward	4.75	2.48	215	"	110	85	109.0
106	"	"	"	1" inert section aft; 1 1/2" spacer forward	5.14	2.69	195	"	150	66	113.0
107	"	9.5	.106	None	2.57	1.347	180	18	55	59	139.0
108	"	"	"	"	"	"	200	18	55	45	136.0
109	"	3.5	.0491	1/2" spacer forward	7.36	3.85	305	32	45	40	109.0
110	"	"	"	1 1/2" spacer forward	8.41	4.40	275	27	120	57	0
111	"	"	"	1" spacer forward	7.90	4.14	295	36	60	65	100.8
112	"	9.5	.1415	1" inert section fwd.	4.58	2.40	255	19	405	34	0
113	"	"	"	1" inert section fwd; 1 1/2" spacer forward	5.14	2.69	257	17		53	103.0
114	"	3.5	.0431	1" inert section aft; 1" spacer aft.	7.90	4.14	195	35	32	41	110.0
				No igniter diffuser							

B. IGNITER DATA AND REMARKS

RUN	WEB THICKNESS (in)	$\dot{m}_{ign}$ lb/sec x 10^2	TOTAL DURATION (sec)	REMARKS
36	.094	2.47	0.25	P_c NOT RECORDED. FAULTY ELECTRICAL CONNECTION
37	"	2.40	"	USABLE DATA
38	"	"	0.27	" "
39	.063	2.22	0.17	" "
42	.055	2.41	0.17	" "
43	"	"	0.16	" "
48	"	2.34	"	" "
49	"	2.33	0.17	" "
50	"	2.28	0.16	" "
51	"	2.40	0.17	" "
52	.039	2.21	0.14	NOT USABLE – LONG DELAY
53	.055	2.17	0.19	USABLE DATA
54	"	2.21	0.195	" "
55	"	2.24	0.17	" "
68	.0465	2.195	0.15	" "
69	"	2.18	"	" "

B. IGNITER DATA AND REMARKS

RUN	WEB THICKNESS (in)	$\dot{m}_{ign}$ lb/sec $\times 10^2$	TOTAL DURATION (sec)	REMARKS
70	.0465	2.255	0.14	USABLE DATA
71	.039	2.21	0.135	MISFIRE
72	.0465	2.185	0.145	USABLE DATA
73	"	2.32	0.165	" "
74	"	2.19	0.15	" "
75	"	2.12	"	" "
76	"	2.15	0.17	UNUSABLE DATA — ANOMALOUS PRESSURE RISE
77	"	2.12	0.16	USABLE DATA
78	"	2.13	0.165	" "
79	"	2.145	0.160	" "
80	"	2.0	0.160	" "
81	"	2.07	0.155	" "
82	"	2.175	"	" "
83	"	2.185	0.150	" "
84	"	2.145	"	" "
85	"	"	"	" "

B. IGNITER DATA AND REMARKS

RUN	WEB THICKNESS (in)	$\dot{m}_{ign}$ lb/sec $\times 10^{-2}$	TOTAL DURATION (sec)	REMARKS
86	.0465	2.28	0.16	DELAY FIRE
87	"	2.07	"	MISFIRE
88	"	2.15	0.145	UNUSABLE DATA — ANOMALOUS PRESSURE TRACE
89	"	——	——	MISFIRE — ONLY MATCH FIRED
90	"	2.105	0.175	USABLE DATA
91	"	2.215	0.136	" "
92	"	2.245	0.140	UNUSABLE DATA — PRESSURE TOO LOW
93	"	2.165	0.153	USABLE DATA
94	"	2.225	0.16	" "
95	"	2.19	0.158	" "
96	"	2.17	0.160	USABLE DATA — SLOW PRESSURE RISE
97	"	2.13	0.164	" " " " "
98	"	1.87	0.178	" "
99	"	1.99	0.169	DELAY FIRE
101	"	2.04	0.168	USABLE DATA ; SAME GRAIN USED IN MISFIRE RUN NO. 100
102	"	2.10	0.158	UNUSABLE DATA — ANOMALOUS PRESSURE TRACE; TEST FOR BACK FLAME SPREADING

B. IGNITER DATA AND REMARKS

RUN	WEB THICKNESS (in)	$\dot{m}_{ign}$ lb/sec x 10^2	TOTAL DURATION (sec)	REMARKS
103	.094	2.36	0.160	USABLE DATA; TEST FOR BACK CHAMBER FILLING
104	.0465	2.18	0.165	DELAY FIRE; " " " " "
105	"	"	0.156	USABLE DATA; " " " " "
106	.094	2.53	0.160	UNUSABLE DATA – ABNORMAL IGNITER BEHAVIOR; TEST FOR BACK CHAMBER FILLING
107	.0465	1.955	"	USABLE DATA; PORT AREA = 0.163 IN.^{2}
108	"	2.10	0.165	" " " " " "
109	"	2.85	0.160	" " TEST FOR BACK CHAMBER FILLING
110	"	1.99	0.163	UNUSABLE DATA; ANOMALOUS PRESSURE TRACE
111	"	2.01	0.158	USABLE DATA; TEST FOR BACK CHAMBER FILLING
112	"	2.15	0.151	DELAY FIRE; TEST FOR BACK FLAME SPREADING
113	"	2.00	0.152	" " " " " " "
114	"	2.09	0.150	USABLE DATA; FORCED IMPINGEMENT AFT OF PROPELLANT LEADING EDGE

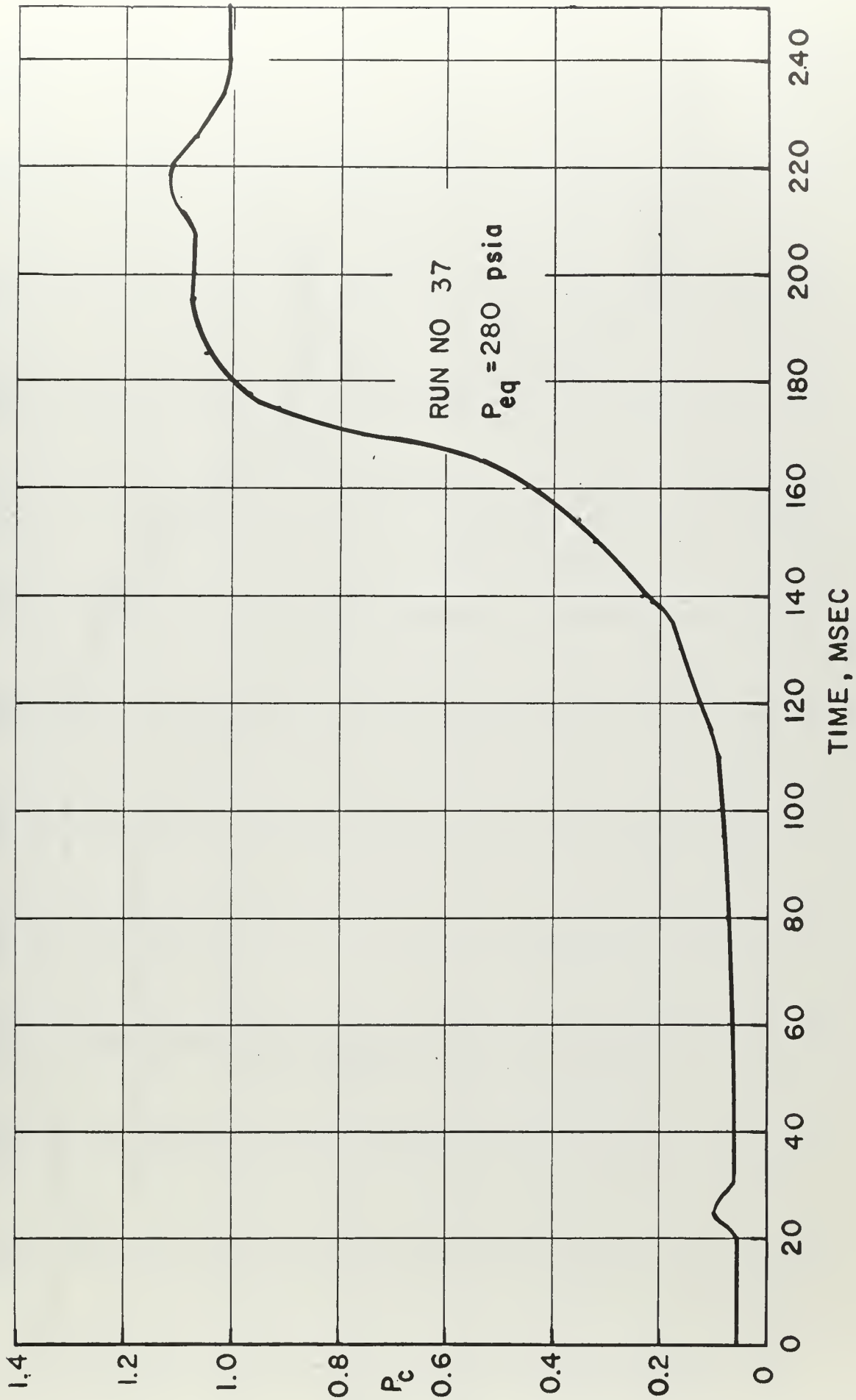
RUN NO 37
P_{eq} = 280 psia
P_c
TIME, MSEC
0
0.2
0.4
0.6
0.8
1.0
1.2
1.4
0
20
40
60
80
100
120
140
160
180
200
220
240

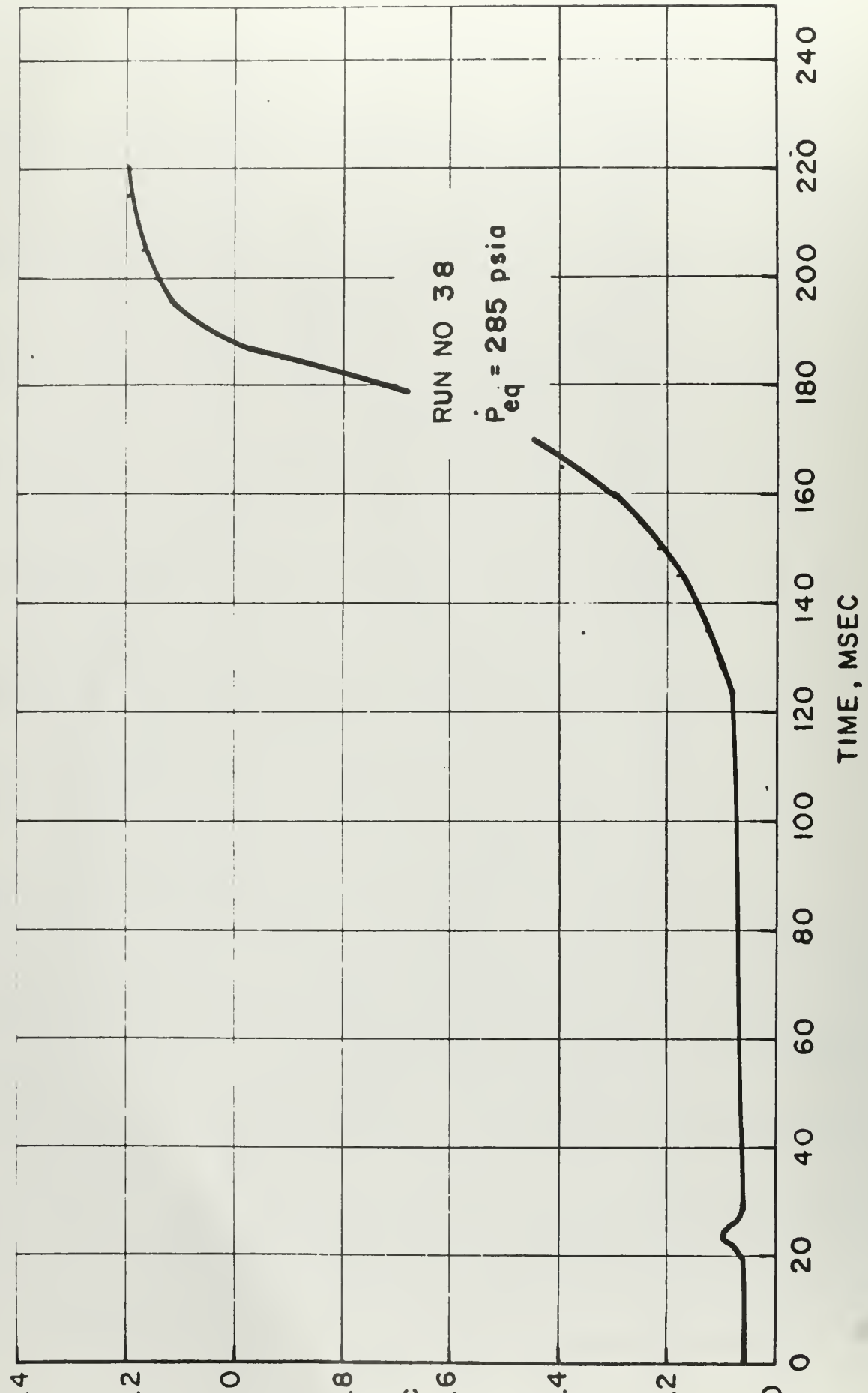
RUN NO 38
$\dot{P}_{eq}$ = 285 psia
P_c
TIME, MSEC
0
0.2
0.4
0.6
0.8
1.0
1.2
1.4
20
40
60
80
100
120
140
160
180
200
220
240

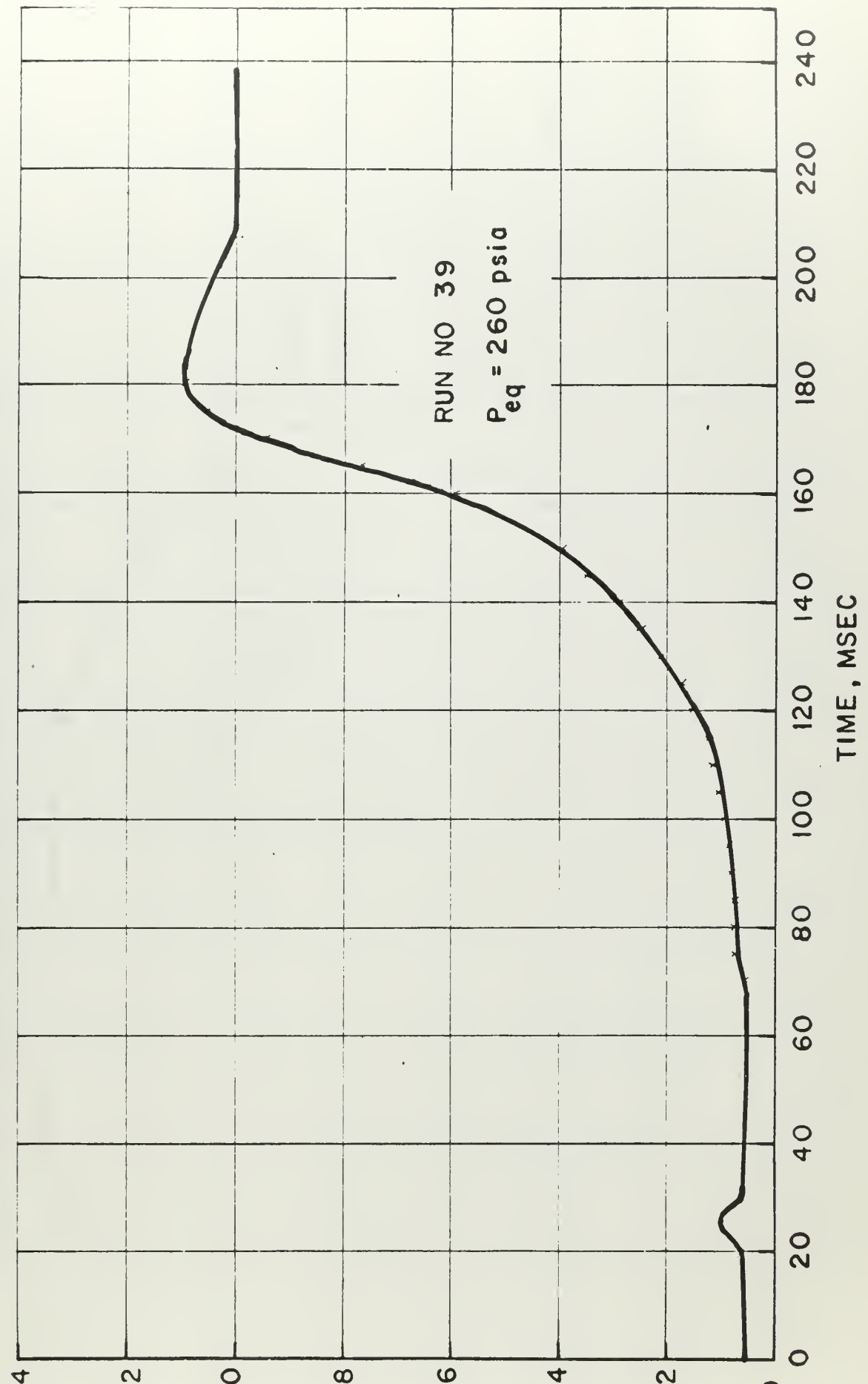
RUN NO 39
P_{eq} = 260 psia
P_c
TIME, MSEC
0
0.2
0.4
0.6
0.8
1.0
1.2
1.4
0
20
40
60
80
100
120
140
160
180
200
220
240

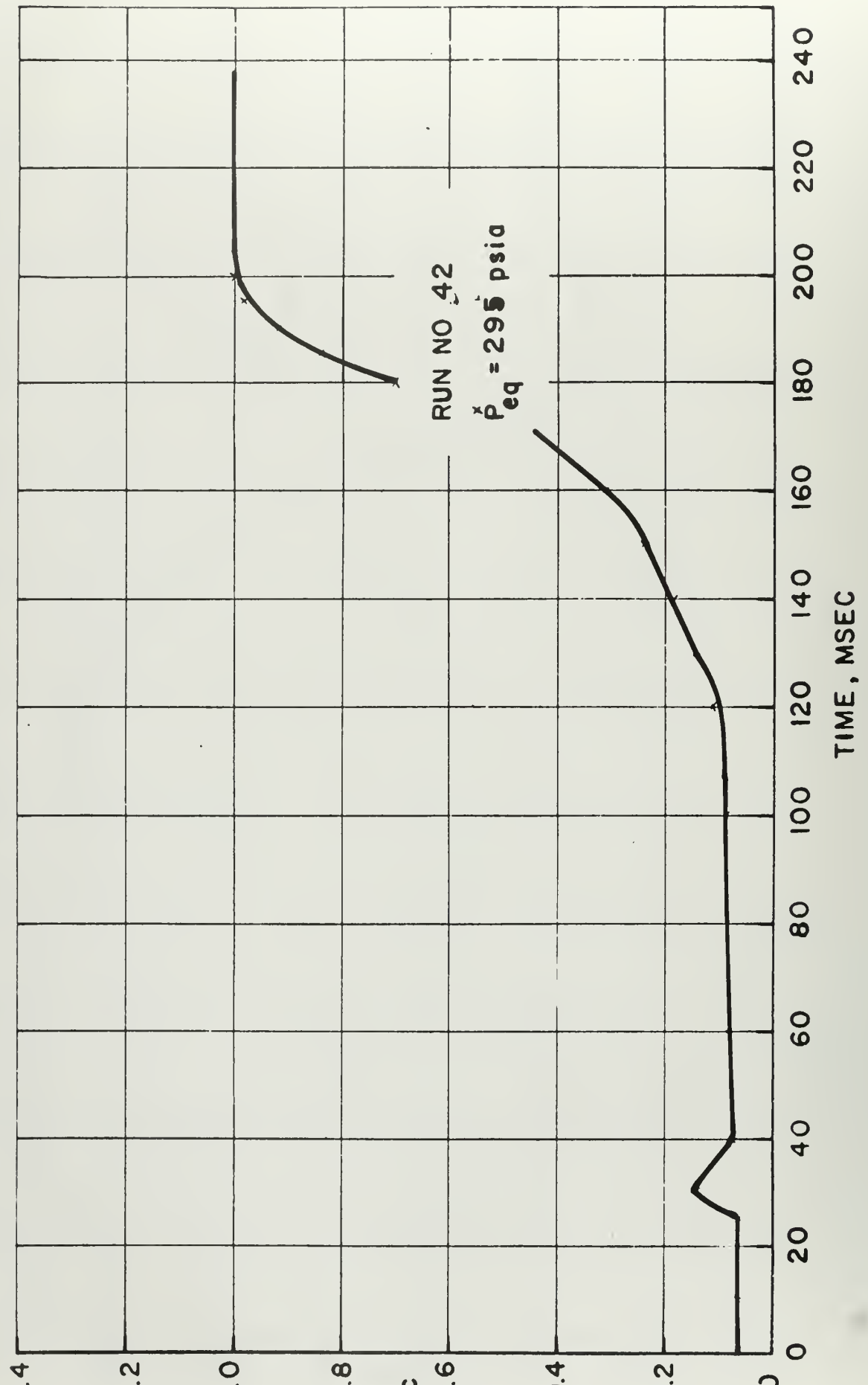
RUN NO 42
$\bar{P}_{eq}$ = 295 psia
P_c
TIME, MSEC
0
20
40
60
80
100
120
140
160
180
200
220
240
0.2
0.4
0.6
0.8
1.0
1.2
1.4

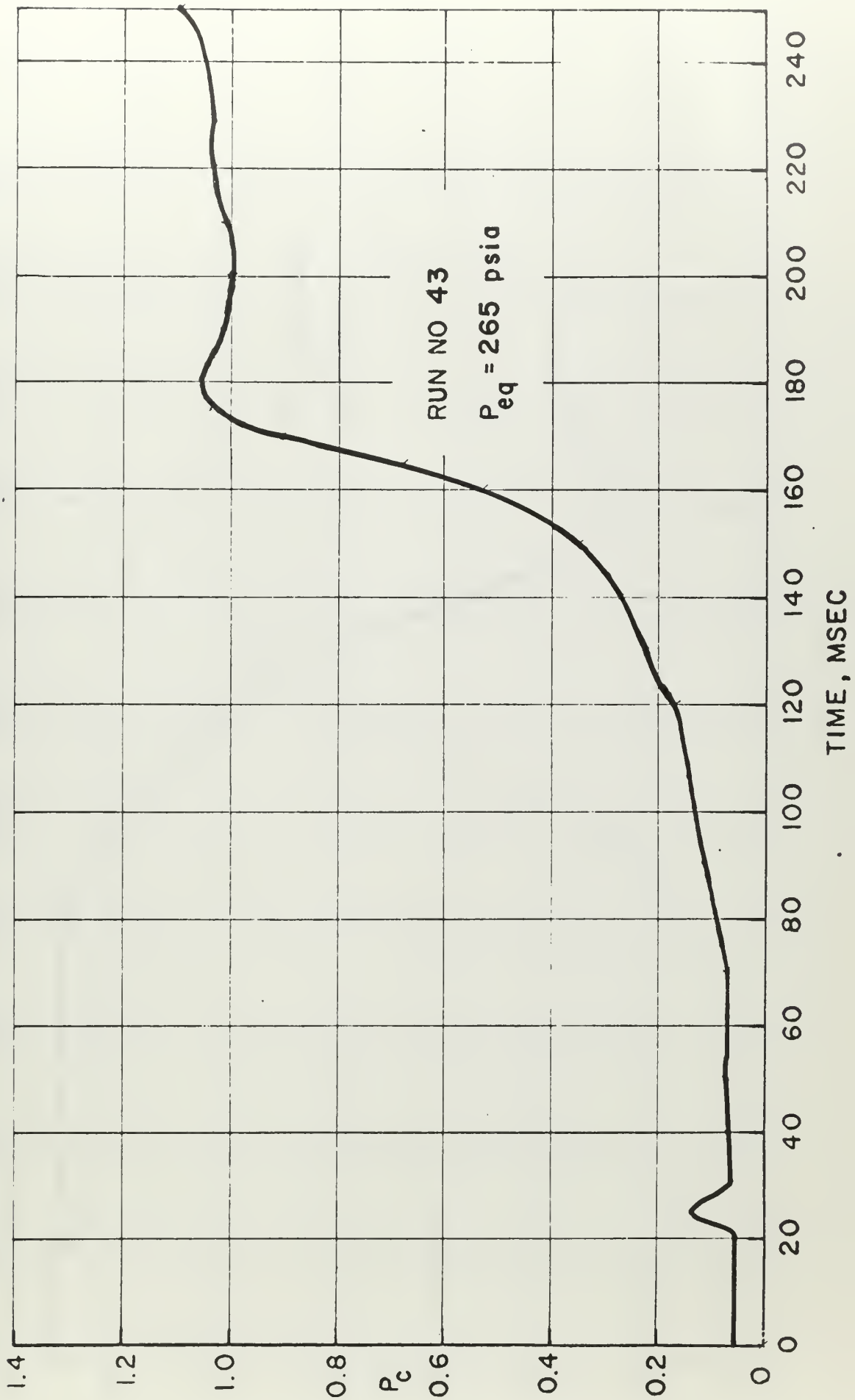
RUN NO 43
P_{eq} = 265 psia
P_c
1.4
1.2
1.0
0.8
0.6
0.4
0.2
0
0
20
40
60
80
100
120
140
160
180
200
220
240
TIME, MSEC

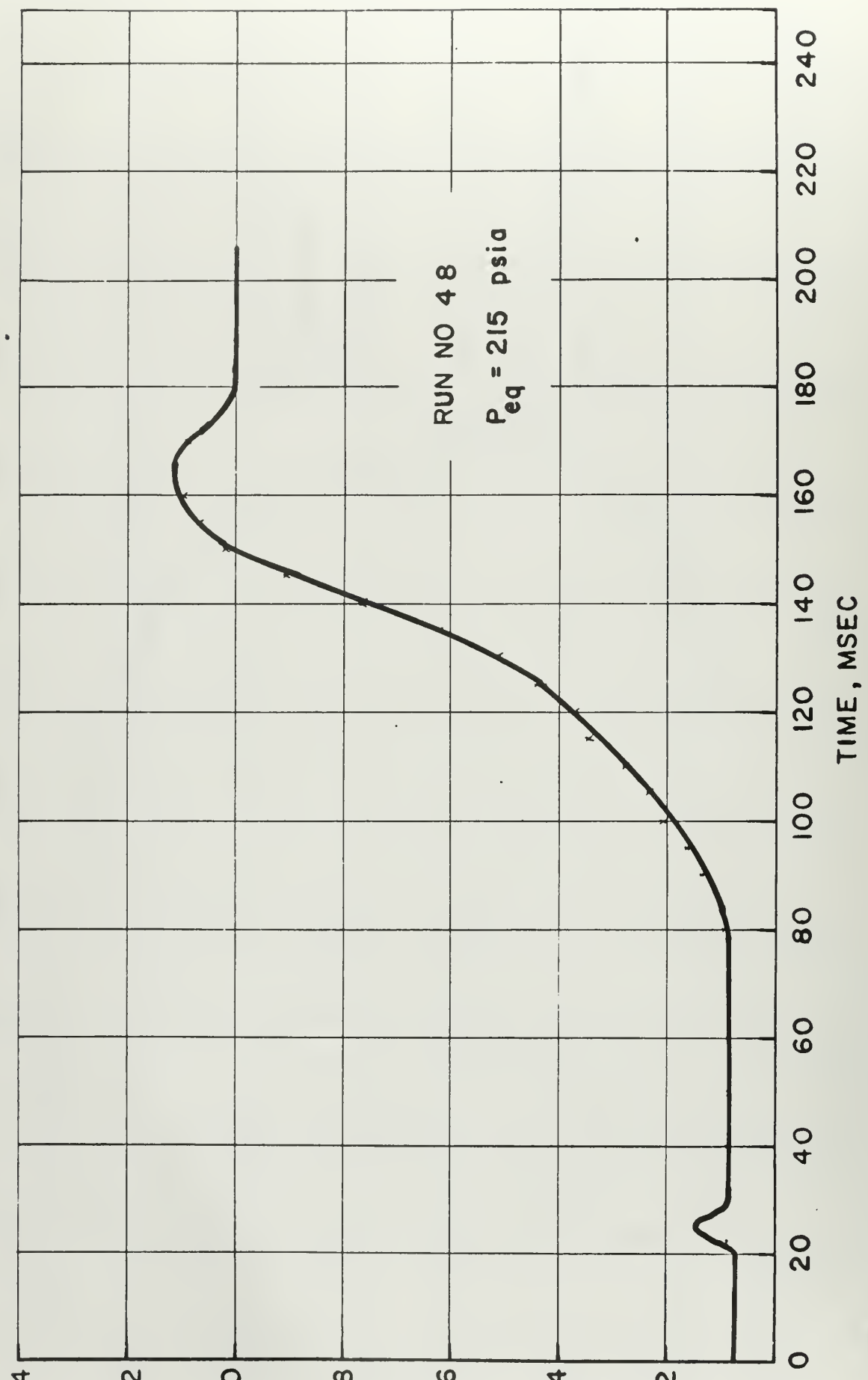
RUN NO 48
P_{eq} = 215 psia
P_c
TIME, MSEC
0
0.2
0.4
0.6
0.8
1.0
1.2
1.4
0
20
40
60
80
100
120
140
160
180
200
220
240

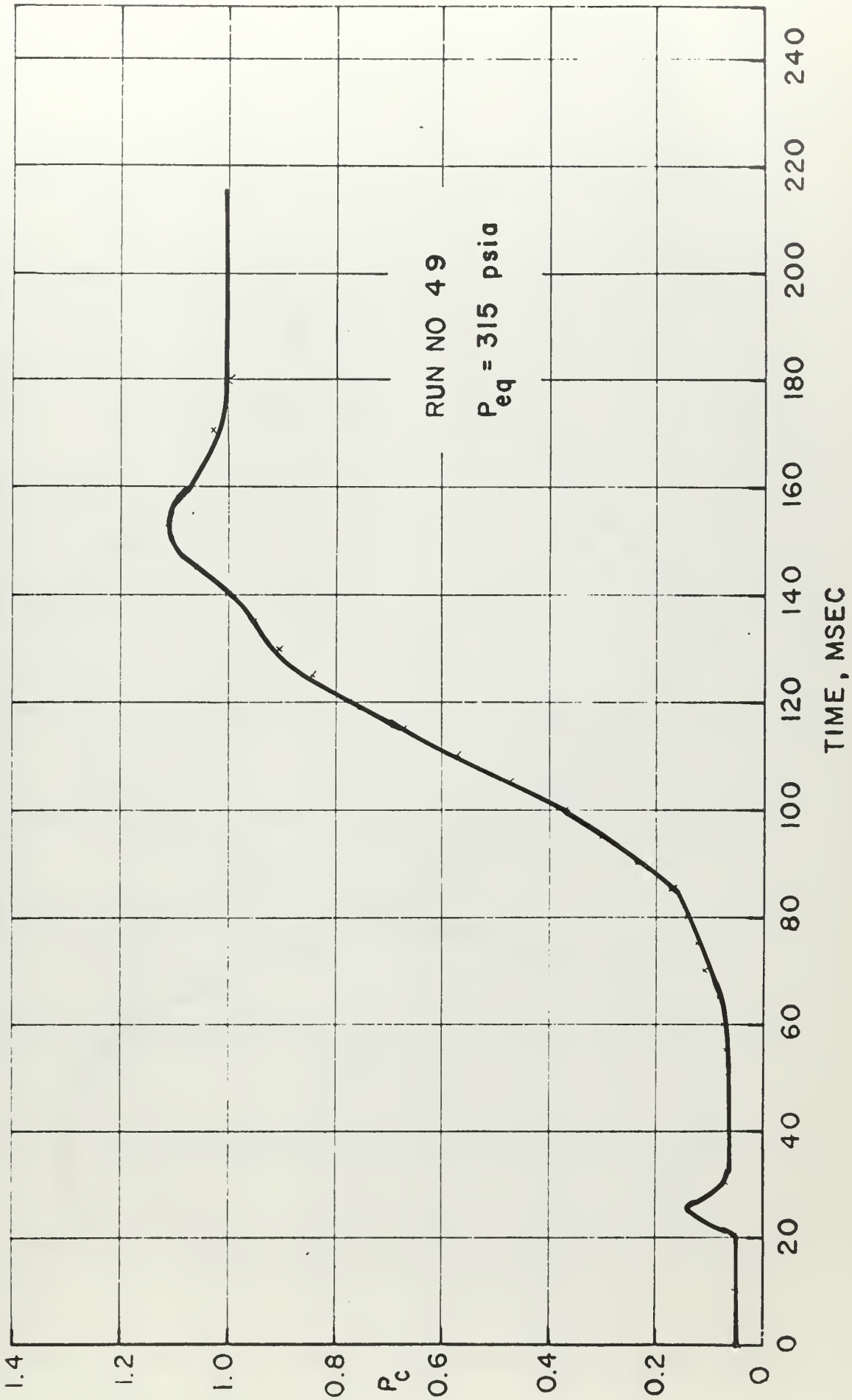
RUN NO 49
P_{eq} = 315 psia
P_c
TIME, MSEC
0
0.2
0.4
0.6
0.8
1.0
1.2
1.4
0
20
40
60
80
100
120
140
160
180
200
220
240

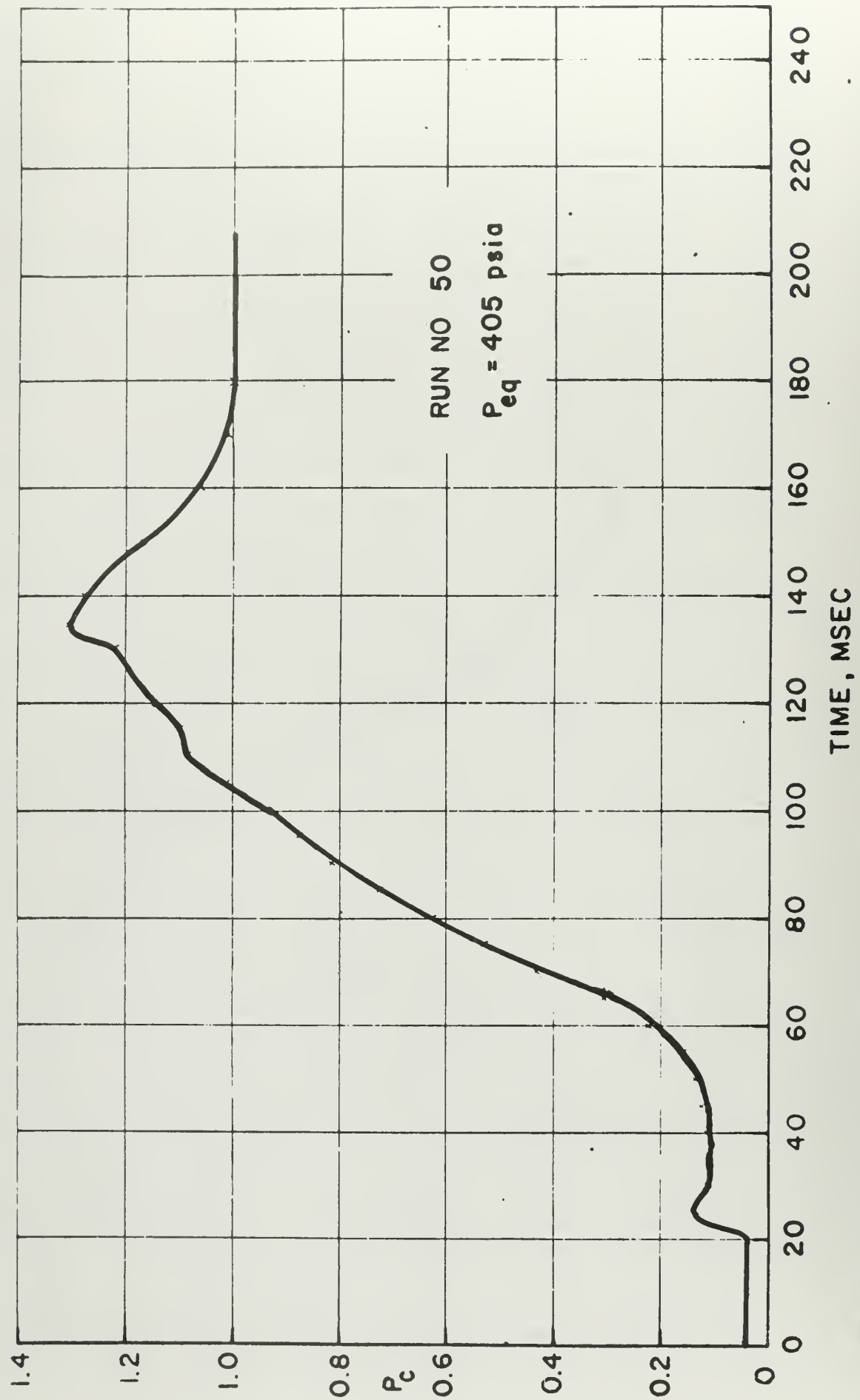
RUN NO 50
P_{eq} = 405 psia
P_c
TIME, MSEC
0
0.2
0.4
0.6
0.8
1.0
1.2
1.4
0
20
40
60
80
100
120
140
160
180
200
220
240

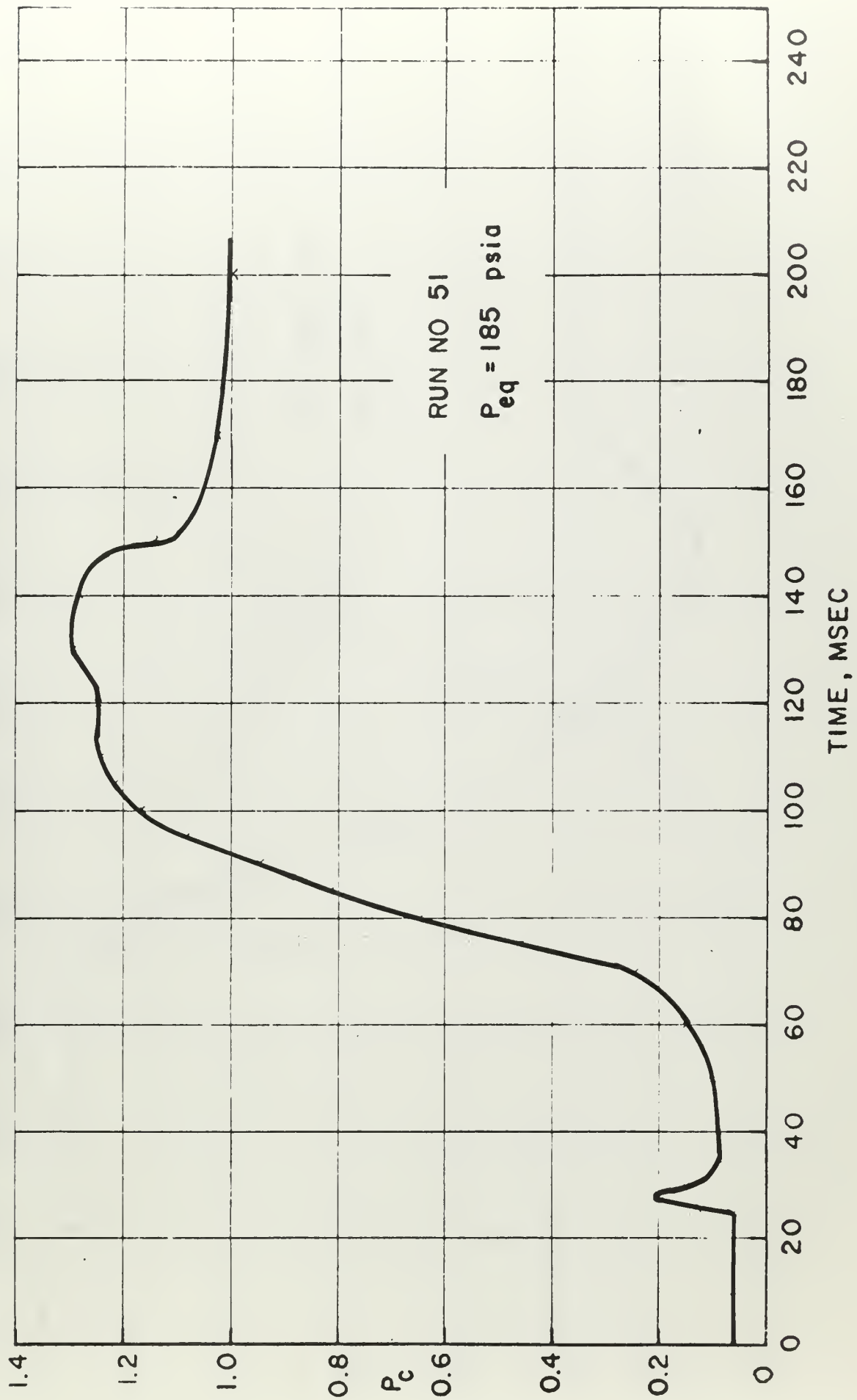
RUN NO 51
P_{eq} = 185 psia
P_c
TIME, MSEC
0
0.2
0.4
0.6
0.8
1.0
1.2
1.4
0
20
40
60
80
100
120
140
160
180
200
220
240

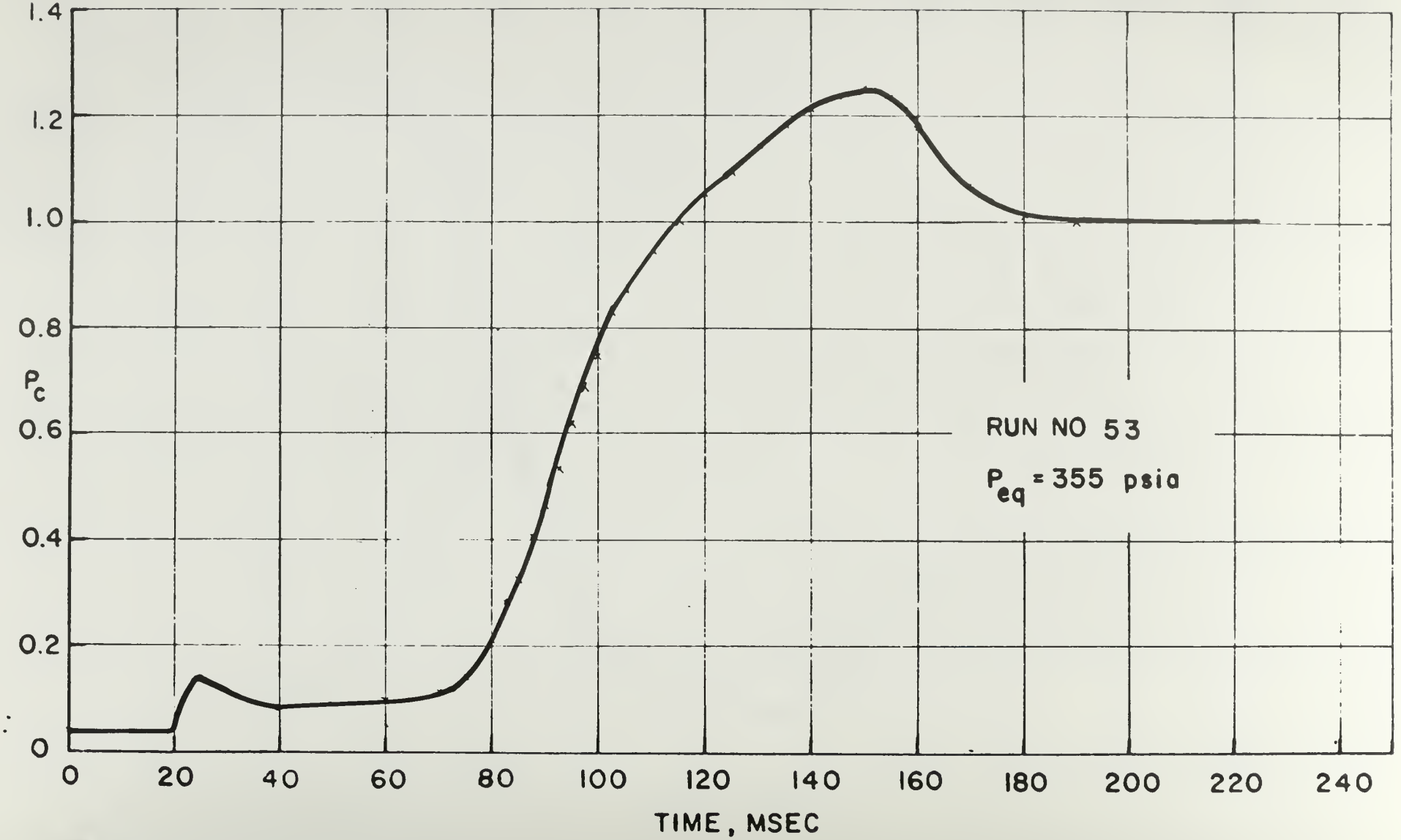
1.4
1.2
1.0
0.8
P_c
0.6
0.4
0.2
0
0
20
40
60
80
100
120
140
160
180
200
220
240
TIME, MSEC
RUN NO 53
P_{eq} = 355 psia

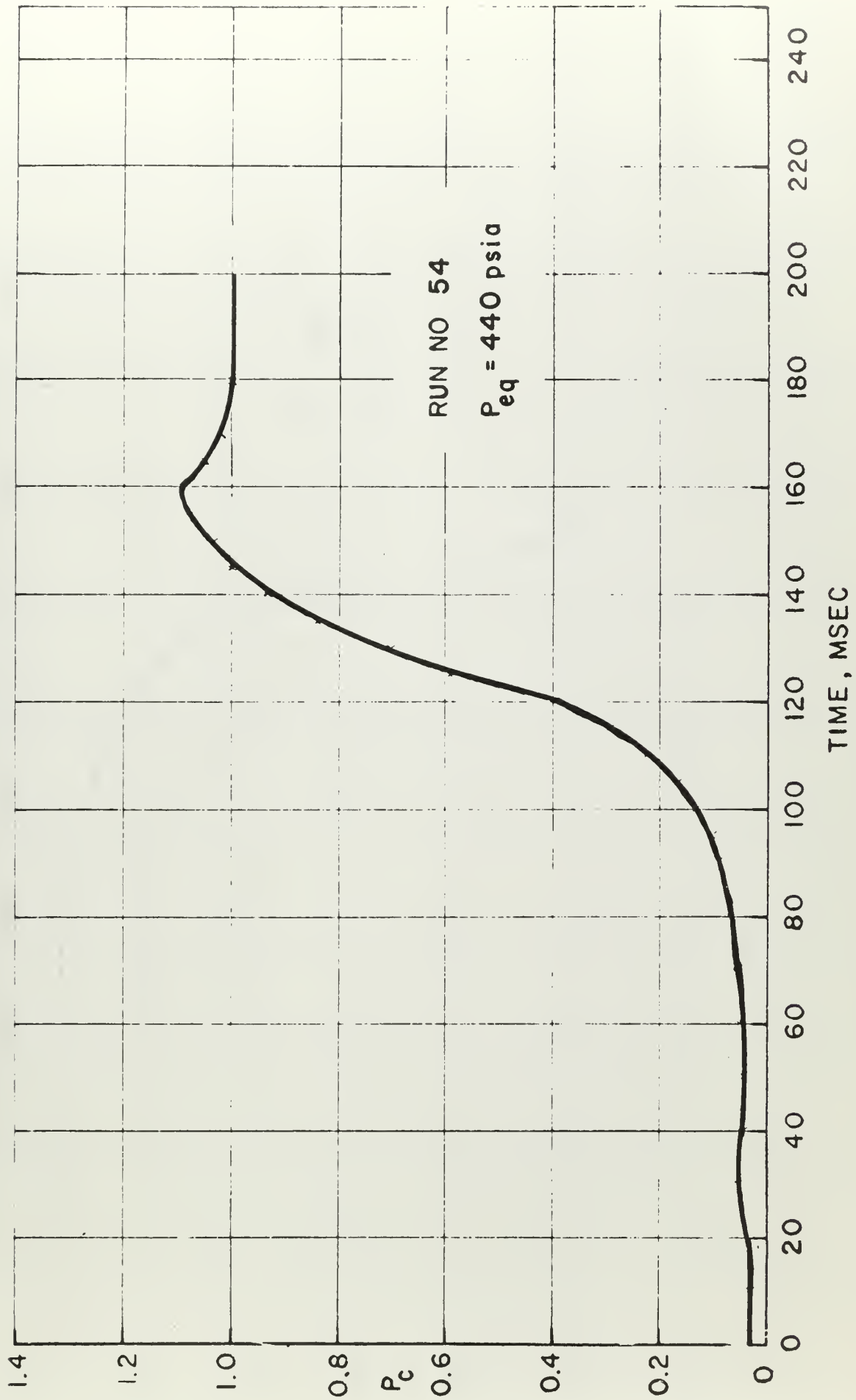
RUN NO 54
P_{eq} = 440 psia
P_c
TIME, MSEC
0
0.2
0.4
0.6
0.8
1.0
1.2
1.4
0
20
40
60
80
100
120
140
160
180
200
220
240

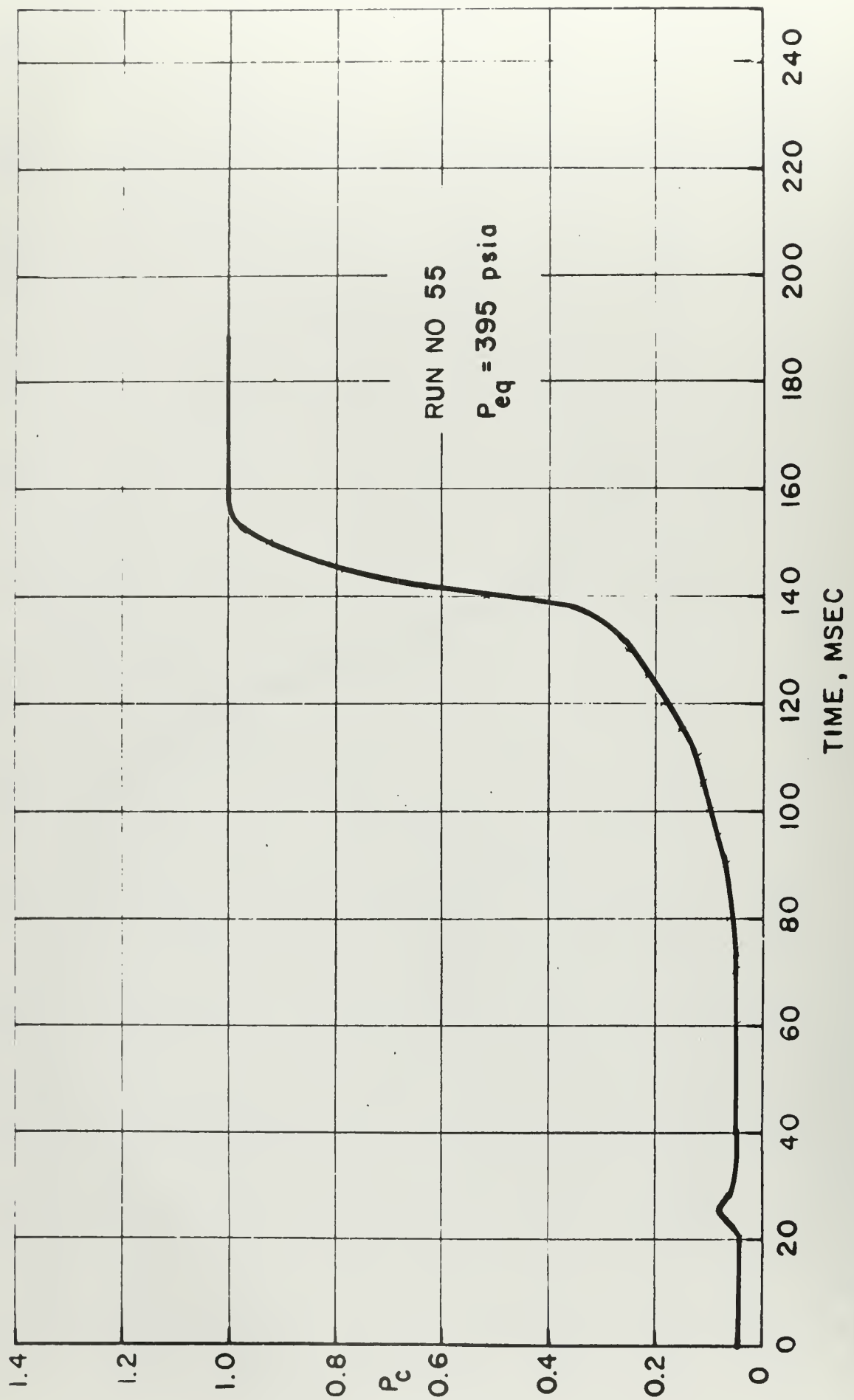
RUN NO 55
P_{eq} = 395 psia
P_c
TIME, MSEC
0
0.2
0.4
0.6
0.8
1.0
1.2
1.4
0
20
40
60
80
100
120
140
160
180
200
220
240

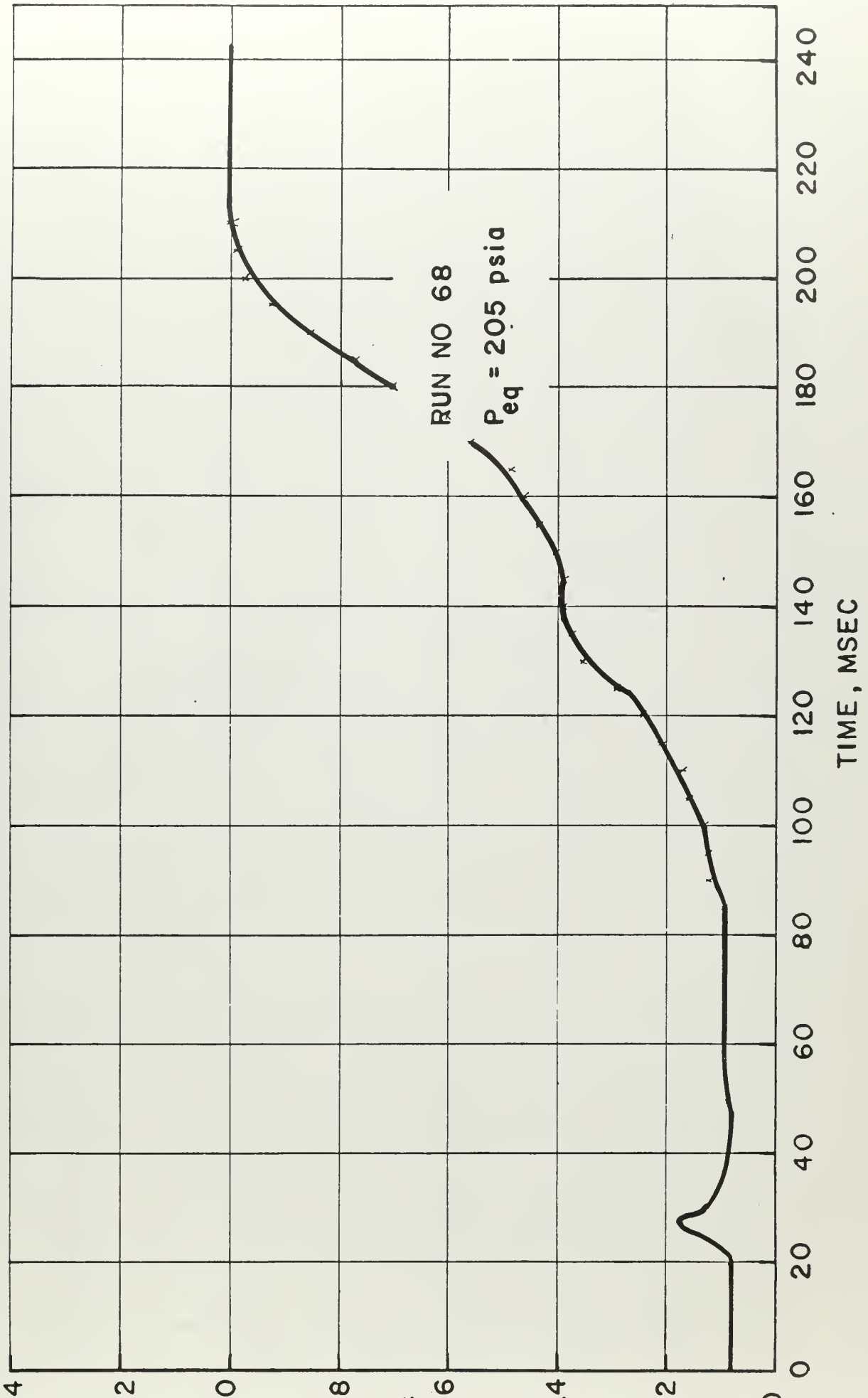
RUN NO 68
P_{eq} = 205 psia
P_c
TIME, MSEC
0
0.2
0.4
0.6
0.8
1.0
1.2
1.4
0
20
40
60
80
100
120
140
160
180
200
220
240

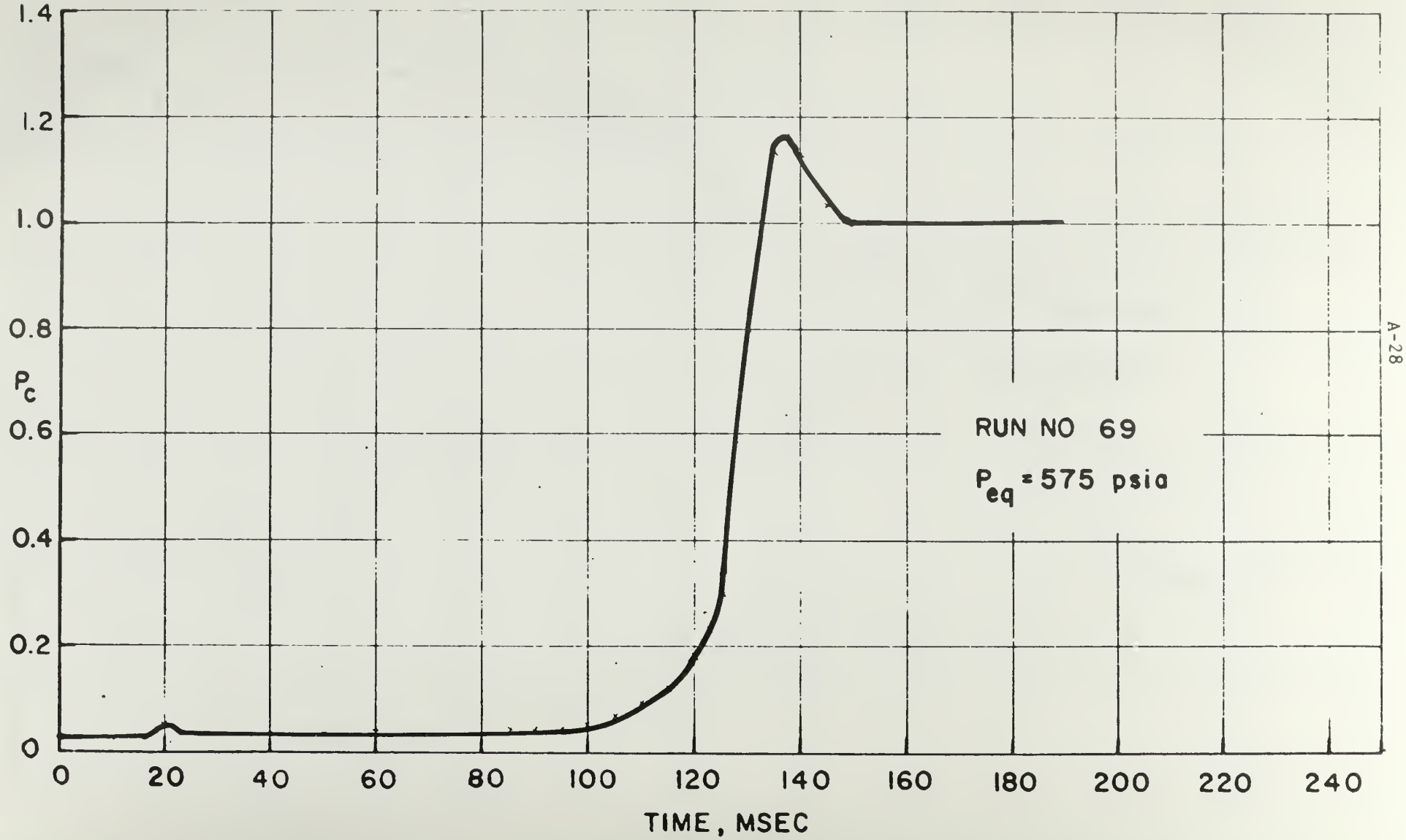
1.4
1.2
1.0
0.8
P_c
0.6
0.4
0.2
0
0
20
40
60
80
100
120
140
160
180
200
220
240
TIME, MSEC
RUN NO 69
P_{eq} = 575 psia

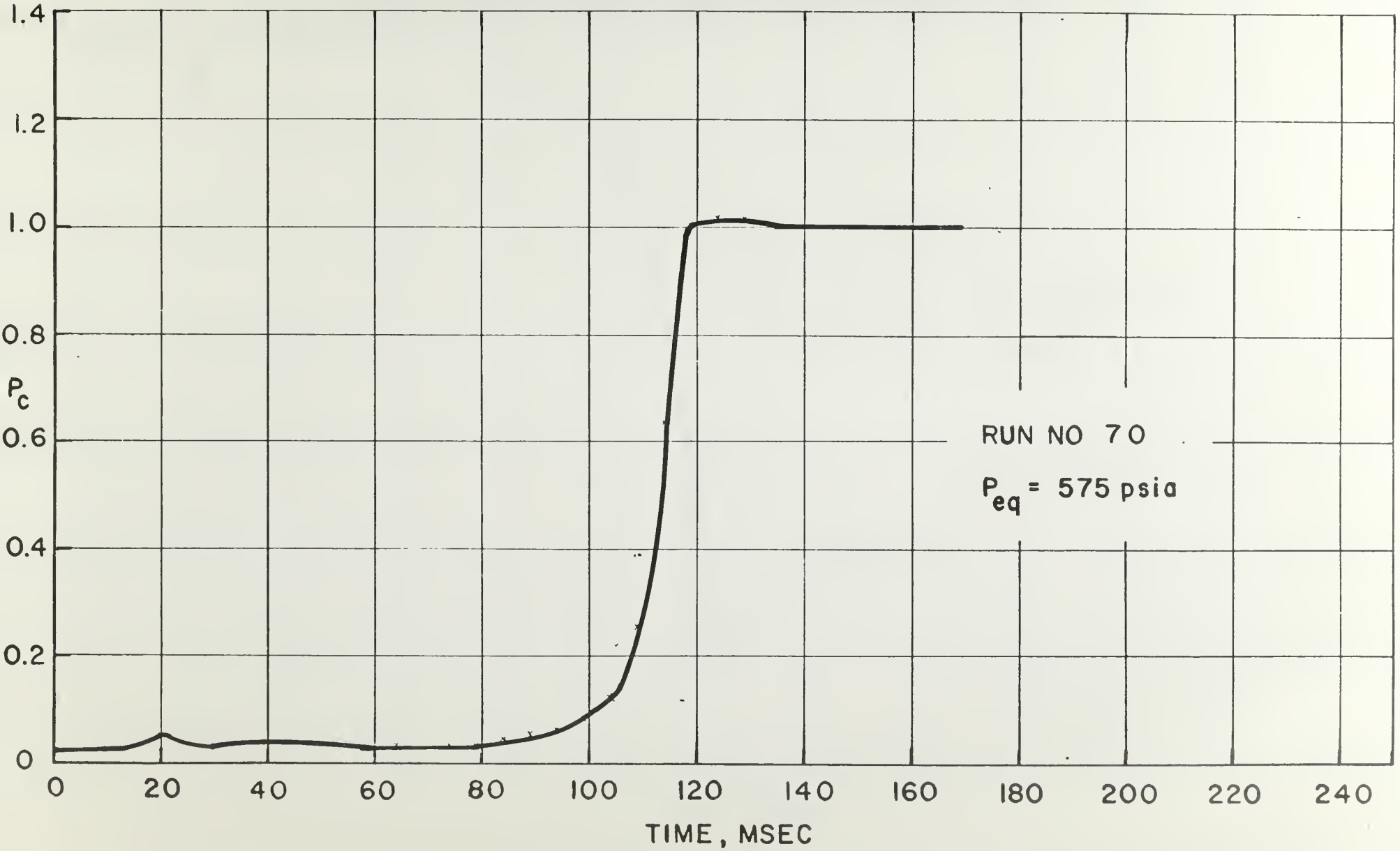
1.4
1.2
1.0
0.8
P_c
0.6
0.4
0.2
0
0
20
40
60
80
100
120
140
160
180
200
220
240
TIME, MSEC
RUN NO 70
P_{eq} = 575 psia

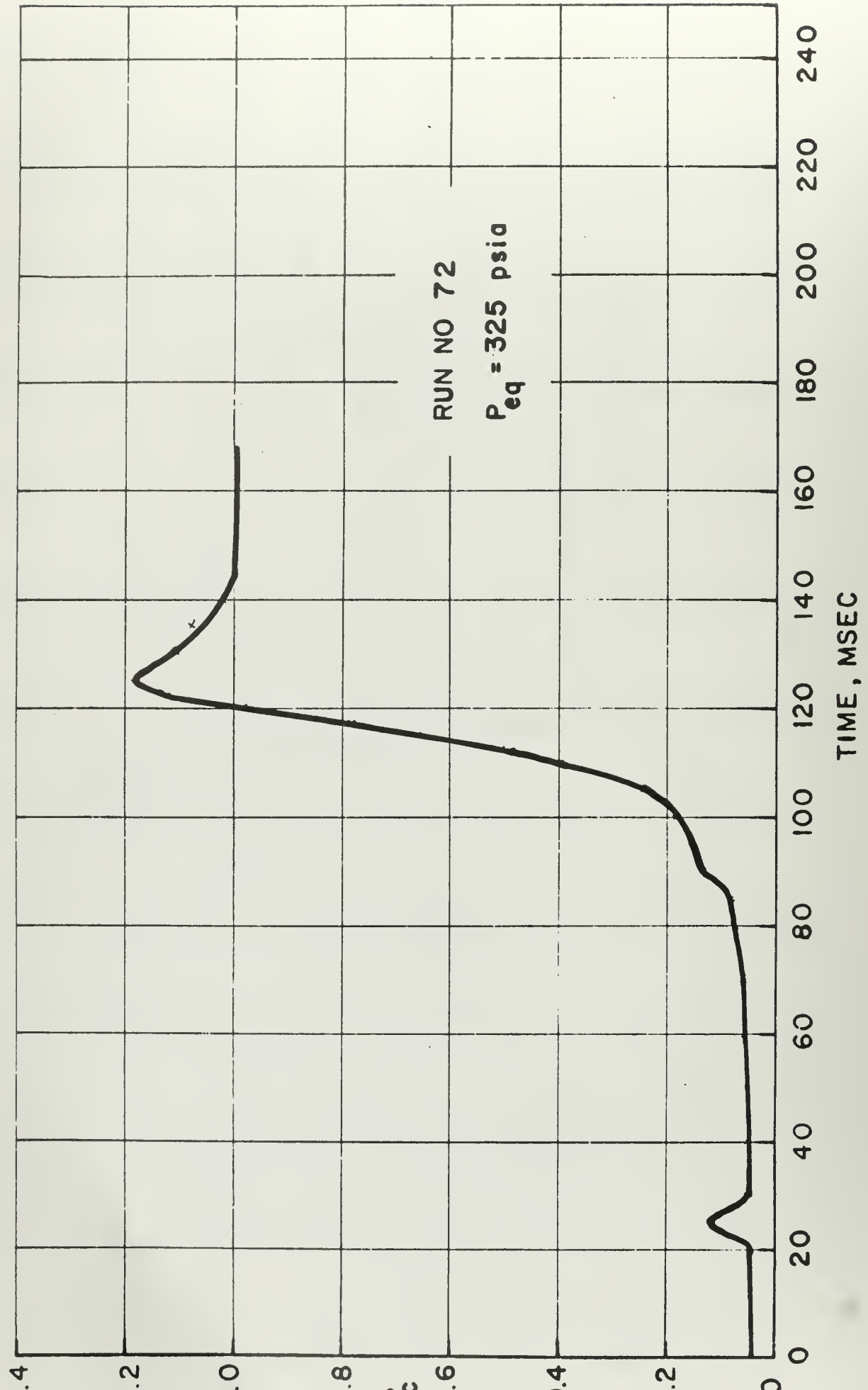
RUN NO 72
P_{eq} = 325 psia
P_c
TIME, MSEC
0
0.2
0.4
0.6
0.8
1.0
1.2
1.4
0
20
40
60
80
100
120
140
160
180
200
220
240

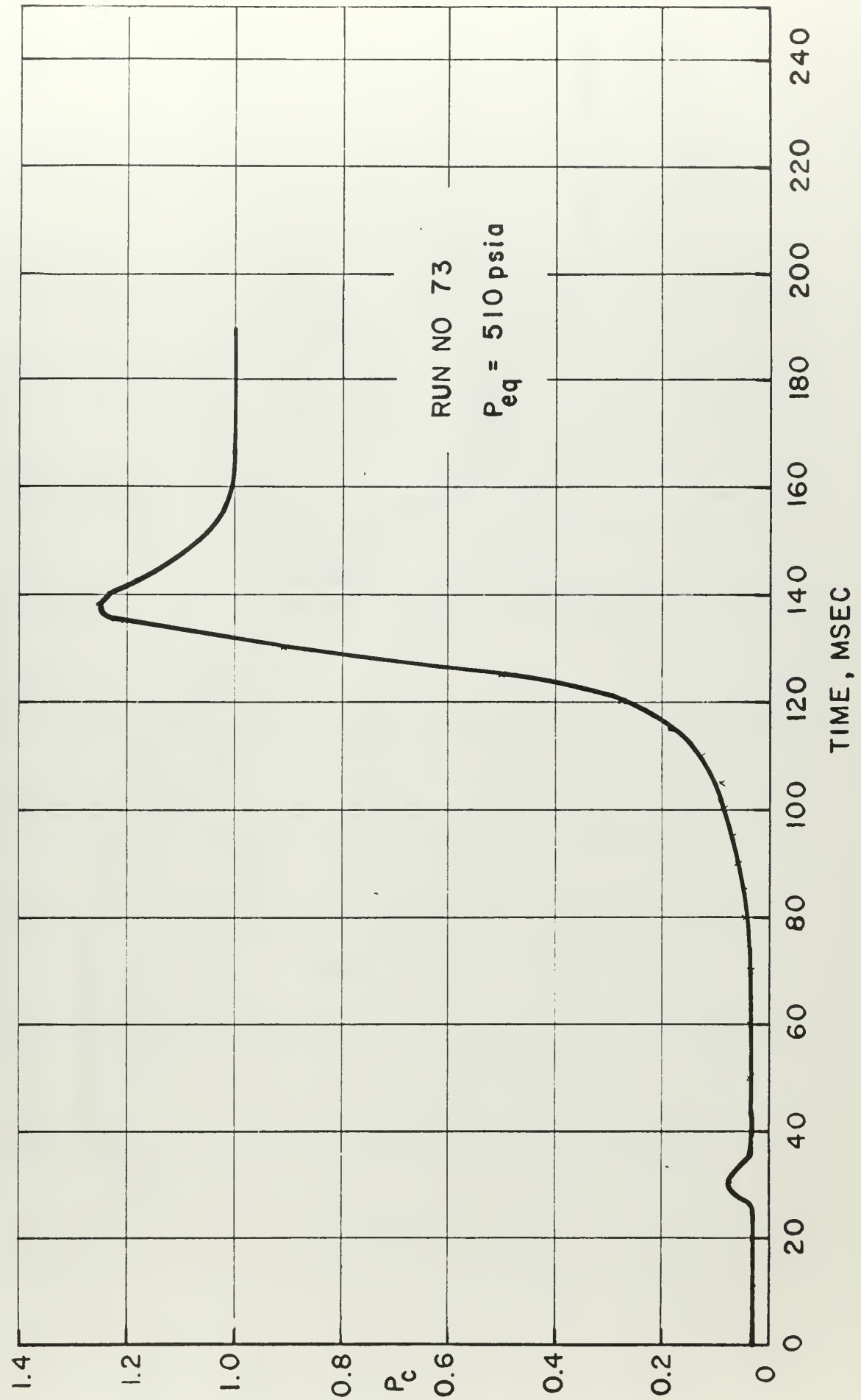
RUN NO 73
P_{eq} = 510 psia
P_c
1.4
1.2
1.0
0.8
0.6
0.4
0.2
0
0
20
40
60
80
100
120
140
160
180
200
220
240
TIME, MSEC

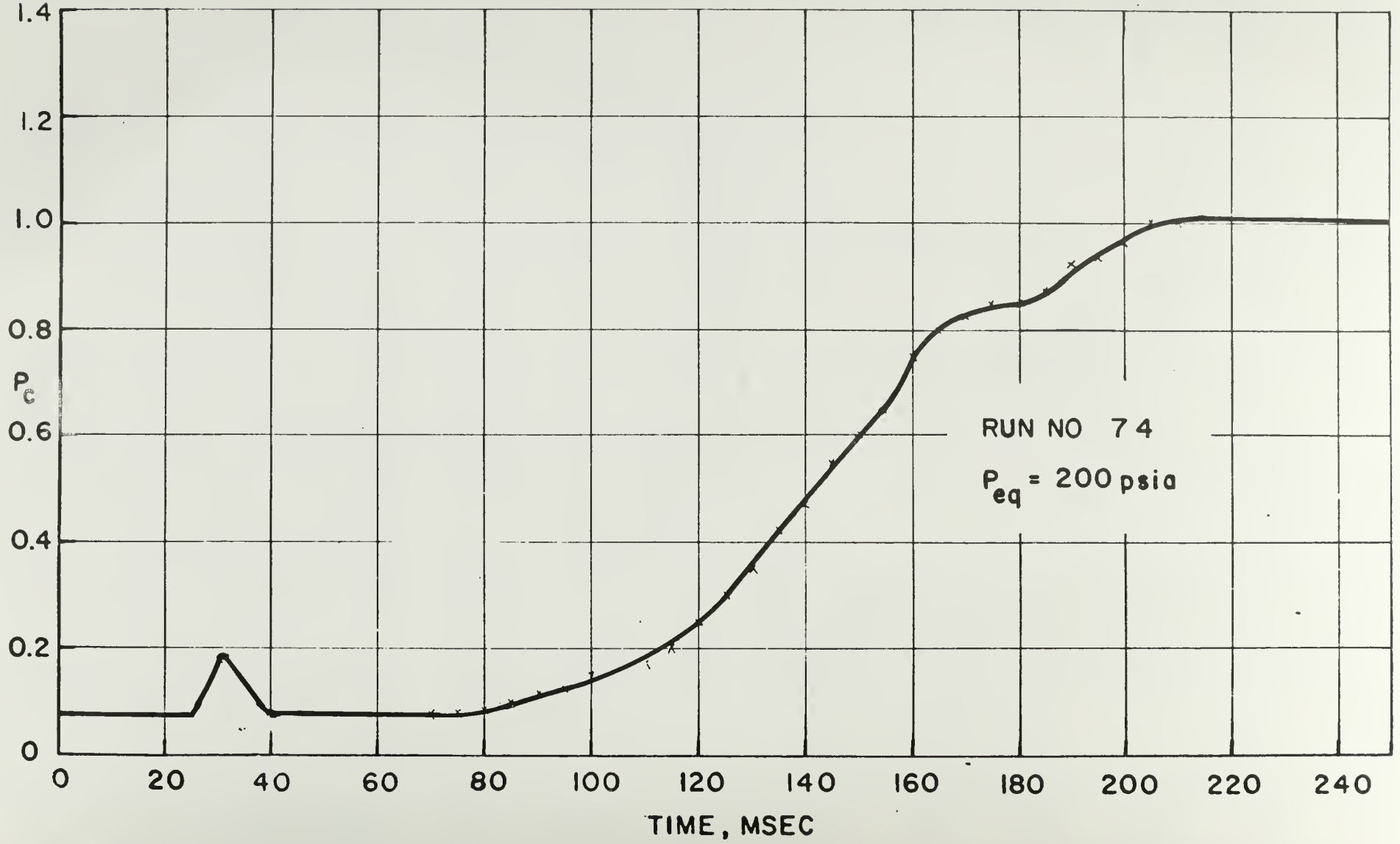
1.4
1.2
1.0
0.8
P_c
0.6
0.4
0.2
0
0
20
40
60
80
100
120
140
160
180
200
220
240
TIME, MSEC
RUN NO 74
P_{eq} = 200 psia

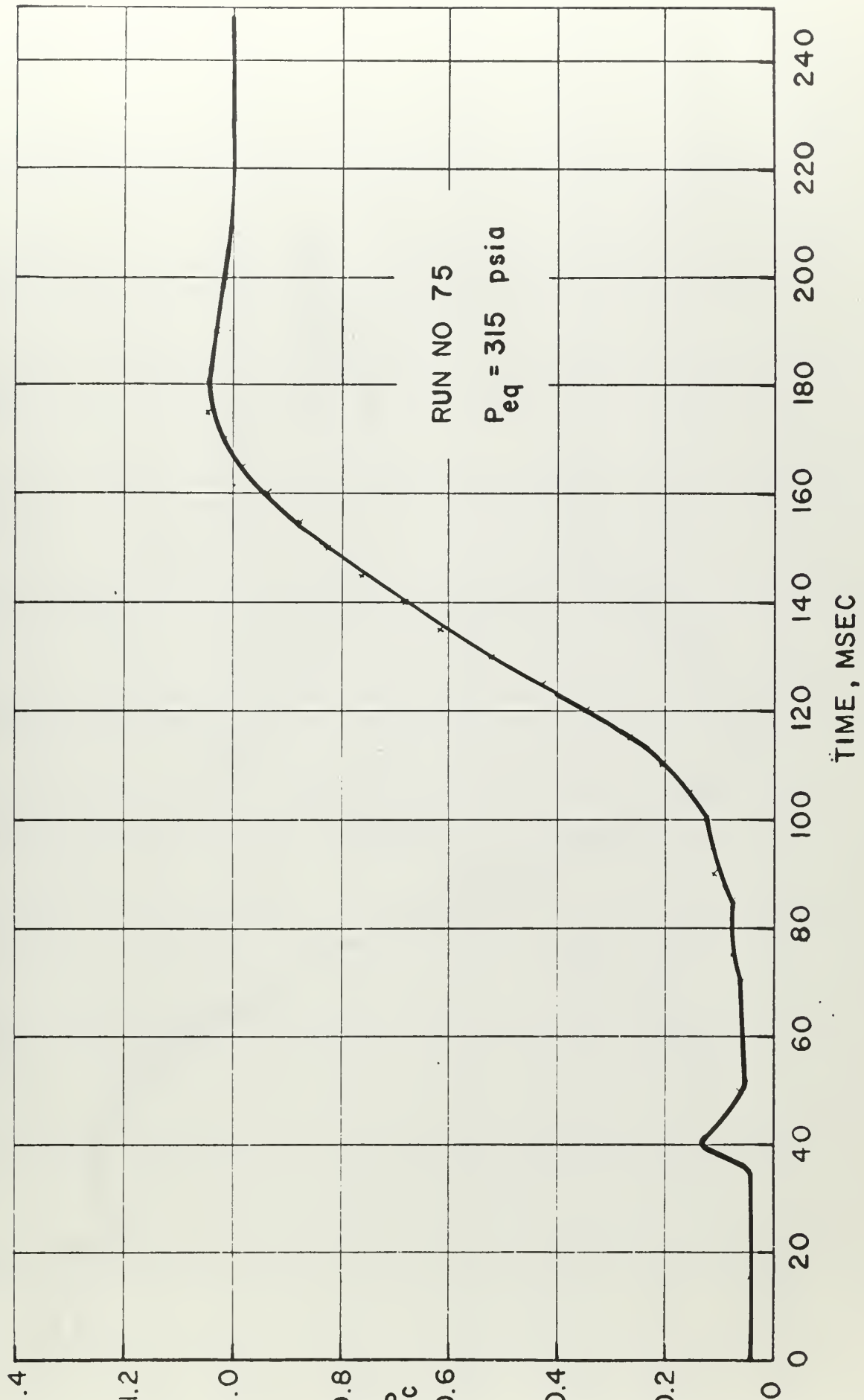
RUN NO 75
P_{eq} = 315 psia
P_c
TIME, MSEC
0
0.2
0.4
0.6
0.8
1.0
1.2
1.4
0
20
40
60
80
100
120
140
160
180
200
220
240

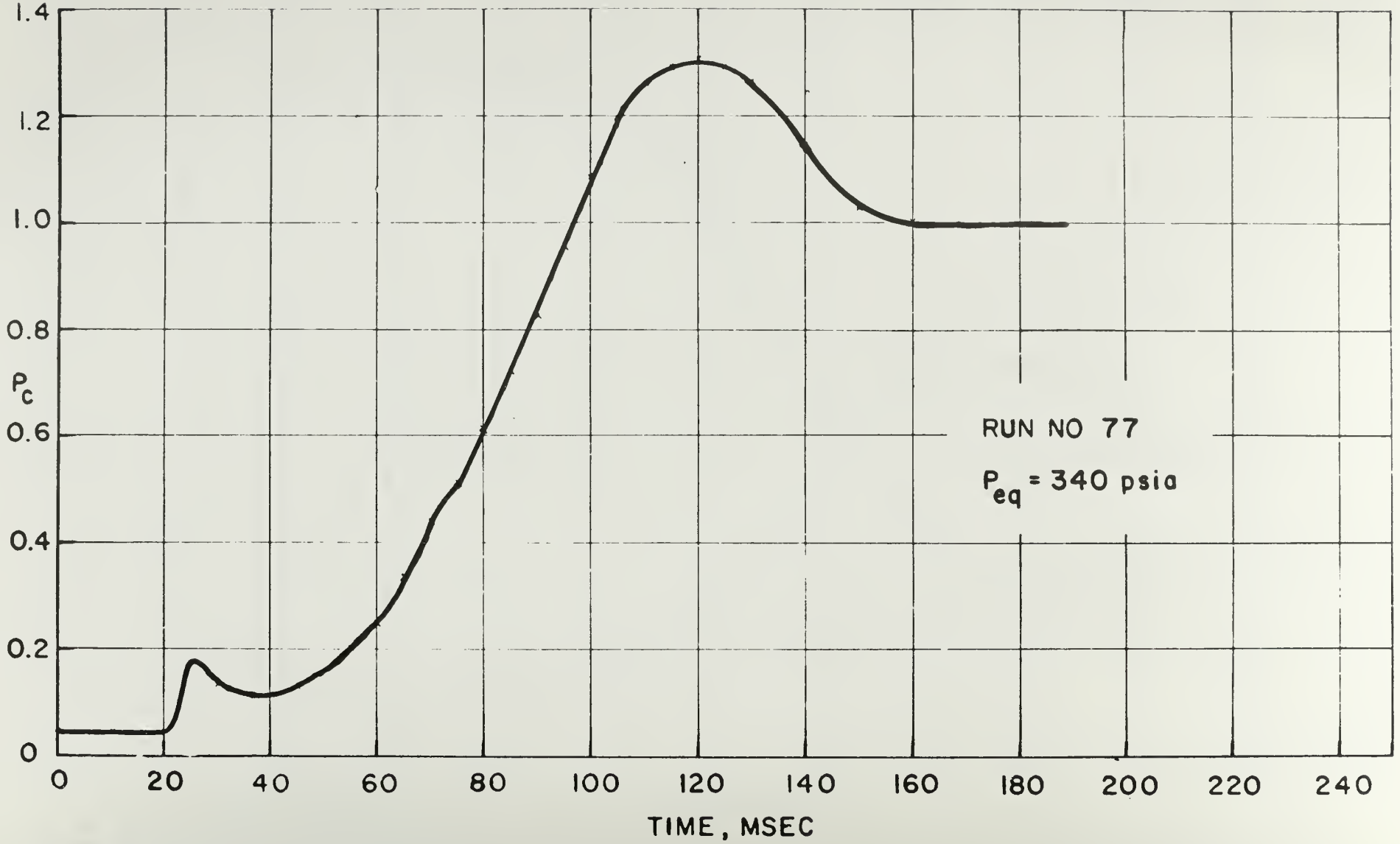
1.4
1.2
1.0
0.8
P_c
0.6
0.4
0.2
0
0
20
40
60
80
100
120
140
160
180
200
220
240
TIME, MSEC
RUN NO 77
P_{eq} = 340 psia

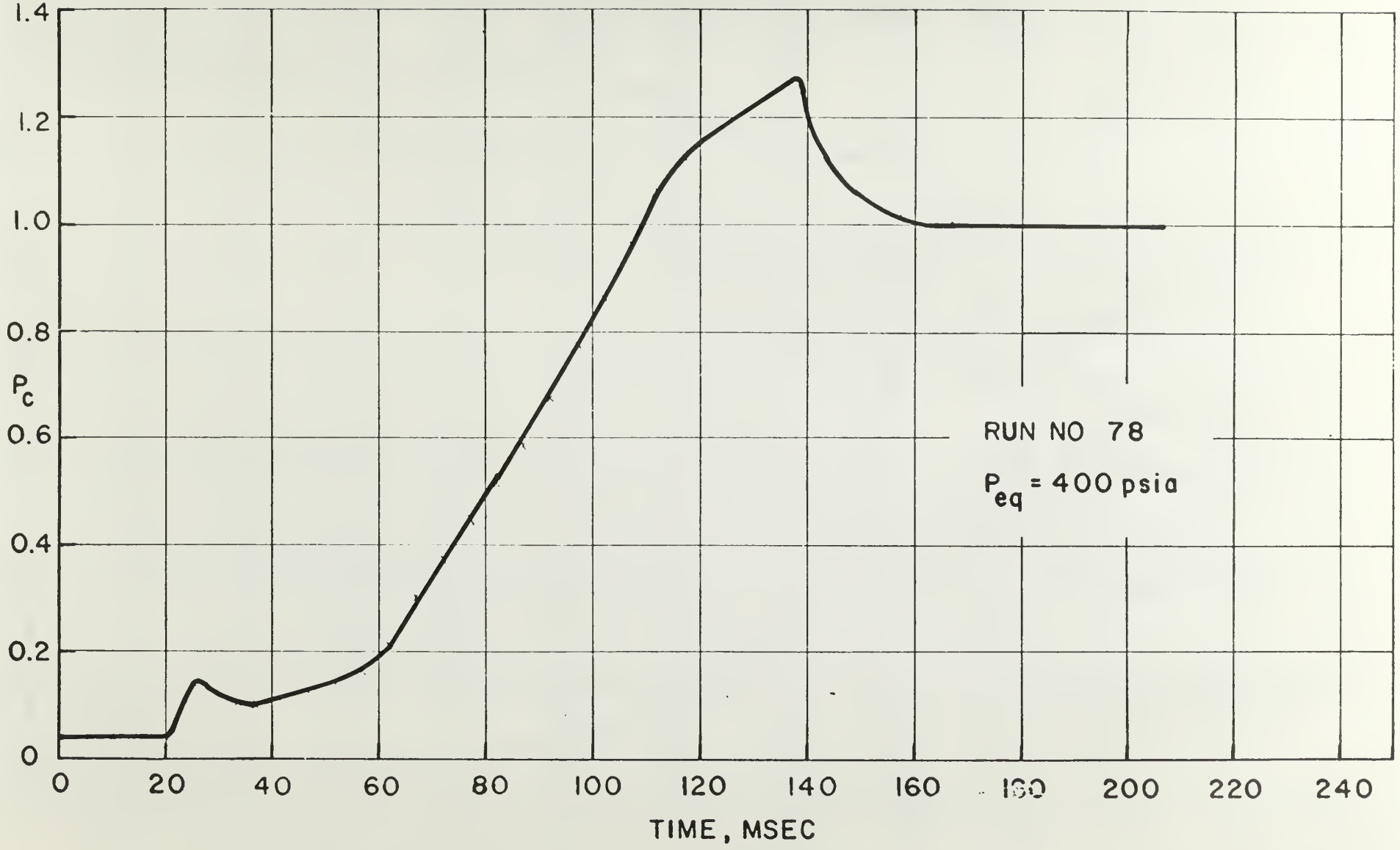
1.4
1.2
1.0
0.8
P_c
0.6
0.4
0.2
0
0
20
40
60
80
100
120
140
160
180
200
220
240
TIME, MSEC
RUN NO 78
P_{eq} = 400 psia

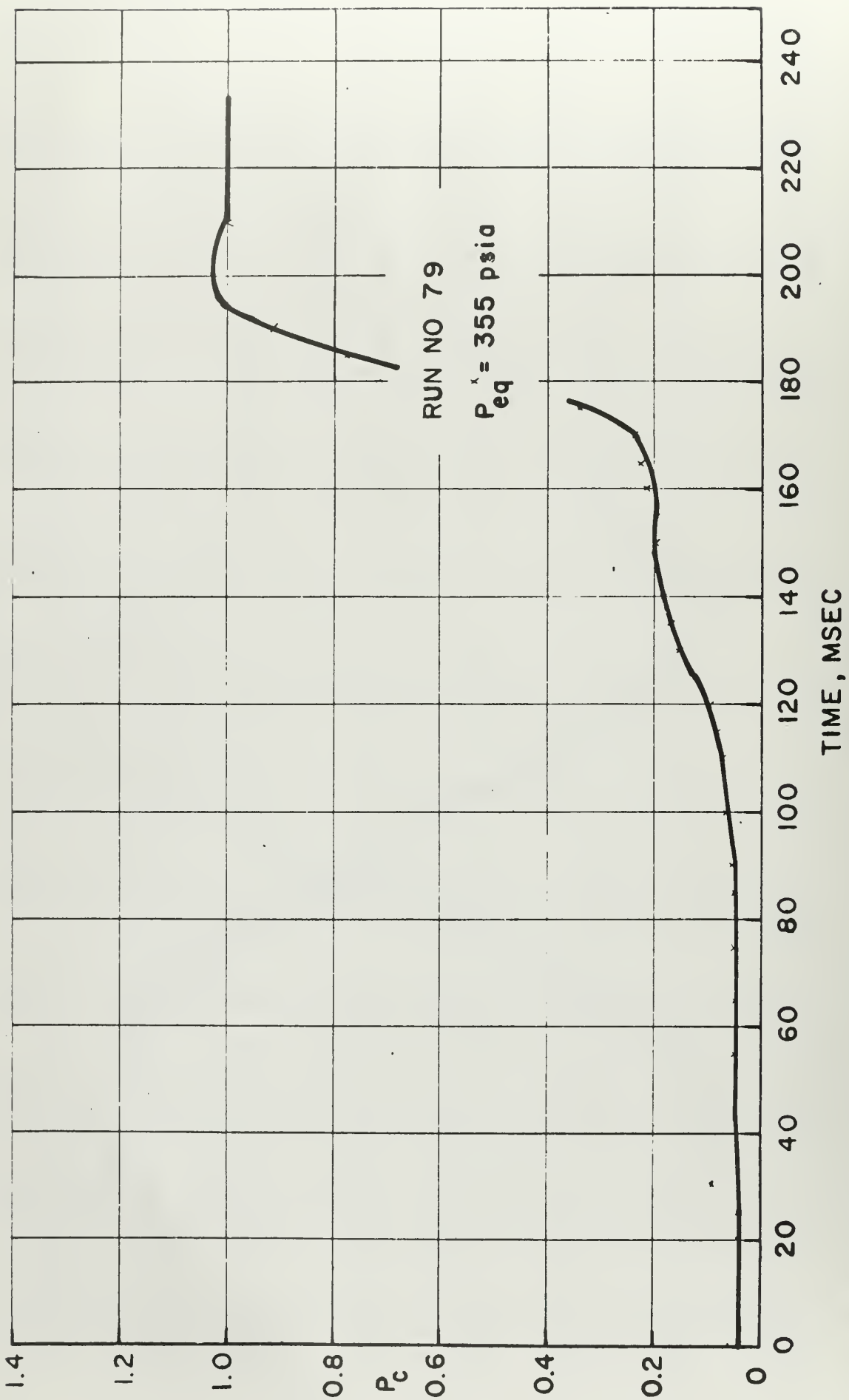
RUN NO 79
P_{eq}' = 355 psia
P_c
1.4
1.2
1.0
0.8
0.6
0.4
0.2
0
0
20
40
60
80
100
120
140
160
180
200
220
240
TIME, MSEC

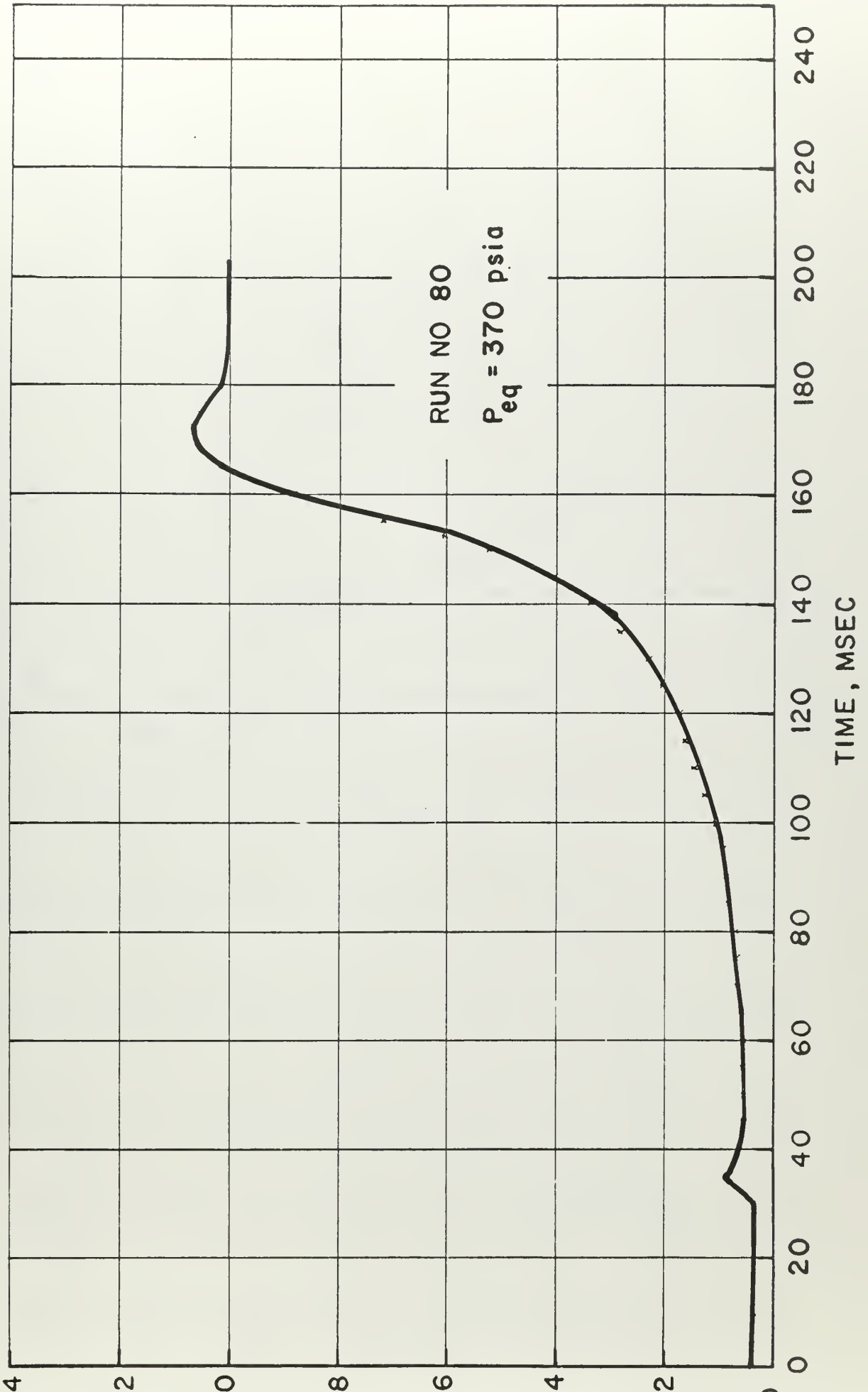
RUN NO 80
P_{eq} = 370 psia
P_c
1.4
1.2
1.0
0.8
0.6
0.4
0.2
0
0
20
40
60
80
100
120
140
160
180
200
220
240
TIME, MSEC

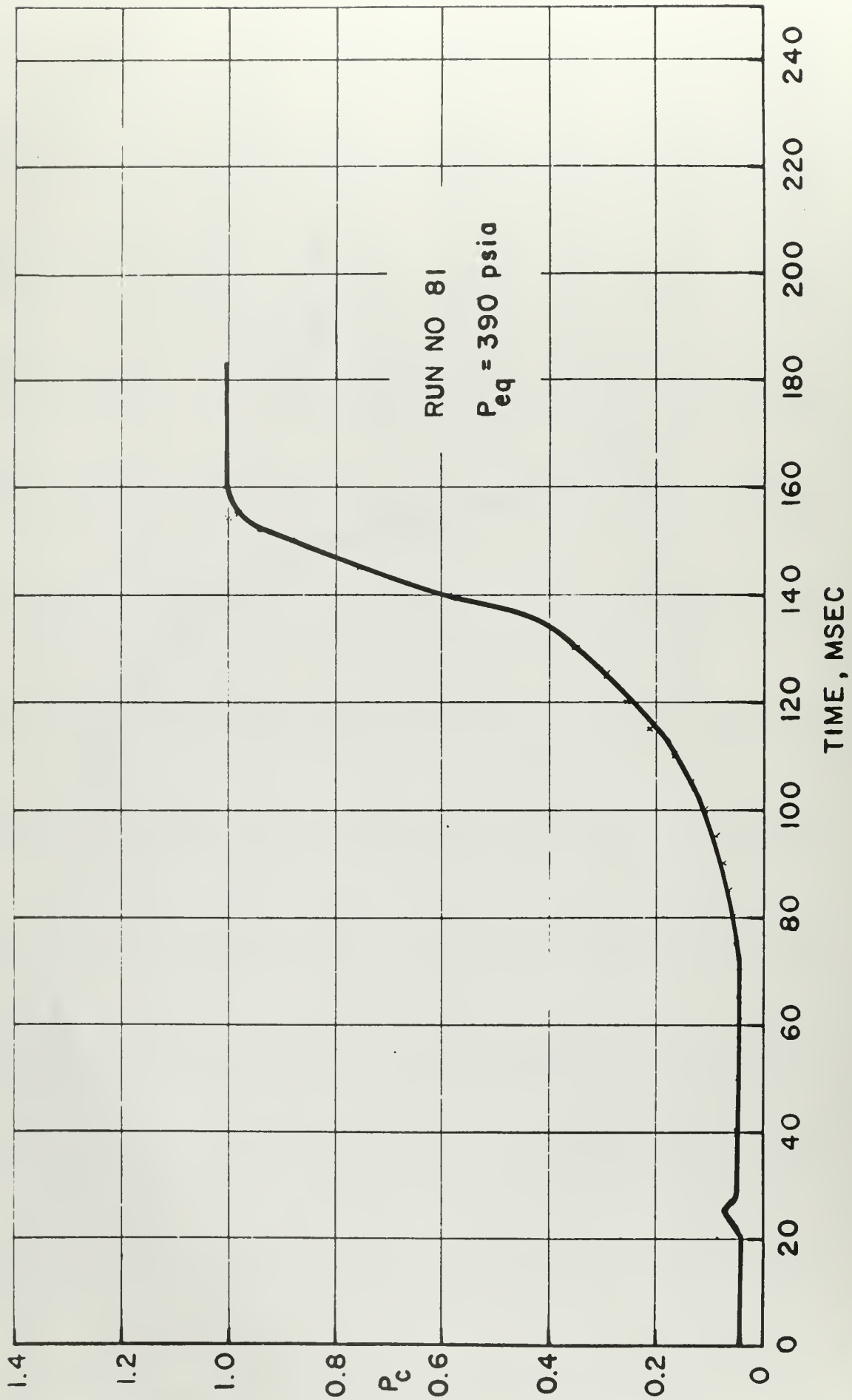
RUN NO 81
P_{eq} = 390 psia
P_c
TIME, MSEC
0
0.2
0.4
0.6
0.8
1.0
1.2
1.4
0
20
40
60
80
100
120
140
160
180
200
220
240

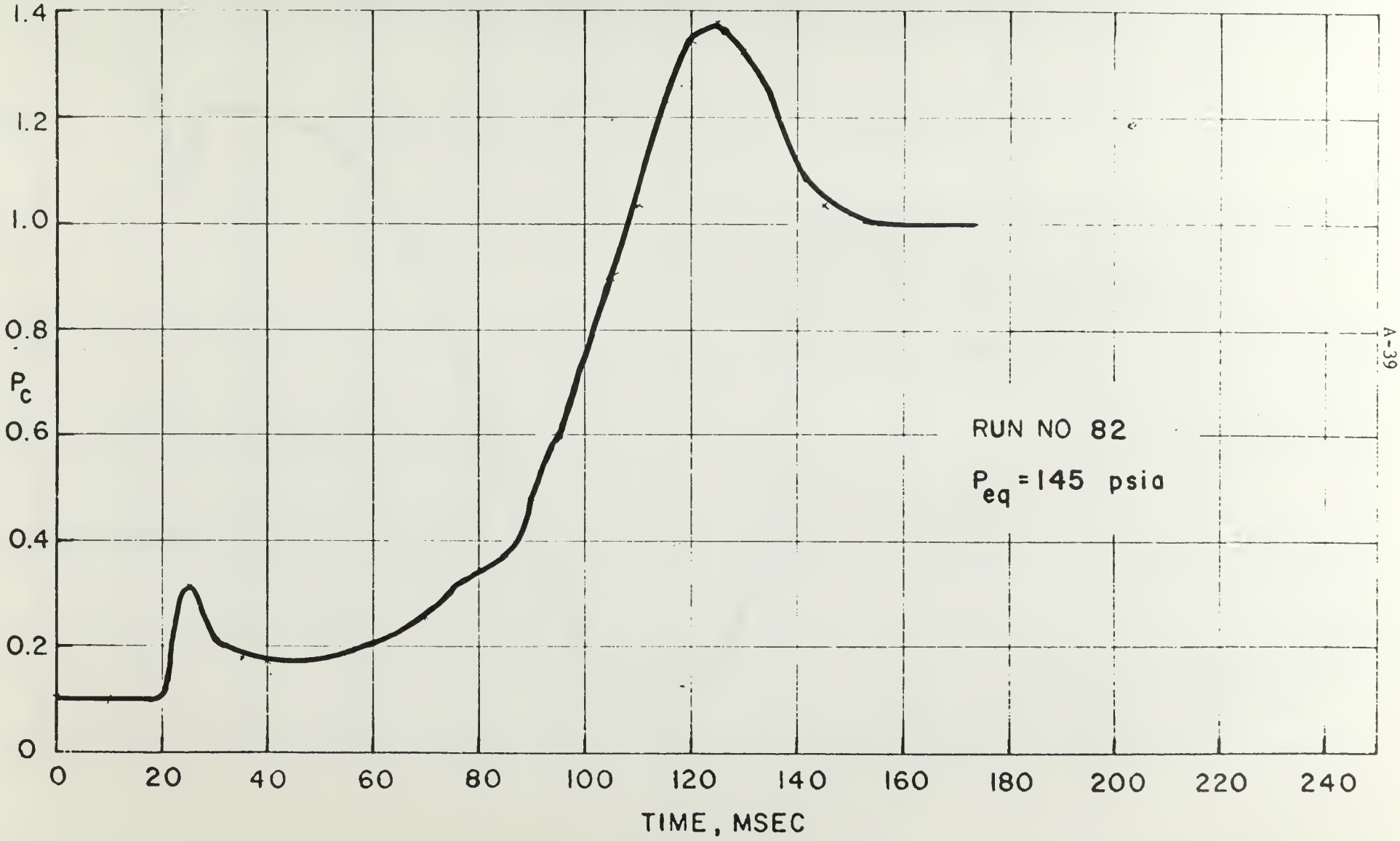
1.4
1.2
1.0
0.8
P_c
0.6
0.4
0.2
0
0
20
40
60
80
100
120
140
160
180
200
220
240
TIME, MSEC
RUN NO 82
P_{eq} = 145 psia

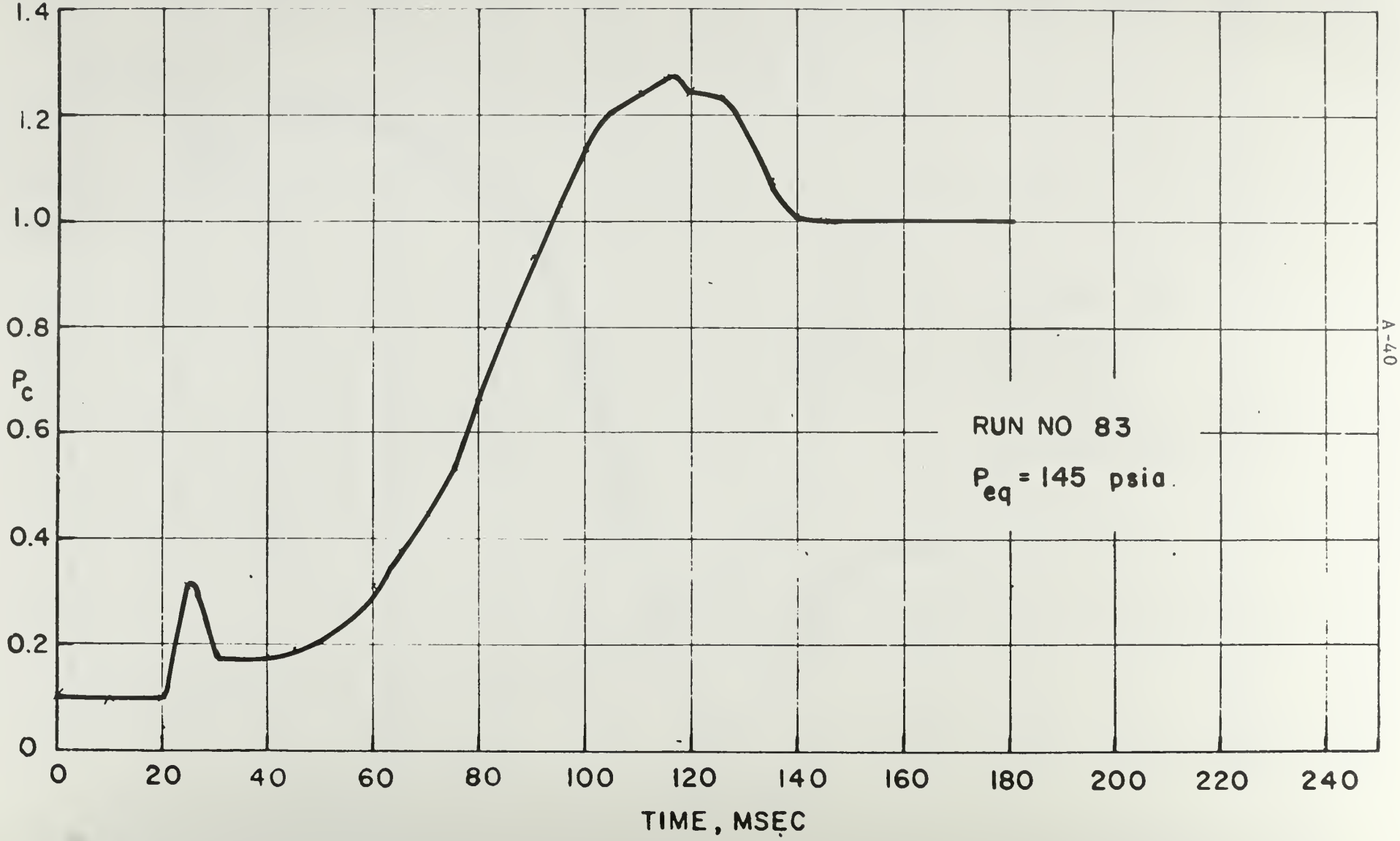
1.4
1.2
1.0
0.8
P_c
0.6
0.4
0.2
0
0
20
40
60
80
100
120
140
160
180
200
220
240
TIME, MSEC
RUN NO 83
P_{eq} = 145 psia

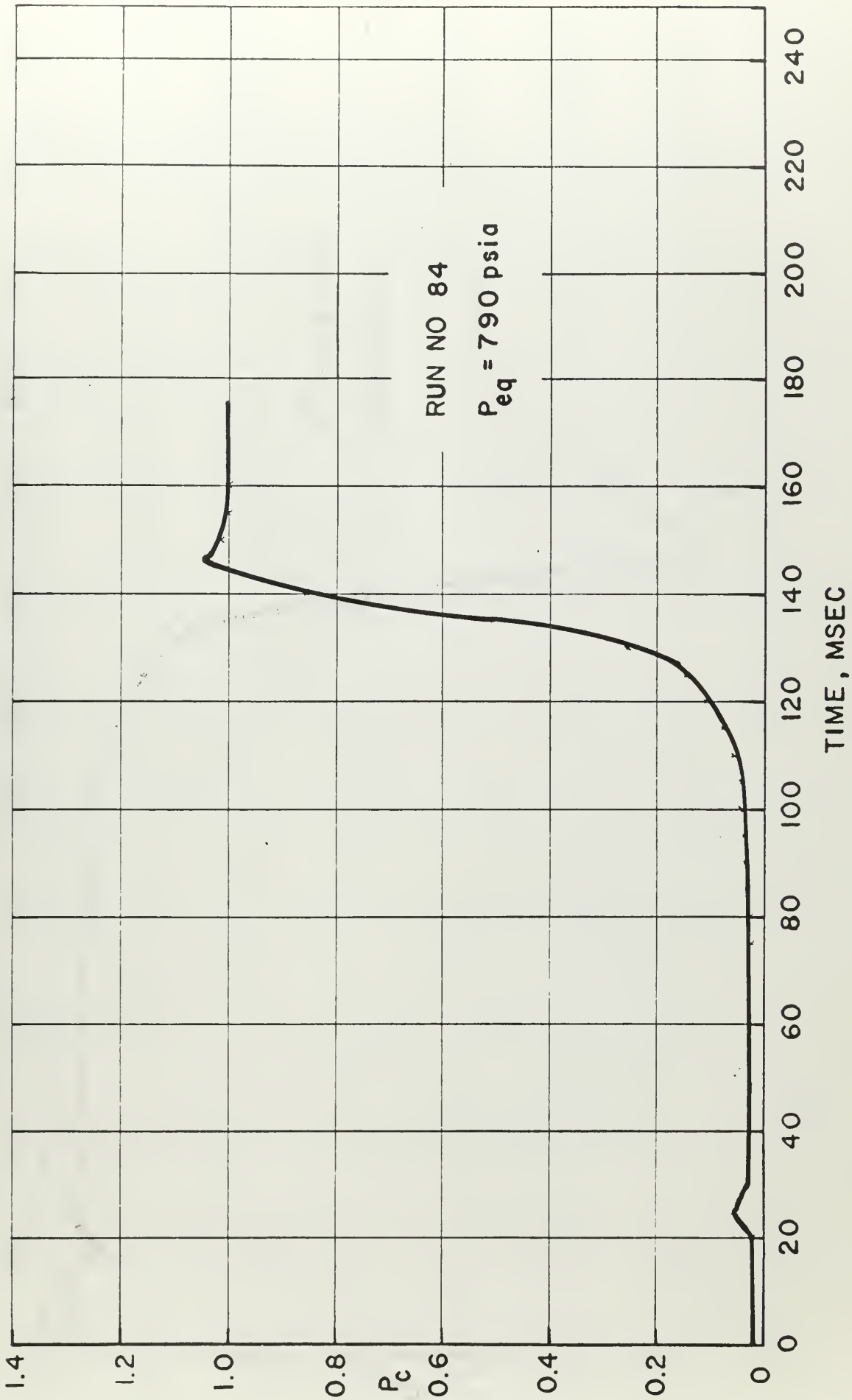
RUN NO 84
P_{eq} = 790 psia
P_c
1.4
1.2
1.0
0.8
0.6
0.4
0.2
0
0
20
40
60
80
100
120
140
160
180
200
220
240
TIME, MSEC

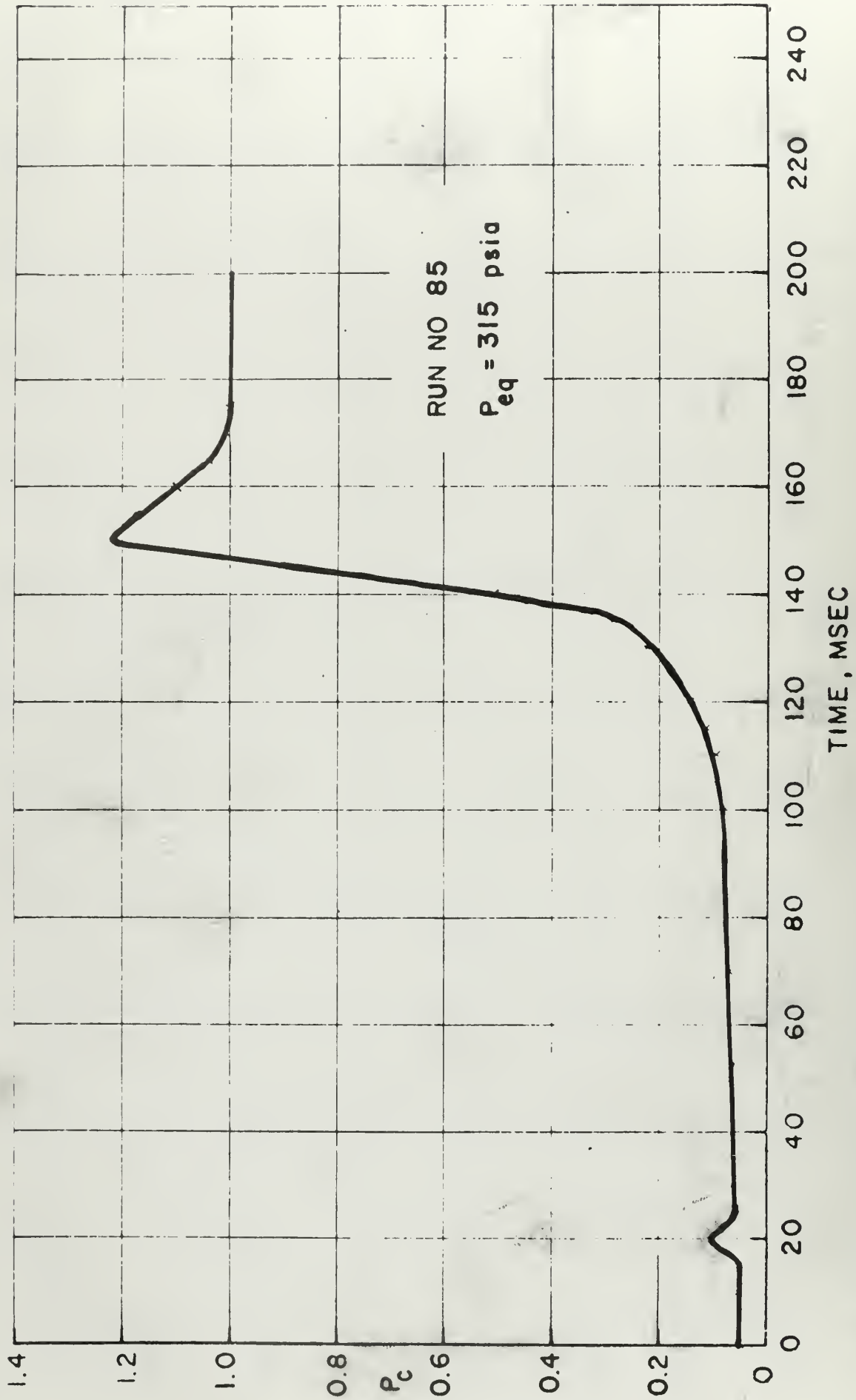
RUN NO 85
P_{eq} = 315 psia
P_c
TIME, MSEC
0
0.2
0.4
0.6
0.8
1.0
1.2
1.4
0
20
40
60
80
100
120
140
160
180
200
220
240

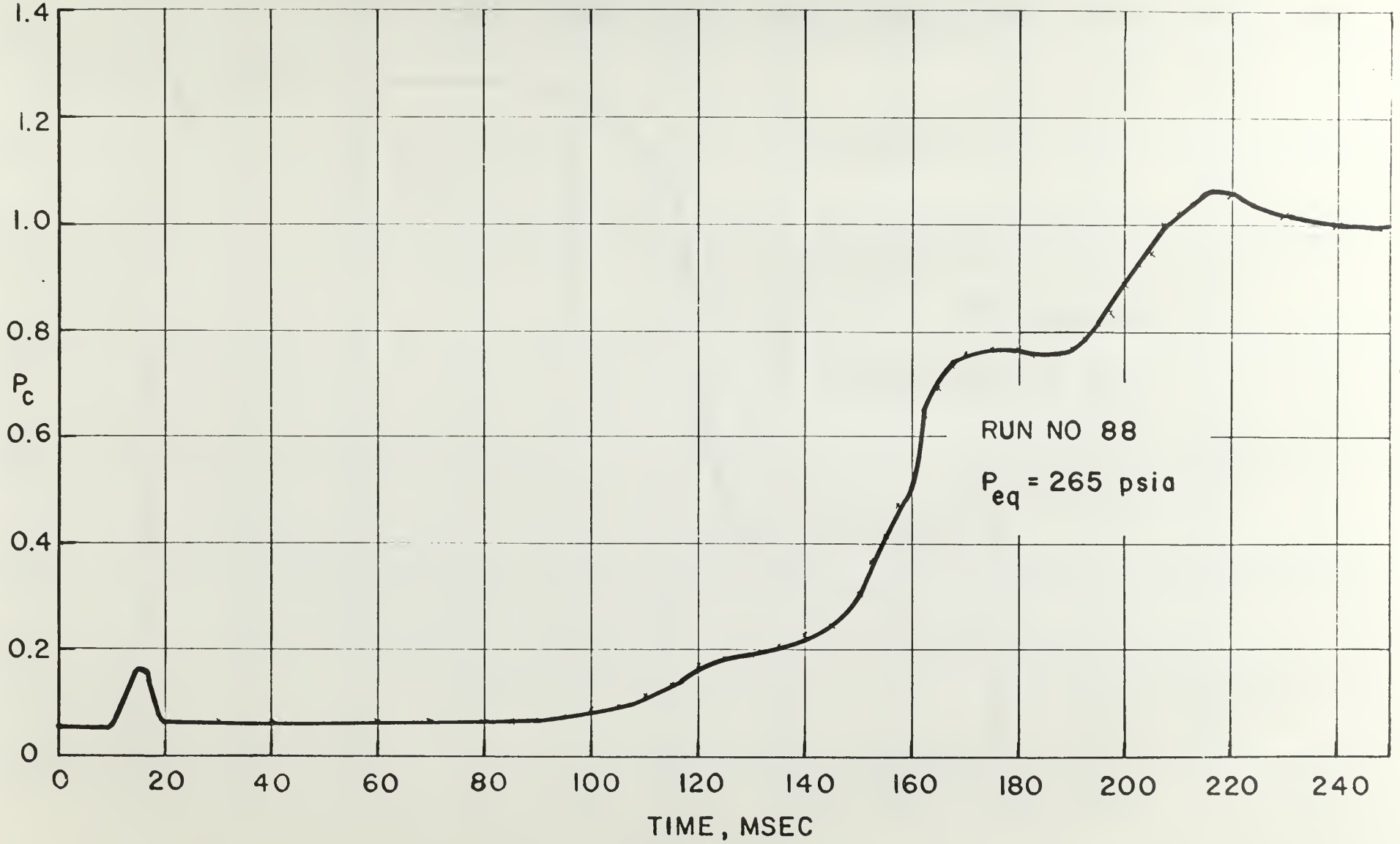
1.4
1.2
1.0
0.8
P_c
0.6
0.4
0.2
0
0
20
40
60
80
100
120
140
160
180
200
220
240
TIME, MSEC
RUN NO 88
P_{eq} = 265 psia

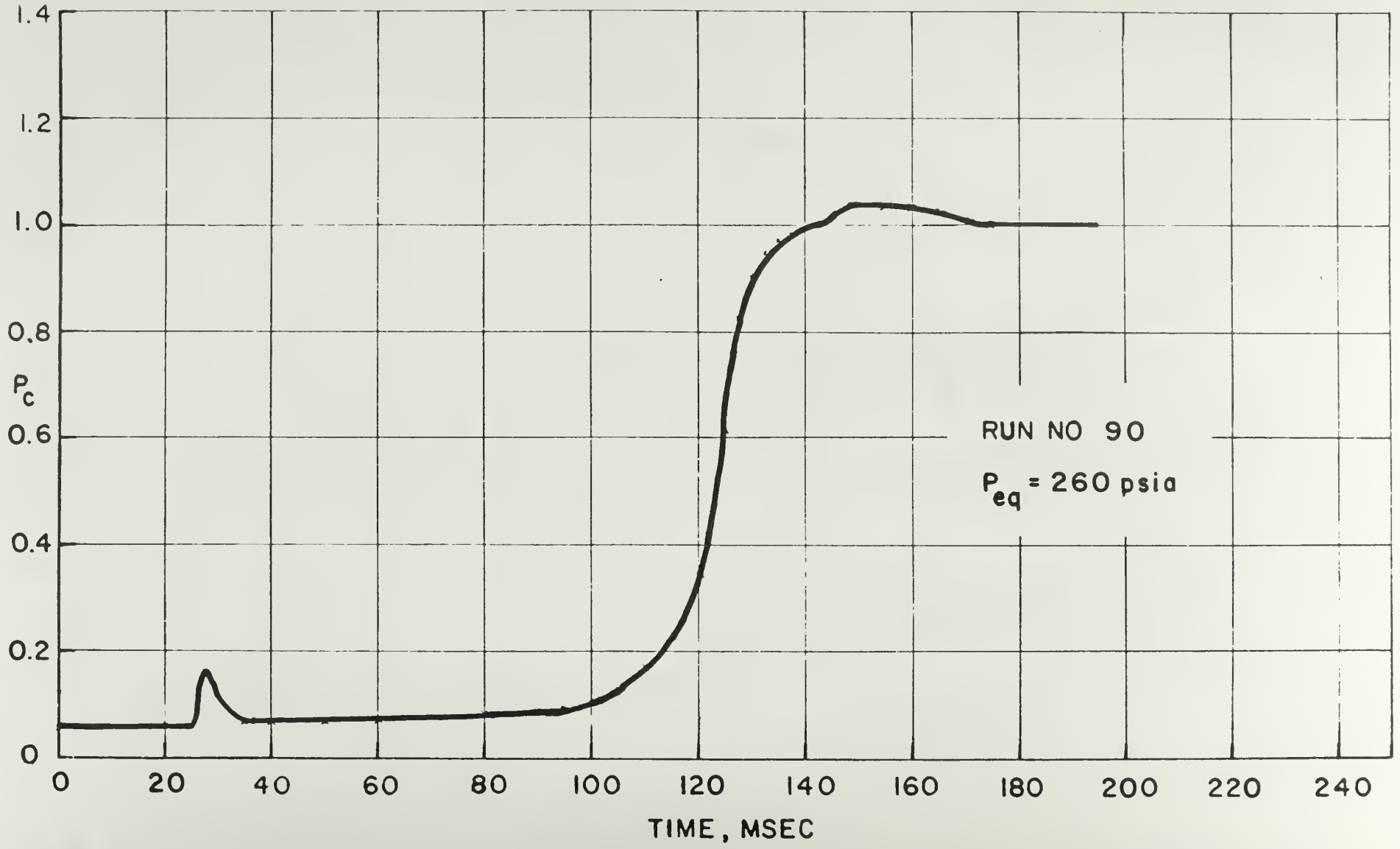
1.4
1.2
1.0
0.8
P_c
0.6
0.4
0.2
0
0
20
40
60
80
100
120
140
160
180
200
220
240
TIME, MSEC
RUN NO 90
P_{eq} = 260 psia

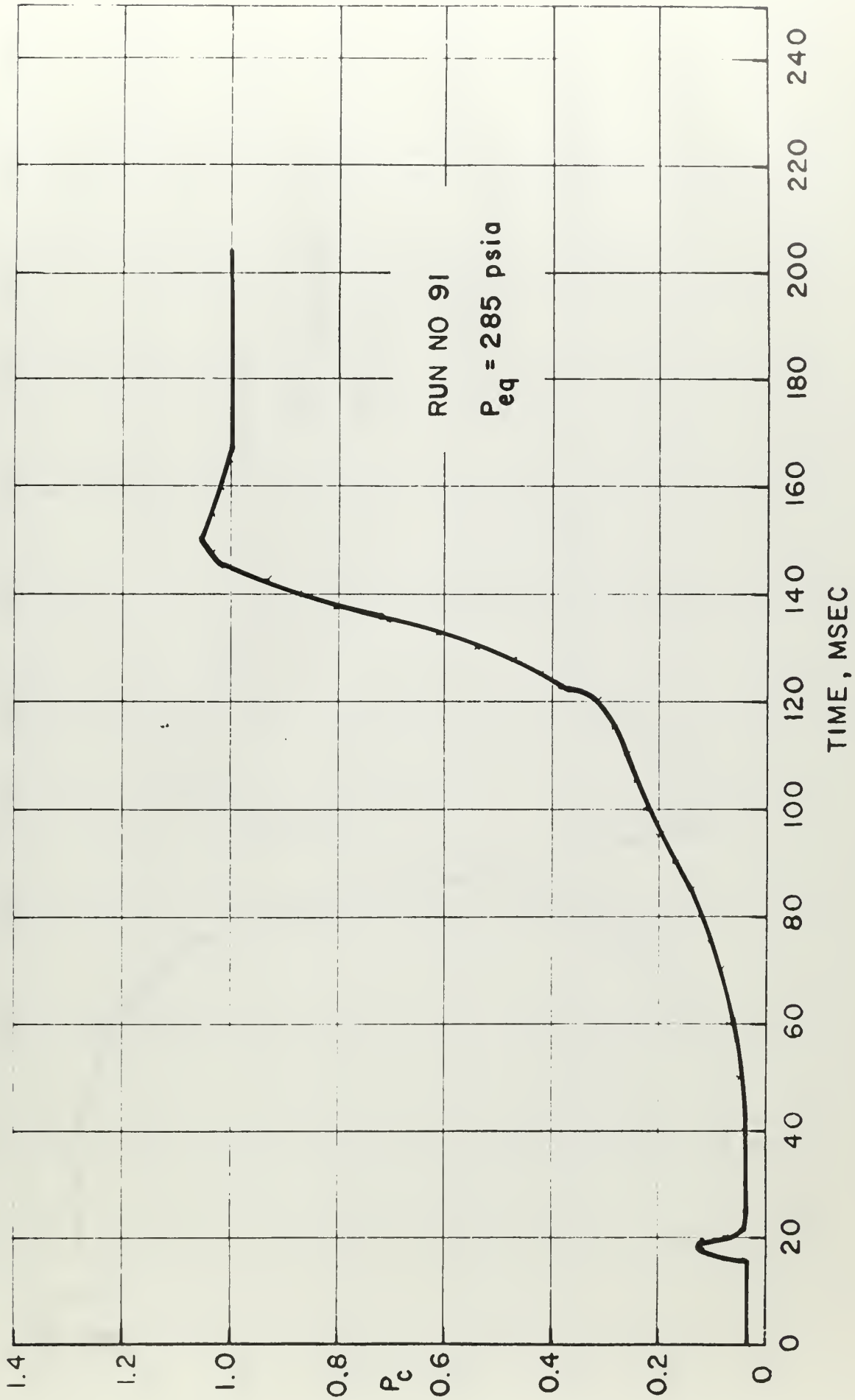
RUN NO 91
P_{eq} = 285 psia
P_c
TIME, MSEC
0
0.2
0.4
0.6
0.8
1.0
1.2
1.4
0
20
40
60
80
100
120
140
160
180
200
220
240

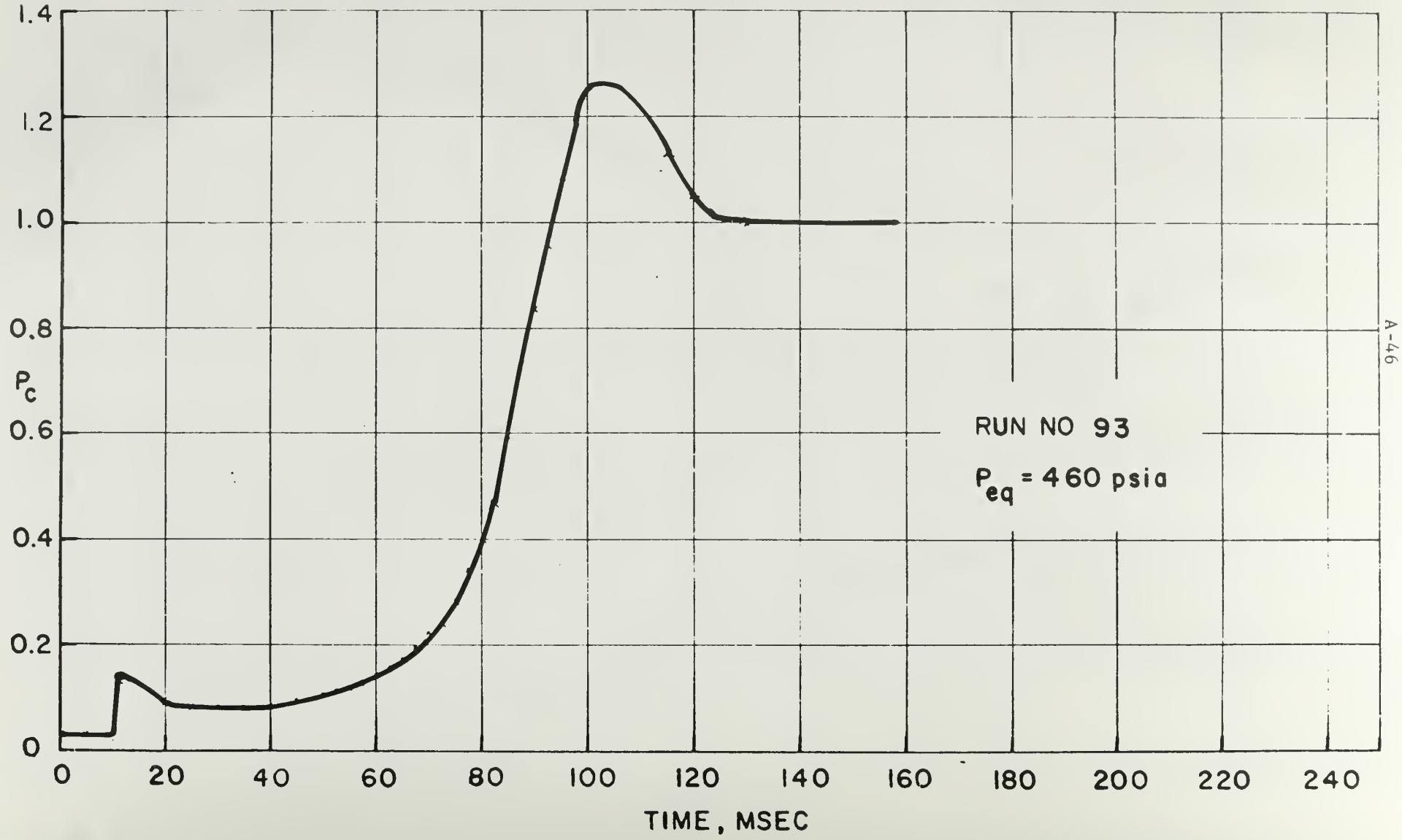
1.4
1.2
1.0
0.8
P_c
0.6
0.4
0.2
0
0
20
40
60
80
100
120
140
160
180
200
220
240
TIME, MSEC
RUN NO 93
P_{eq} = 460 psia

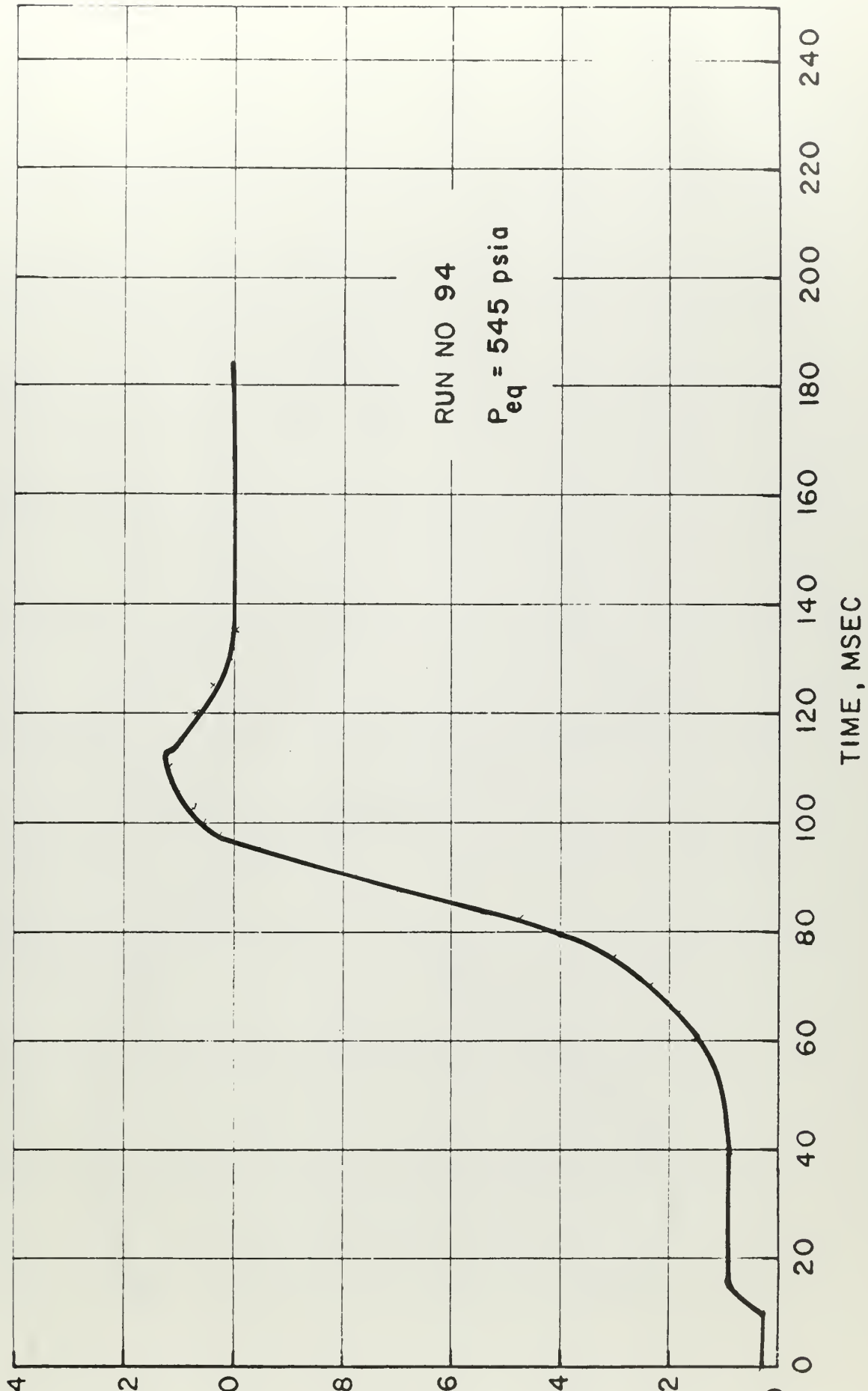
RUN NO 94
P_{eq} = 545 psia
P_c
1.4
1.2
1.0
0.8
0.6
0.4
0.2
0
0
20
40
60
80
100
120
140
160
180
200
220
240
TIME, MSEC

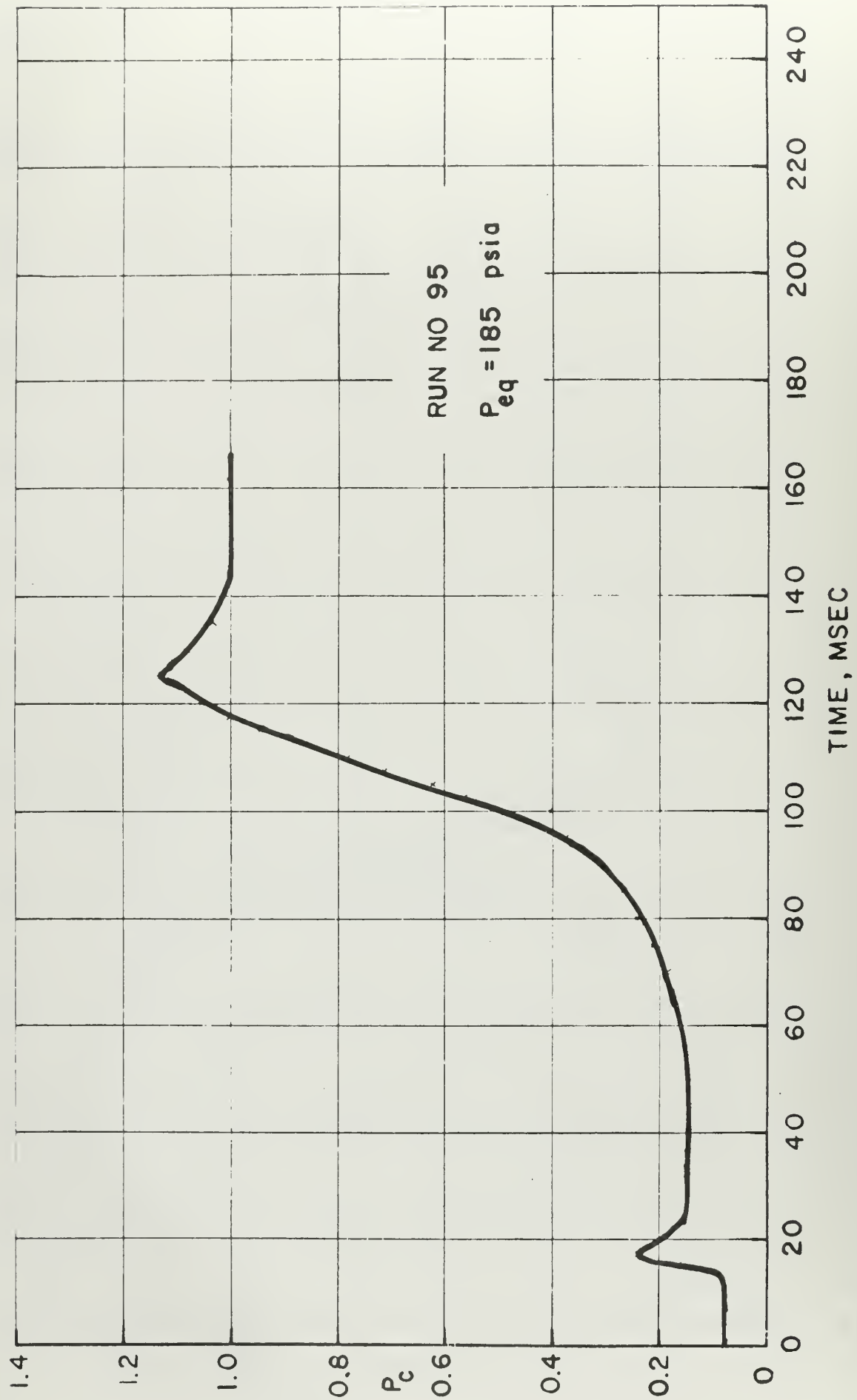
RUN NO 95
P_{eq}=185 psia
P_c
TIME, MSEC
0
0.2
0.4
0.6
0.8
1.0
1.2
1.4
0
20
40
60
80
100
120
140
160
180
200
220
240

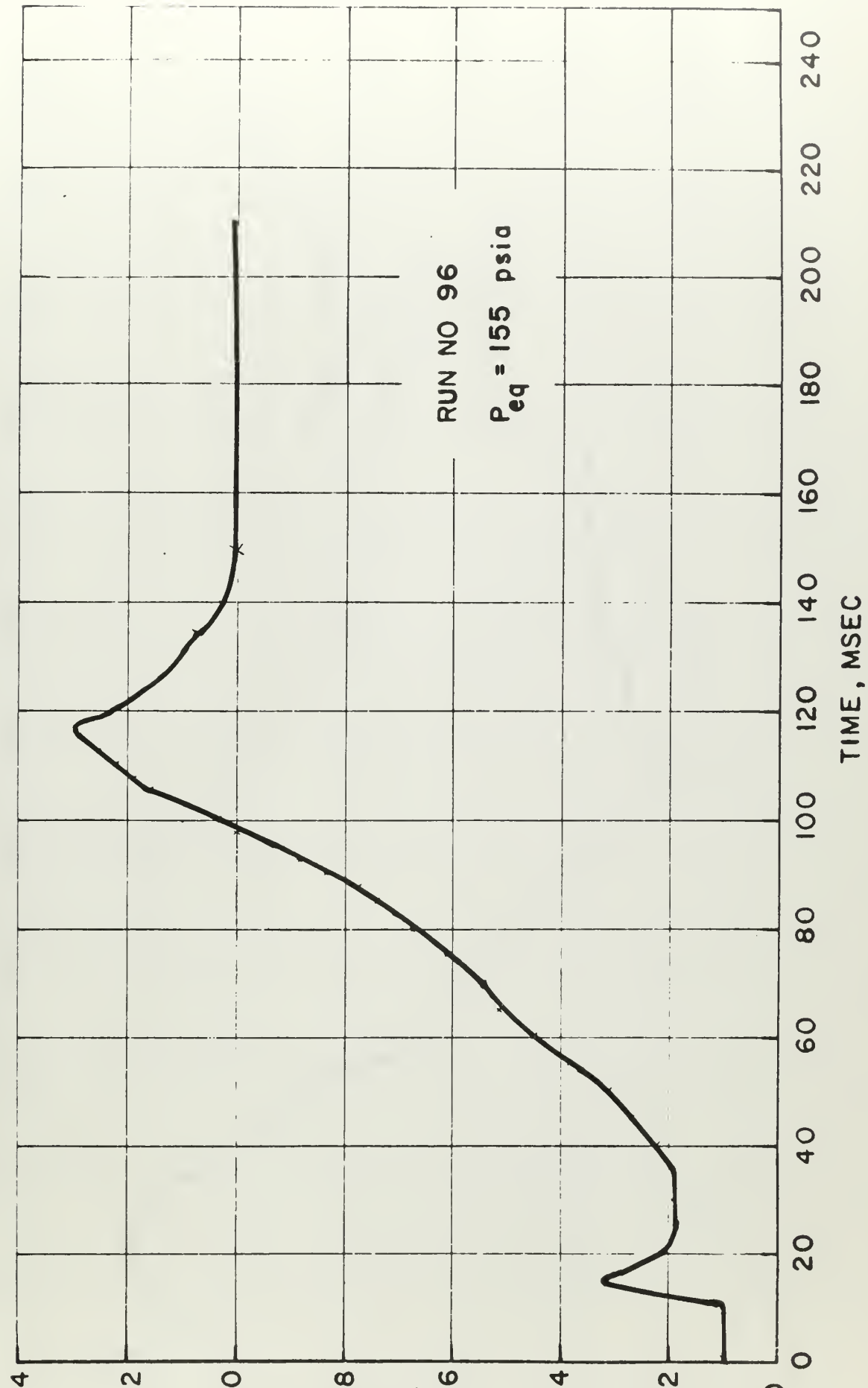
RUN NO 96
P_{eq} = 155 psia
P_c
TIME, MSEC
0
0.2
0.4
0.6
0.8
1.0
1.2
1.4
0
20
40
60
80
100
120
140
160
180
200
220
240

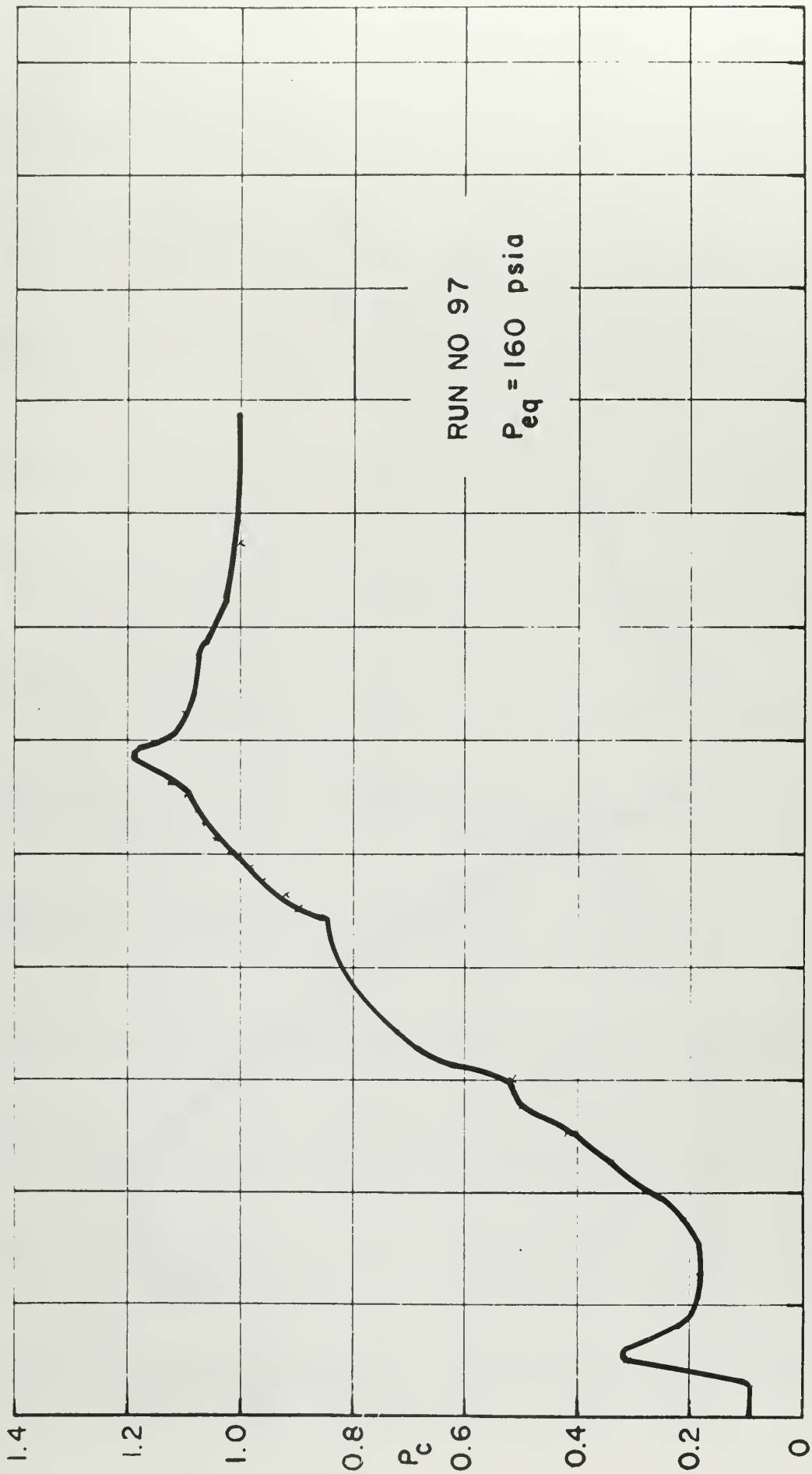
RUN NO 97
P_{eq} = 160 psia
P_c
TIME, MSEC
0
0.2
0.4
0.6
0.8
1.0
1.2
1.4
20
40
60
80
100
120
140
160
180
200
220
240

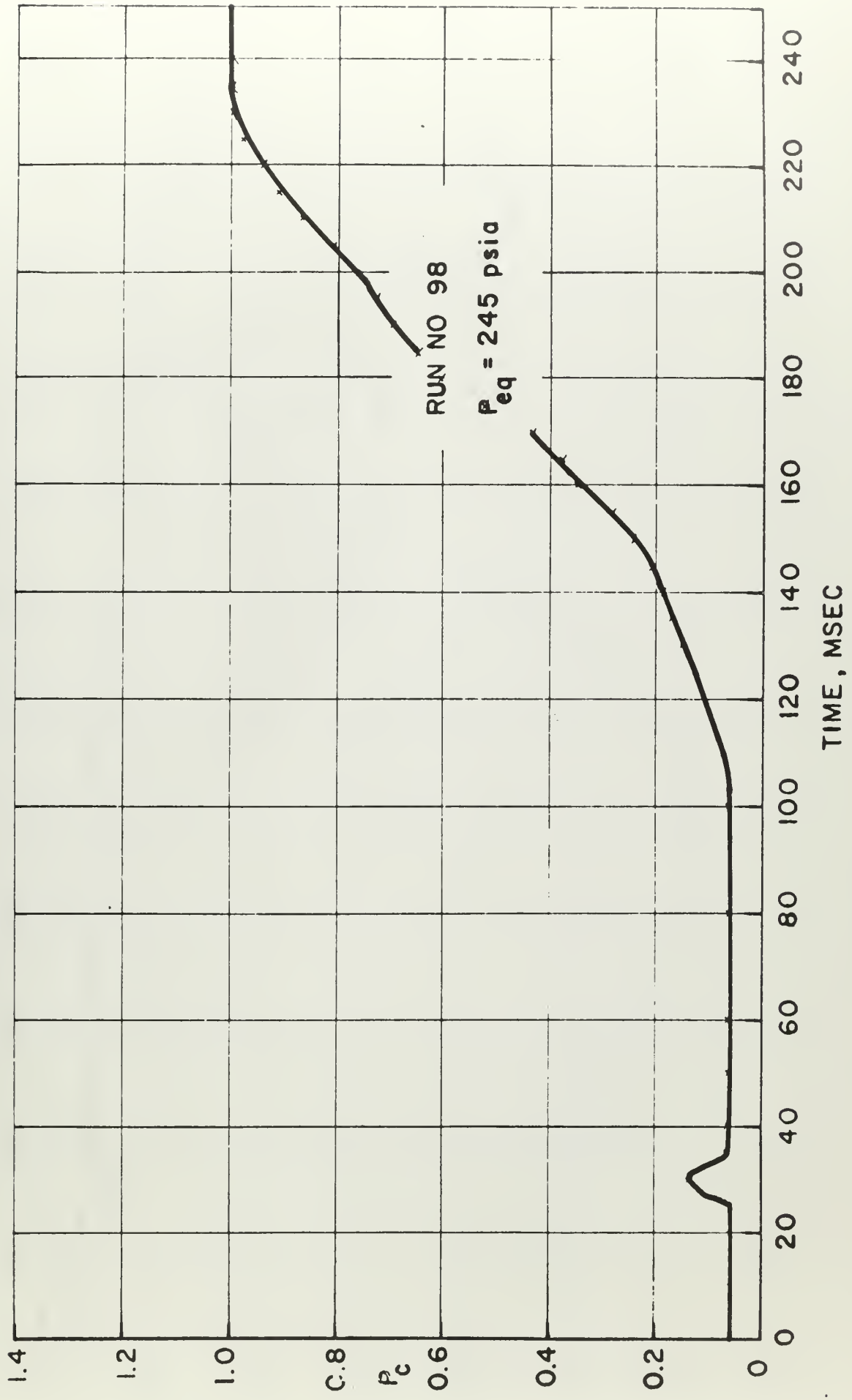
RUN NO 98
P_{eq} = 245 psia
P_c
1.4
1.2
1.0
0.8
0.6
0.4
0.2
0
0
20
40
60
80
100
120
140
160
180
200
220
240
TIME, MSEC

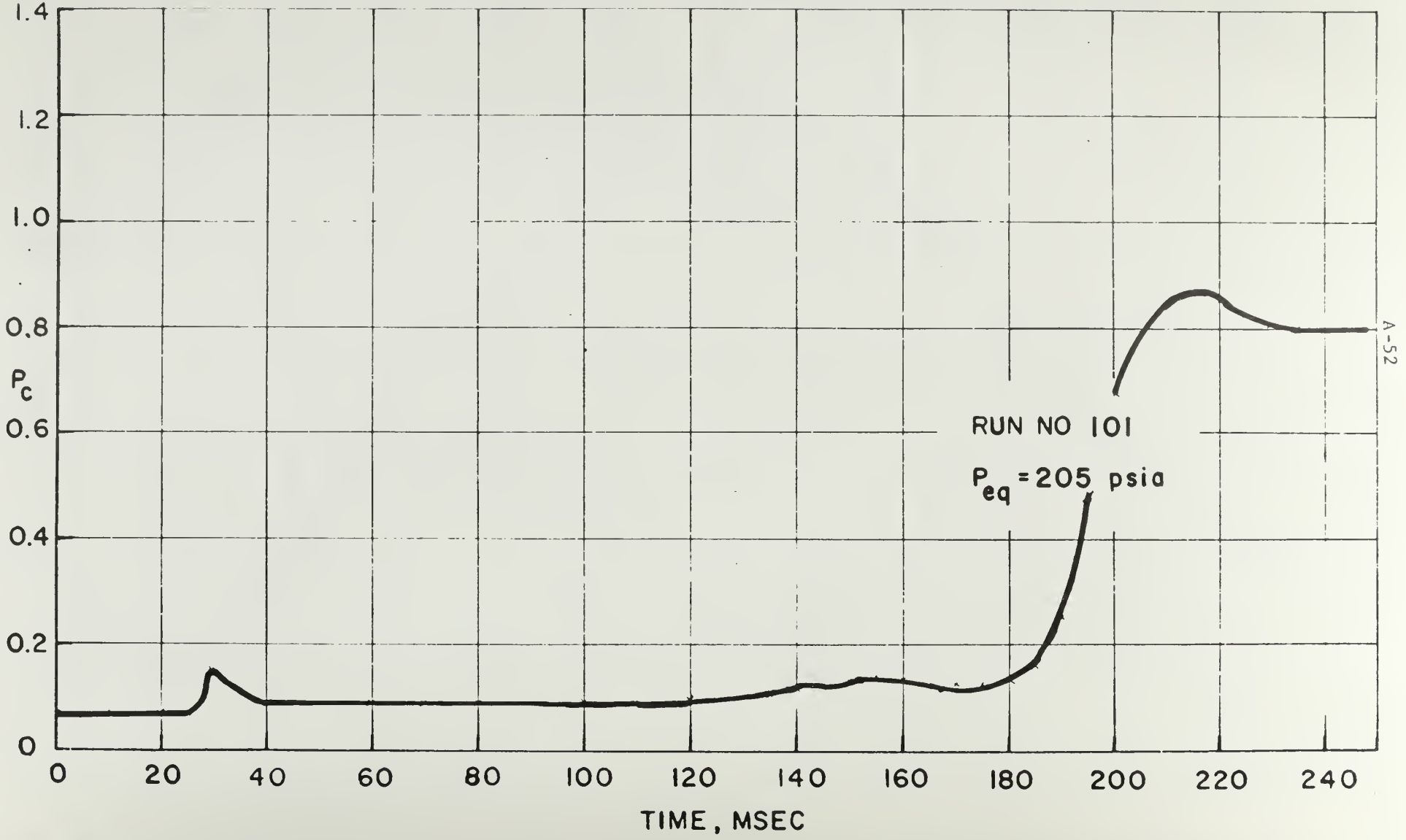
1.4
1.2
1.0
0.8
P_c
0.6
0.4
0.2
0
0
20
40
60
80
100
120
140
160
180
200
220
240
TIME, MSEC
RUN NO 101
P_{eq} = 205 psia

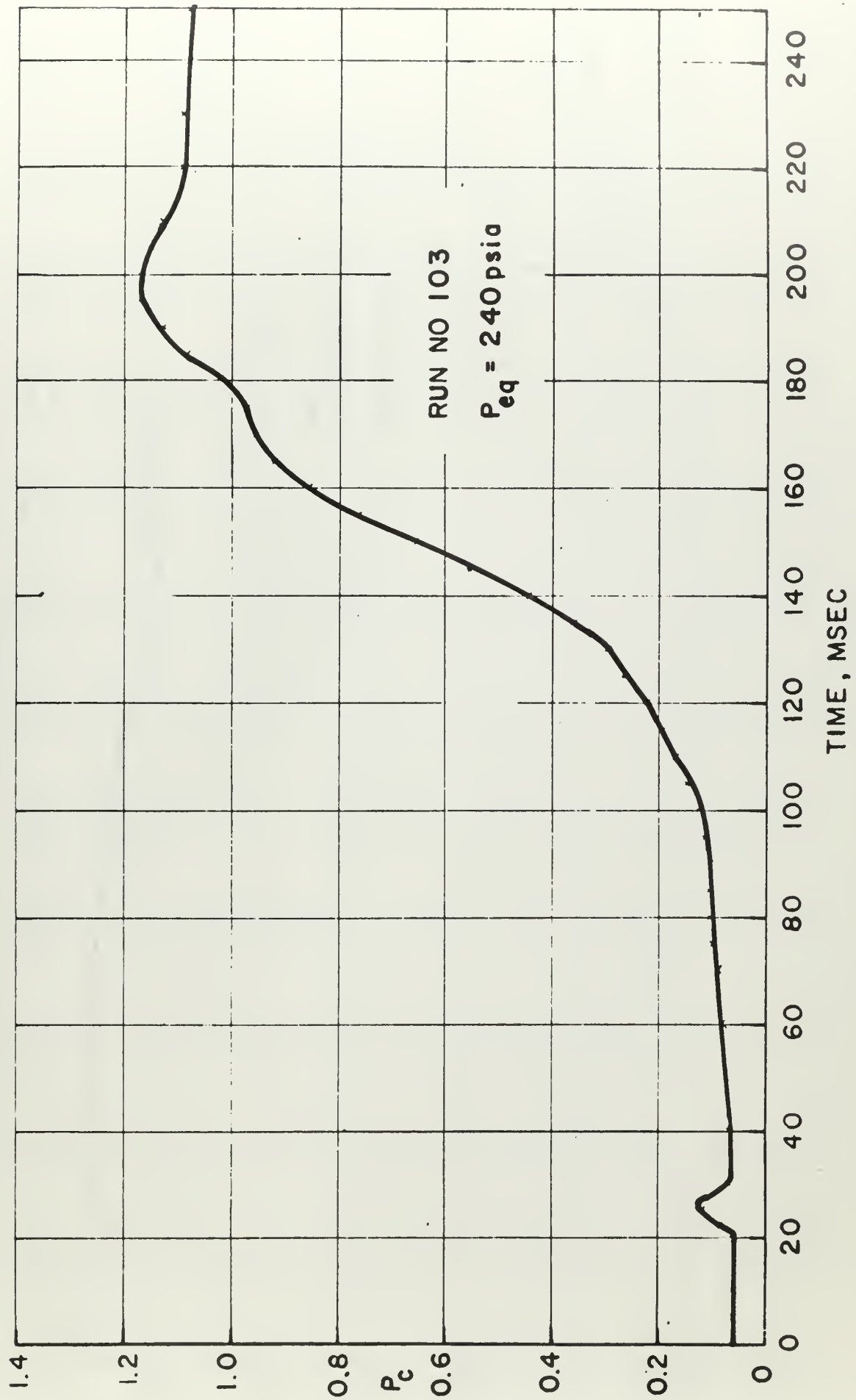
RUN NO 103
P_{eq} = 240 psia
P_c
TIME, MSEC
0
0.2
0.4
0.6
0.8
1.0
1.2
1.4
0
20
40
60
80
100
120
140
160
180
200
220
240

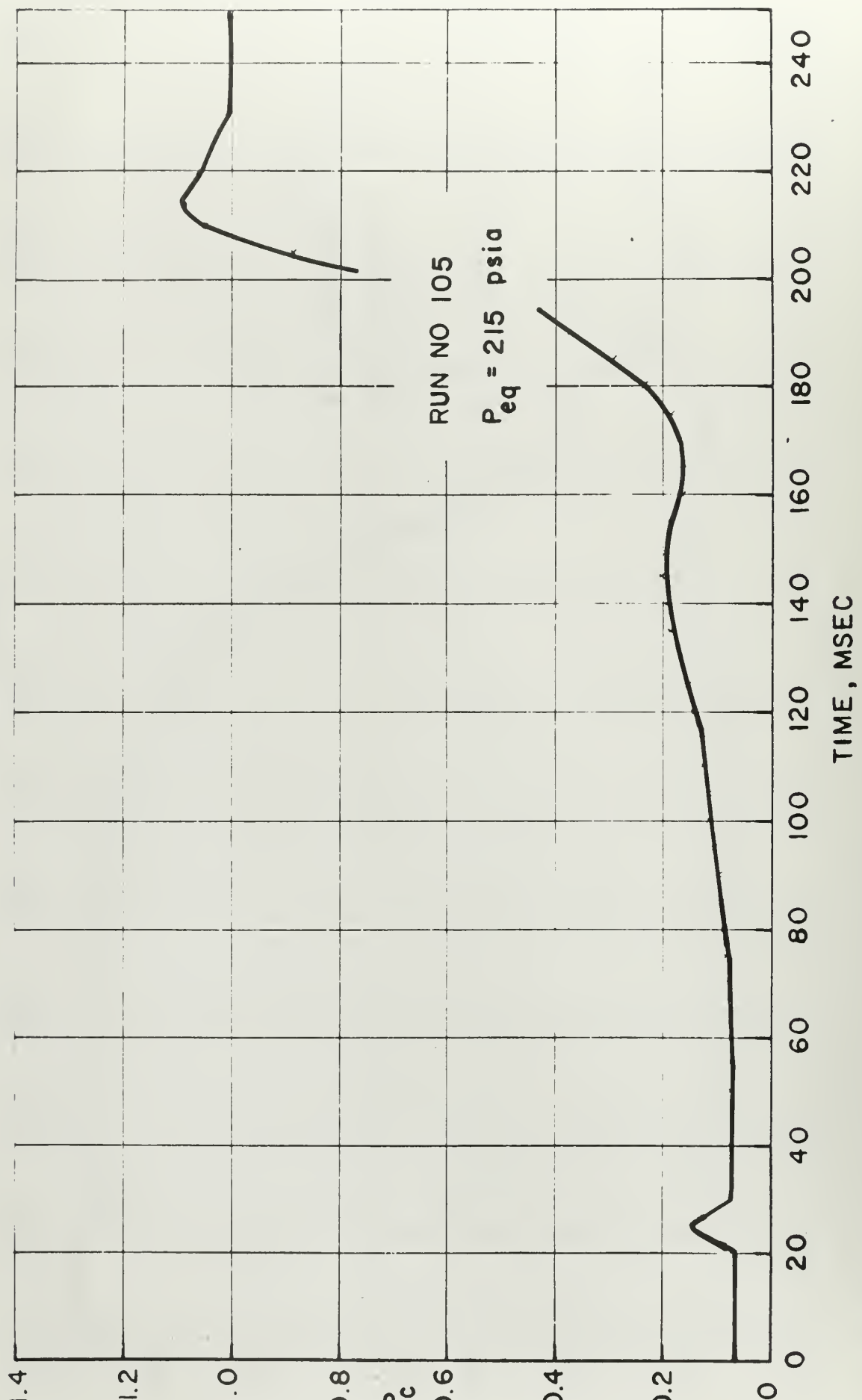
RUN NO 105
P_{eq} = 215 psia
P_c
TIME, MSEC
0
0.2
0.4
0.6
0.8
1.0
1.2
1.4
0
20
40
60
80
100
120
140
160
180
200
220
240

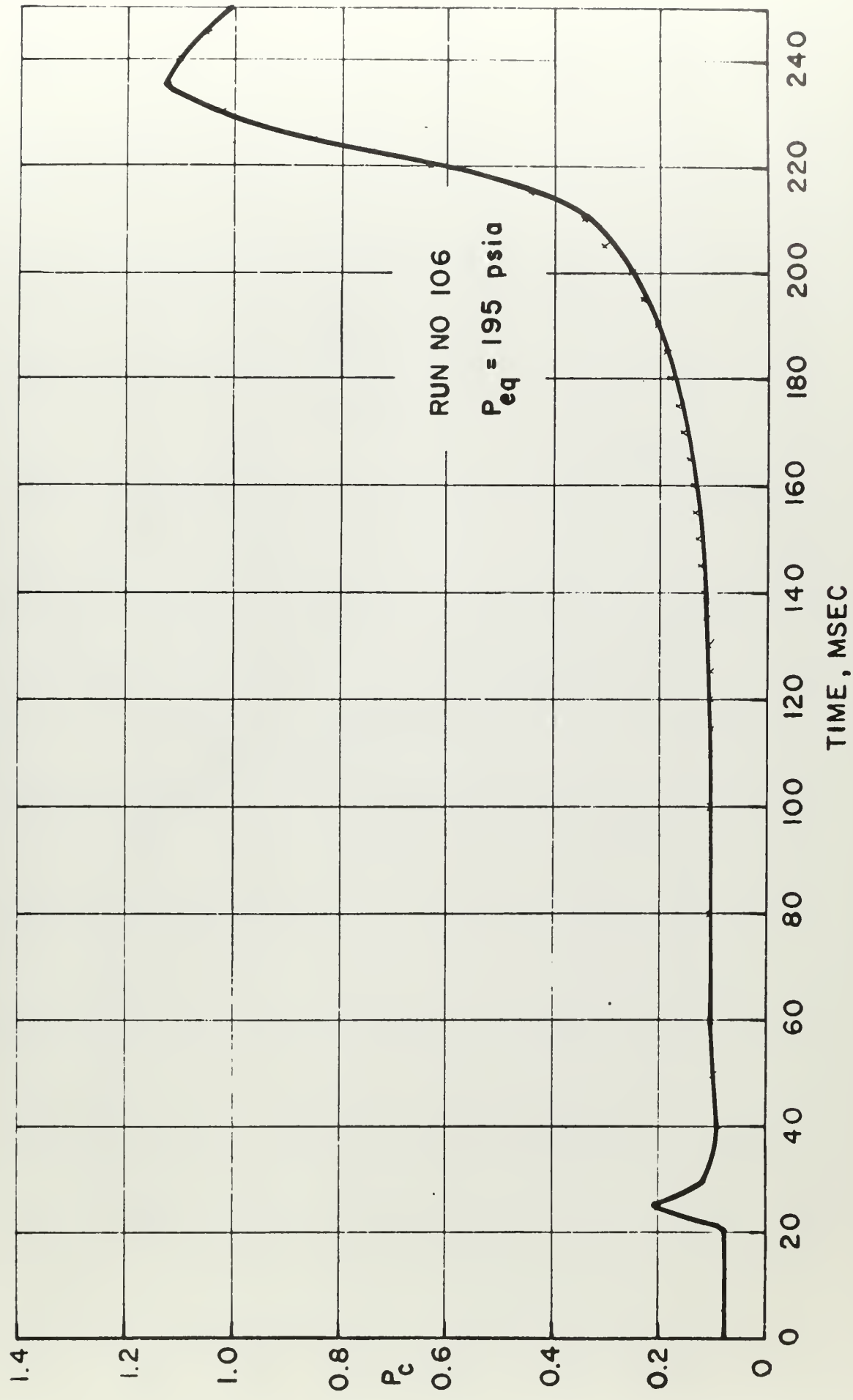
RUN NO 106
P_{eq} = 195 psia
P_c
1.4
1.2
1.0
0.8
0.6
0.4
0.2
0
0
20
40
60
80
100
120
140
160
180
200
220
240
TIME, MSEC

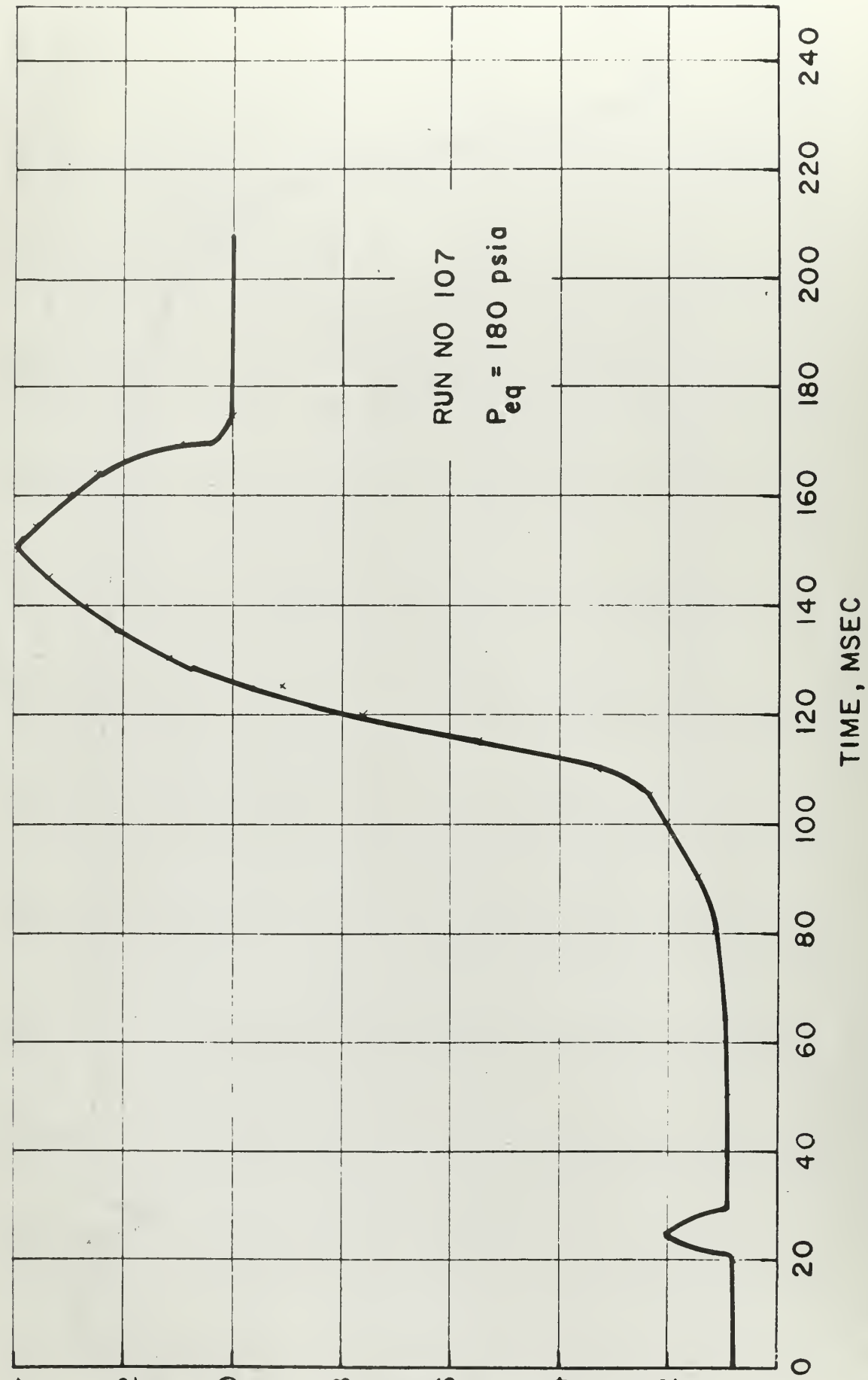
RUN NO 107
P_{eq} = 180 psia
P_c
1.4
1.2
1.0
0.8
0.6
0.4
0.2
0
0
20
40
60
80
100
120
140
160
180
200
220
240
TIME, MSEC

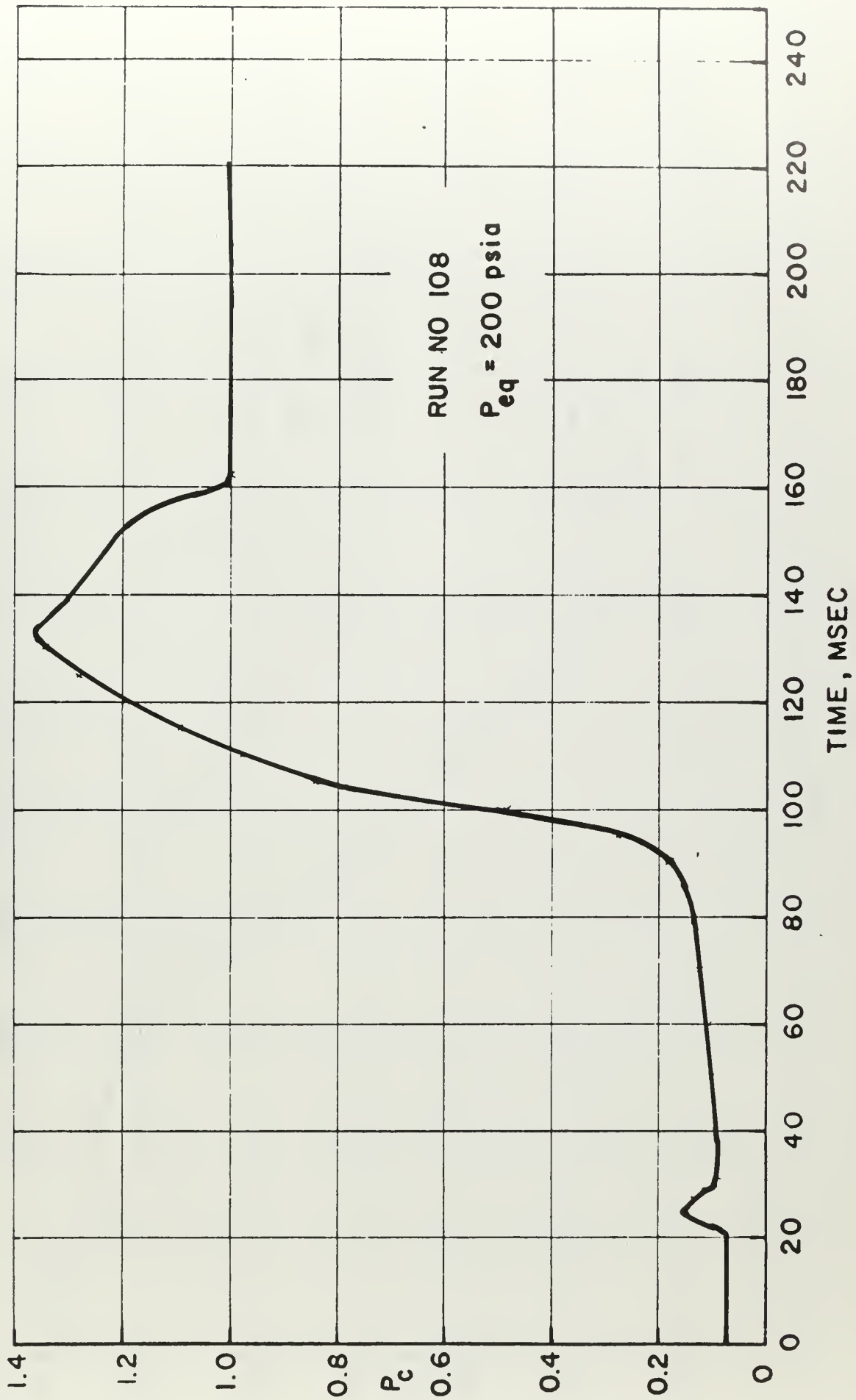
RUN NO 108
P_{eq} = 200 psia
P_c
1.4
1.2
1.0
0.8
0.6
0.4
0.2
0
0
20
40
60
80
100
120
140
160
180
200
220
240
TIME, MSEC

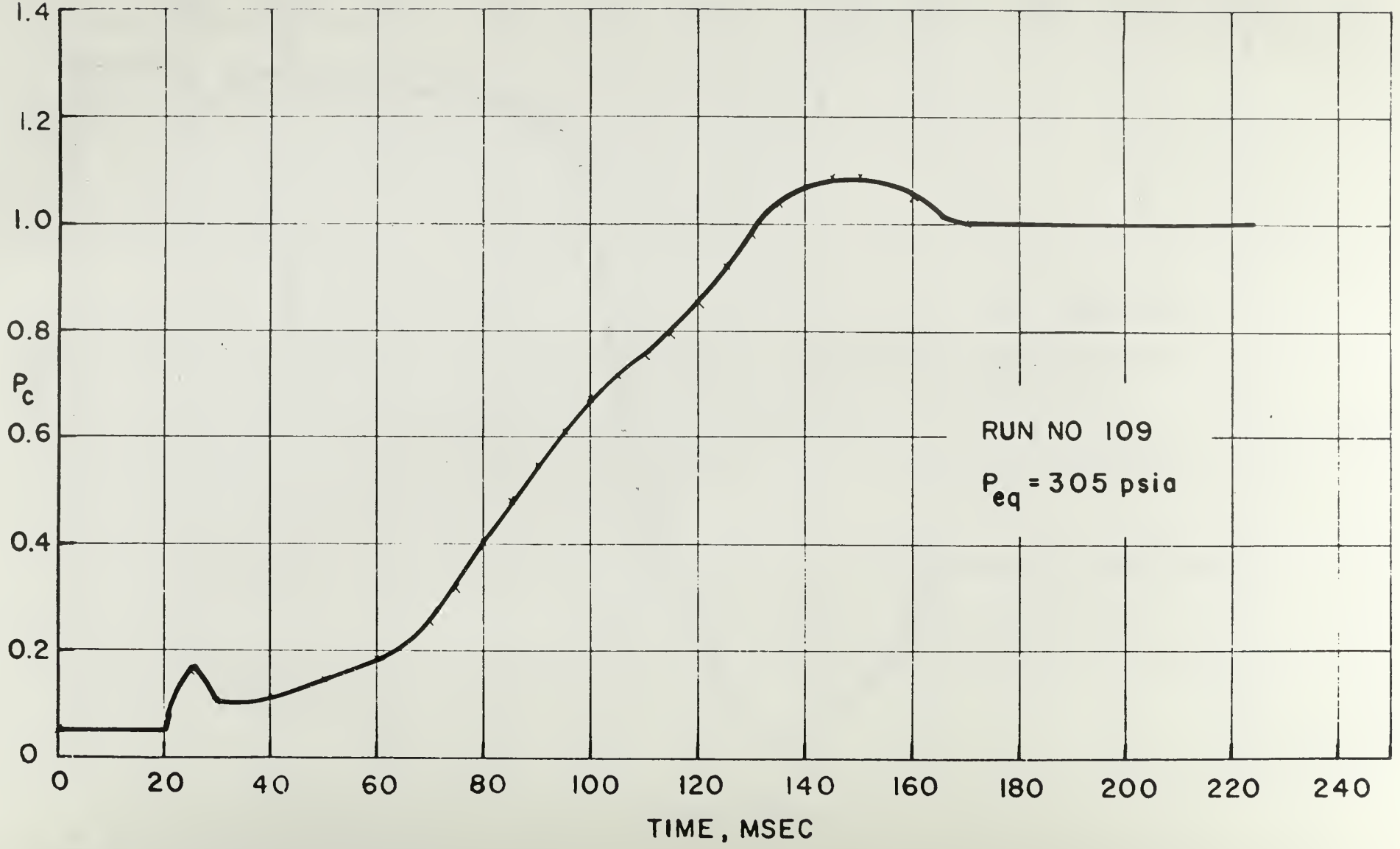
1.4
1.2
1.0
0.8
P_c
0.6
0.4
0.2
0
0
20
40
60
80
100
120
140
160
180
200
220
240
TIME, MSEC
RUN NO 109
P_{eq} = 305 psia

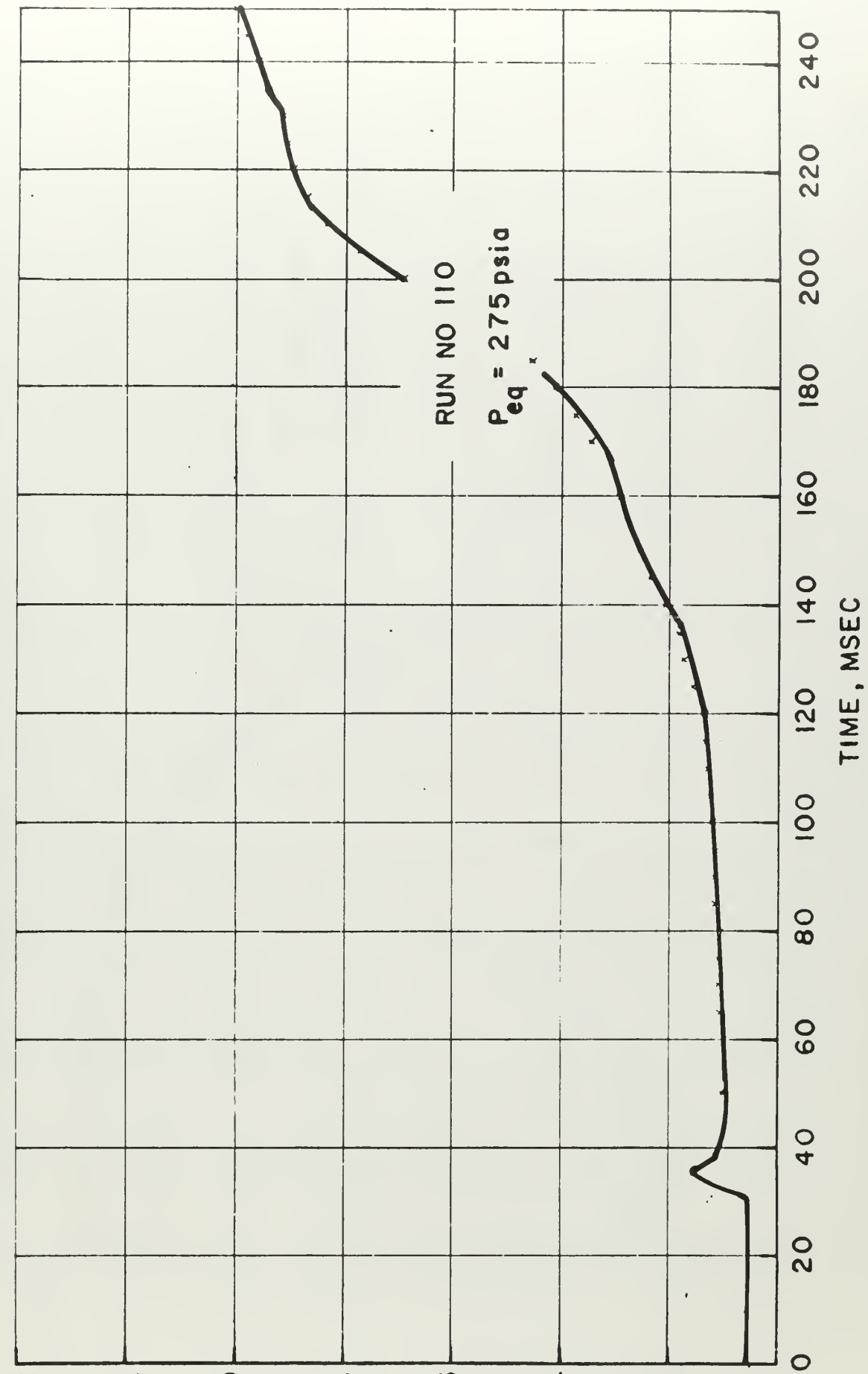
RUN NO 110
P_{eq} = 275 psia
P_c
1.4
1.2
1.0
0.8
0.6
0.4
0.2
0
0
20
40
60
80
100
120
140
160
180
200
220
240
TIME, MSEC

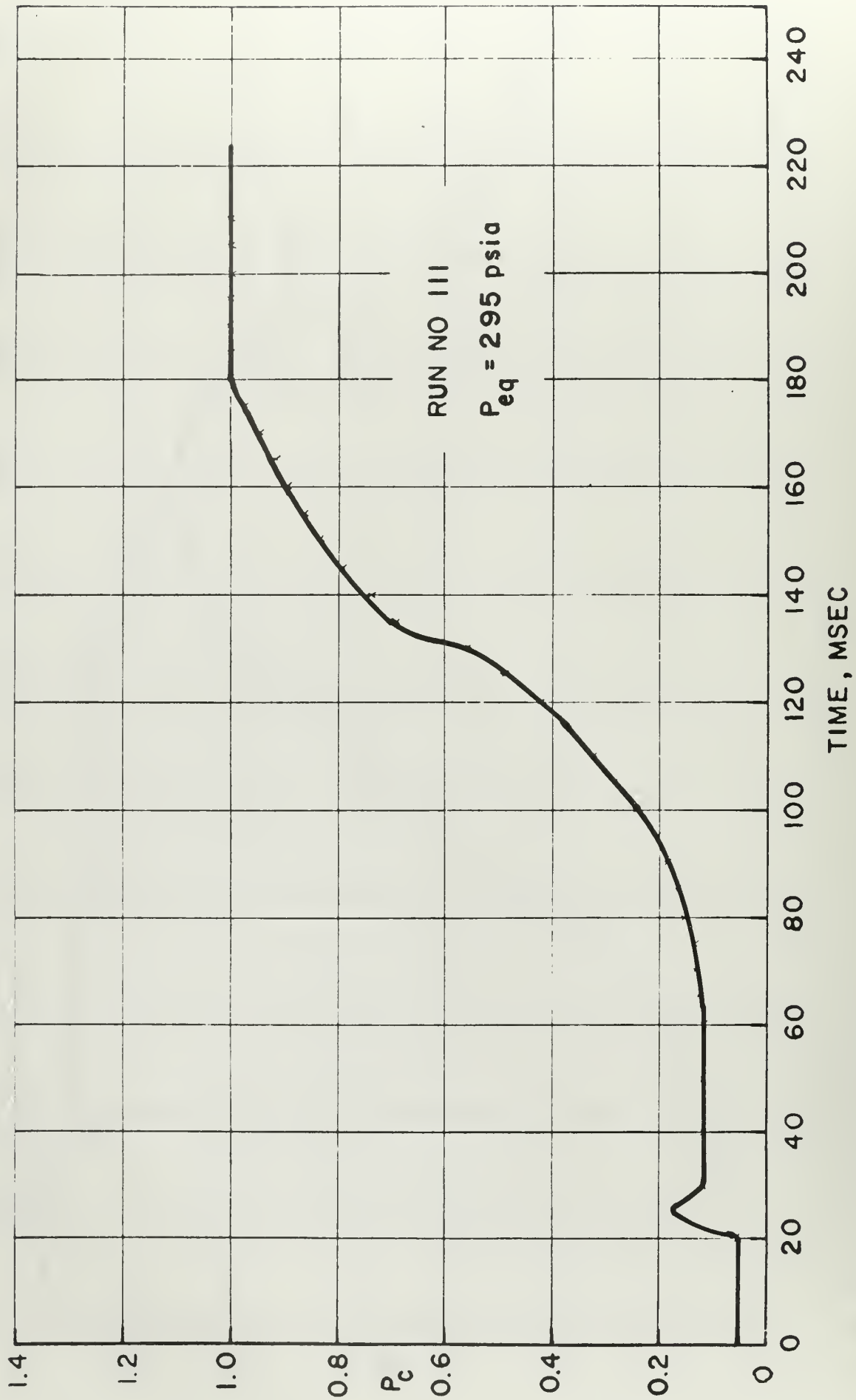
RUN NO 111
P_{eq} = 295 psia
P_c
1.4
1.2
1.0
0.8
0.6
0.4
0.2
0
0
20
40
60
80
100
120
140
160
180
200
220
240
TIME, MSEC

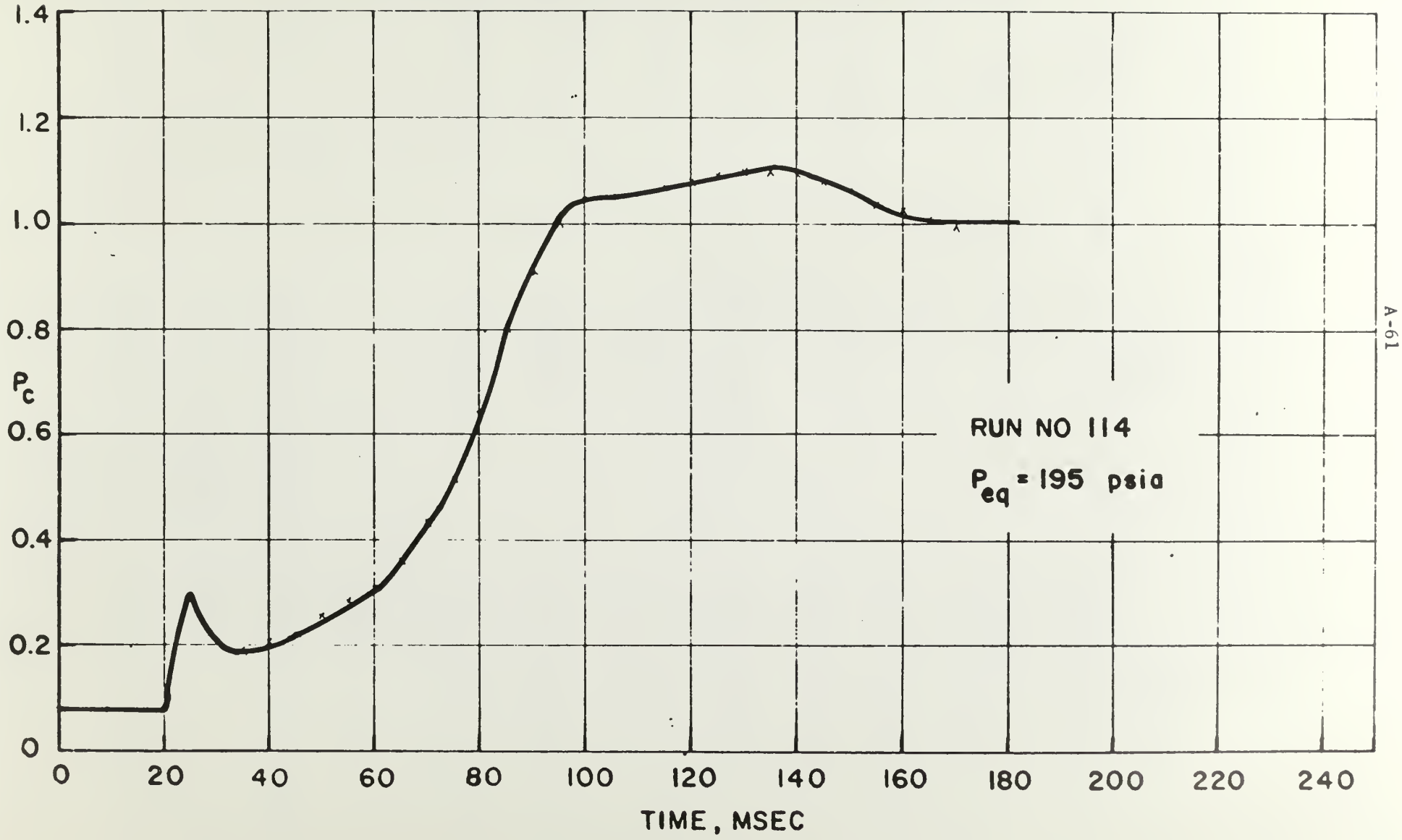
1.4
1.2
1.0
0.8
P_c
0.6
0.4
0.2
0
0
20
40
60
80
100
120
140
160
180
200
220
240
TIME, MSEC
RUN NO 114
P_{eq} = 195 psia

APPENDIX B

COMMERCIALLY AVAILABLE EXPERIMENTAL APPARATUS AND MATERIALS

Item	Purpose	Manufacturer
Tape Recorder, Honeywell Model 8100	Data Recording	Honeywell, Inc. 4800 East Dry Creek Road Denver, Colorado
Visicorder Oscillograph Honeywell Model 1508	Data Recording	Honeywell, Inc. 4800 East Dry Creek Road Denver, Colorado
Magnetic Recording Tape Type 42J	Data Recording	Memorex Corporation Santa Clara, California
Lino-Writ 5 Oscillograph Paper	Data Recording	E. I. DuPont 380 Allwood Road Clifton, New Jersey
Dana Amplifiers, D.C. Type 3520	Amplification of input signals to tape and oscillograph	Dana Laboratories, Inc. 630 Young Street Santa Anna, California
D.C. Voltmeter, Digital	Calibrations & Monitor	United Systems Corporation 918 Woodley Road Dayton 3, Ohio
Vacuum Tube Voltmeter Model 400 HR	Calibration of Equipment	Hewlett-Packard Company 395 Page Mill Road Palo Alto, California
Wide Range Oscillator Model 200 CDR	Calibration of Equipment	Hewlett-Packard Company 395 Page Mill Road Palo Alto, California
Tektronix Scope Model 521	Systems Monitor	Tektronix, Inc. Portland 7, Oregon
B & F Transducer Conditioning Module Type 1-211A2	Transducer Power Supply and Calibrator	B & F Instruments, Inc. 3644 N. Lawrence Avenue Philadelphia 40, Penna.
Pressure Transducer Type PT-76	Pressure Measurement	Dynisco Cambridge, Massachusetts
Deadweight Tester 0-2000 psi Model 472	Transducer Calibration	Amthor Inst. Testing Co. Brooklyn, New York

Item	Purpose	Manufacturer
Sequence Timer Model RC-J2889	Equipment Control	Industrial Timer Corp. State Electronics 36 Route 10, Hanover, N.J.
Gates Power Supply G3030F	Control Power	Gates Electronics Corp. New York, New York
Conax Thermocouple Gland Type MTG-20-A2	Igniter Feed Through	Conax Corporation 2300 Wazden Avenue Buffalo, New York
Electric Match Assembly Type 14104	Ignition	Atlas Chemical Company Ordinance Material Dept. Wilmington, Delaware
1/2" Stainless Steel Rupture Discs	Motor Protection	Black, Sivalls & Bryson, Inc. Wayne, Pennsylvania
Blow-Out Assembly 1/2" Safety Head Assy.	Motor Protection	Black, Sivalls & Bryson, Inc. Wayne, Pennsylvania
Fuller RL-3700 Potting Compound	Blow-Out Disc Protection	W. P. Fuller & Company P. O. Box 3727 Terminal Annex Los Angeles 54, California
Gage 0-2000 psi 12"	Calibration Gage	Heise Bourdon Tube Company Newton, Connecticut
Grove Reducing Regulator Model 15H	Calibration Pressure Control	Grove Regulator Company 6529 Hollis Street Oakland, California
Mixer, ARC Vertical Model 60LP	Propellant mixing	Atlantic Research Corp. Shirley Hwy. at Edsall Rd. Alexandria, Virginia
Phenolic Tubing Nema "L"	Propellant shells	Synthane Corporation Oaks, Pennsylvania
Teflon Rod	Molds & Mandrels	Commercial Plastics Newark, New Jersey

LIST OF CHEMICALS

Item	Purpose	Manufacturer
Ammonium Perchlorate	Oxidizer	American Potash & Chemical Corp. 3000 W. Sixth Street Los Angeles, California
(A) standard AMS-C66F	Non-Spherical Std.	
(B) rounded class I 2-10% + 50 mesh 91-99% + 200 mesh	Spherical Std.	
(C) 5 micron nominal at 50% point	Spherical fine 5μ	
(D) 45 micron at 50% point	Spherical 45μ	
PBAA Propellant		
PBAA Polymer	Fuel Binder	American Synthetic Rubber Corporation P.O. Box 360 Louisville 1, Kentucky
Epoxy Resin (shell) (EPON 828)	Fuel Binder	Miller-Stephenson Chemical Company Philadelphia 8, Penna.
Plastisol Propellant		
Fluid Ball Powder Type A	Propellant	Associated Products Operation Olin Matheson Chem. Co. East Alton, Illinois
TEGDN	Propellant	Propellex, Div. of Chromalloy Corporation P. O. Box 187 Edwardsville, Illinois
Inhibitors		
E-POX-E Glue No. EPX-1	Igniter Inhibiter	The Woodhill Chemical Corp. Cleveland, Ohio
Silicone Rubber RTV580	Grain end inhibitor transducer diaphragm protection	General Electric Silicone Products Dept. Waterford, New York